

4. MIDDLE VALLEY: DEAD DOG AREA (SITE 1036)¹

Shipboard Scientific Party²

HOLE 857D

Position: 48°26.517'N, 128°42.651'W
Date occupied: 5 September 1996
Date departed: 7 September 1996
Time on hole: 2 days, 8 hr, 30 min
Date occupied: 9 September 1996
Date departed: 11 September 1996
Time on hole: 1 day, 23 hr
Total time on hole: 4 days, 7 hr, 30 min
Bottom felt (drill pipe measurement from rig floor, m): 2431.5
Distance between rig floor and sea level (m): 12.1
Water depth (drill pipe measurement from sea level, m): 2419.4
Comments: Fished CORK and thermistor string placed during Leg 139. Replaced CORK and thermistor string.

HOLE 858G

Position: 48°27.360'N, 128°42.531'W
Date occupied: 22 August 1996
Date departed: 24 August 1996
Time on hole: 1 day, 5 hr, 15 min
Date occupied: 1 September 1996
Date departed: 5 September 1996
Time on hole: 3 days, 23 hr
Total time on hole: 5 days, 4 hr, 15 min
Bottom felt (drill pipe measurement from rig floor, m): 2431.5
Distance between rig floor and sea level (m): 11.3
Water depth (drill pipe measurement from sea level, m): 2414.9
Total depth (from rig floor, m): 2727.5
Number of cores (including cores having no recovery): 1
Total core recovered (m): 0.81
Comments: After the CORK was recovered, the hole was drilled from 236.0 to 296.0 mbsf. One wash core (19W) was recovered before reCORKing was done. Cores 17W and 18W are material scraped from inside of the retrieved CORK housing.

HOLE 1036A

Position: 48°27.3703'N, 128°42.5849'W
Date occupied: 15 September 1996
Date departed: 16 September 1996
Time on hole: 16 hr, 45 min
Bottom felt (drill pipe measurement from rig floor, m): 2419.0
Distance between rig floor and sea level (m): 11.6
Water depth (drill pipe measurement from sea level, m): 2407.4
Total depth (from rig floor, m): 2457.5
Number of cores (including cores having no recovery): 6
Total core recovered (m): 34.79
Core recovery (%): 90.4
Oldest sediment cored:
Depth (mbsf): 38.5
Nature: siltstone and silty claystone

HOLE 1036B

Position: 48°27.384'N, 128°42.6069'W
Date occupied: 16 September 1996
Date departed: 16 September 1996
Time on hole: 11 hr
Bottom felt (drill pipe measurement from rig floor, m): 2426.0
Distance between rig floor and sea level (m): 11.6
Water depth (drill pipe measurement from sea level, m): 2414.4
Total depth (from rig floor, m): 2478.3
Number of cores (including cores having no recovery): 6
Total core recovered (m): 46.72
Core recovery (%): 89.3
Oldest sediment cored:
Depth (mbsf): 52.3
Nature: mud with silty bioturbated layer

HOLE 1036C

Position: 48°27.3982'N, 128°42.6309'W
Date occupied: 16 September 1996
Date departed: 17 September 1996
Time on hole: 15 hr, 30 min
Bottom felt (drill pipe measurement from rig floor, m): 2425.1
Distance between rig floor and sea level (m): 11.6

¹Fouquet, Y., Zierenberg, R.A., Miller, D.J., et al., 1998. *Proc. ODP, Init. Repts.*, 169: College Station, TX (Ocean Drilling Program).

²Shipboard Scientific Party is given in the list preceding the Table of Contents.

Water depth (drill pipe measurement from sea level, m): 2413.5

Total depth (from rig floor, m): 2479.3

Number of cores (including cores having no recovery): 6

Total core recovered (m): 46.87

Core recovery (%): 86.5

Oldest sediment cored:

Depth (mbsf): 54.2

Nature: sandstone

Principal results: Site 1036 was drilled at the active Dead Dog Vent Field (DDVF) to (1) constrain the fluid flow rates and pathways for hydrothermal fluid and seawater entrained into the hydrothermal upflow zone, (2) study the mode of formation of the hydrothermal mounds, (3) test a model that predicted the mounds grow by seafloor mineral precipitation and inflationary growth, (4) determine the effects of hydrothermal activity on sediment diagenesis and alteration, and (5) determine the presence, continuity, and nature of a suspected cap rock horizon at 30 meters below seafloor (mbsf). Another primary goal of operations in and around the DDVF was to replace the existing Circulation Obviation Retrofit Kit (CORK) and thermistor strings in two boreholes (Holes 858G and 857D) as part of an active hydrologic flow experiment designed to enable temporal monitoring of changes in seafloor temperature and pore pressure.

To meet these objectives, we drilled Holes 1036A, 1036B, and 1036C along a northwest-southeast transect from the top to the margin of the 7-m-high Dead Dog active hydrothermal mound. Old CORKs were removed in Holes 857D and 858G, new ones were set in their place, and the boreholes were reinstrumented. Pop-Up Pore Pressure Instruments (PUP-PIs) were also deployed in the area of Dead Dog Mound to monitor pore-pressure variations during operations.

Three of the major lithologic units known from Middle Valley were recognized (Units I, II, and IV). Lithologic Unit I is Holocene to upper Pleistocene silty clay of dominantly hemipelagic origin and has a relatively consistent thickness between holes. Three subunits were defined on the basis of hydrothermal/diagenetic alteration. Subunit IA lacks distinctive hydrothermal or diagenetic products. Subunit IB is distinguished from Subunit IA by the presence of authigenic carbonate. Subunit IC contains authigenic anhydrite as disseminated crystals, nodules, and cements, and is a distinctive alteration facies of the hydrothermal system.

Lithologic Unit II is characterized by hemipelagic silty clays interbedded with silt to fine sand turbidites. Two of the subunits characterizing this interval were recovered from Site 1036; Subunit IIB is characterized by the occurrence of diagenetic carbonates within the turbiditic sediments. Subunit IIC is distinguished by the presence of anhydrite cements and nodules.

Lithologic Unit IV is a clastic mixture of white anhydrite crystals, now partly altered to gypsum, very fine-grained pyrrhotite with subordinate pyrite and sphalerite, and greenish gray clay, probably a Mg-bearing smectite. This unit was only recovered at Hole 1036A, which is less than 10 m away from an active chimney surrounded by an apron of anhydrite chimney debris. The angularity and size of the clasts, as well as the relief of the mound, dictate that these clasts are derived from the collapse of chimneys formed at vents on Dead Dog Mound.

Drilling at Site 1036 showed that flat-lying Subunits IA and IIA have not been significantly displaced since deposition. The relief of the Dead Dog Mound is close to the stratigraphic thickness of chimney-derived rubble; hence, the mound is nearly entirely a buildup of rubble and is not caused by authigenic hydrothermal mineral precipitation in the subsurface or tectonic uplift. The upper boundaries of the carbonate and anhydrite alteration subunits deepen away from the mound, reflecting the decreasing geothermal gradients.

Although Hole 1036A is less than 10 m west of an active vent, no major hydrothermal vein network was intercepted at depth, and most sediments are not highly lithified by hydrothermal alteration. Only a few hydraulic breccias and some anhydrite veins are observed. The absence of a stockwork zone underlying the mound and the lack of extensive indura-

tion suggest that the Dead Dog hydrothermal mound is an immature feature, consistent with the occurrence of collapsed chimney material overlying very young sediments.

Biostratigraphic zonation of the quaternary sequence at Middle Valley is limited to planktonic foraminifers, because other fossils such as diatoms, radiolarians, and calcareous nannofossils are poorly preserved in hydrothermal settings. Planktonic foraminifers are abundant to common to 9.94, 18.61, and ~26 mbsf in the core from Holes 1036A, 1036B, and 1036C, respectively. The depth where foraminifers disappear roughly coincides with the shallowest occurrence of weakly indurated sediments. Regional sedimentation rates constrained by the depth to a 125 k.y. horizon identified by foraminifer assemblages range from 17 to 33 cm/k.y., which is surprisingly slow considering the young age of the basement and the total thickness of the sediment filling Middle Valley.

High gamma and wet bulk densities correspond to the occurrence of carbonate nodules in cores from Holes 1036A, 1036B, and 1036C. Both measures of bulk densities indicate a general increase downsection. This is correlated to a decrease of porosity from 70% at the surface to 50% or less at 40 mbsf. Near the vent, porosity in cores from Hole 1036A drops abruptly to <30% at ~30 mbsf near the contact between lithologic Units I and II. The depth at which the magnetic susceptibility of sediments decreases to near zero (magnetic "wipeout" zone) increases with distance from the vent and may be related to hydrothermal alteration and the shallowing of isotherms near the vent. Magnetic peaks in the deeper cores from Holes 1036A and 1036B within the magnetic wipeout zone are caused by local pyrrhotite precipitation. The natural remnant magnetization of cores from Site 1036 was measured for quasi-continuous sections. Hydrothermal activity significantly affects the paleomagnetic signal and overprints the record of the Brunhes Chron, with the level of affected sediment decreasing with proximity to the hydrothermal vent.

The pore fluids from Hole 1036A have a composition distinct from those in other holes located further from hydrothermal venting. Composition similar to that of seawater above 20 mbsf suggests vigorous local recharge. Between 20 and 30 mbsf, increase in the Mg and decrease in the Ca and Na concentrations indicate a significant modification of the pore-water composition. This implies high-temperature (>200°C) alteration in the vicinity of a fluid conduit, caused by heat supply from upflowing fluid. This alteration process appears to involve downwelled seawater that is subsequently transported laterally through this section. In Holes 1036B and 1036C, pore fluids are modified by thermally enhanced diagenesis of clay minerals and anhydrite precipitation. Below 40 mbsf in Hole 1036B, pore fluids are dominated by a hydrothermal component with a composition similar to the Dead Dog fluid end-member. The upper boundary of hydrothermal penetration was not observed in Hole 1036C because the depth of influence of the hydrothermal fluids rapidly decreases away from the vent.

Pore water collected from Hole 1036C cores contains methane and hydrocarbon derived from the high-temperature alteration of organic matter. Hydrothermal petroleum is found in discrete horizons in sediments from Hole 1036A (12–17 mbsf), Hole 1036B (24–35 mbsf), and Hole 1036C (32–35 mbsf). This petroleum has migrated only a short distance ahead of the heat front and resides at an in situ temperature of 100°–150°C. CO₂ increases near the oil horizon, but there is no correlation between methane and the oil horizon. Total organic carbon (TOC) decreases with increasing depth in Hole 1036A close to the vent and increases with depth in Hole 1036C at the base of the mound.

Upon recovery of the old CORK housing from Hole 858G, we discovered that the inside of the CORK body was coated with hydrothermal precipitates, predominantly anhydrite but with abundant pyrrhotite and pyrite. Naturally occurring hydrothermal chimneys from the DDVF are predominantly composed of anhydrite, with only minor amounts of pyrite and trace amounts of pyrrhotite. Although the seals in the CORK had clearly failed because of the high temperature, examination of the location of the precipitates and the still-open flow channels suggests that the fluid flow originated in the sediment underlying the reentry funnel and that flow out of the cased hole may not have contributed to the precipitation of hydrothermal minerals in the CORK.

A water sampler temperature probe (WSTP) run 20 m into the casing indicated fluid temperatures in excess of 220°C. The fluid sample collected contained a mixture of seawater and hydrothermal fluid that extrapolates to a hydrothermal end-member similar to fluids sampled in the vent field using the *Alvin*. A temperature run with the Ultra High Temperature Multisensor Memory (UHT-MSM) dewatered tool confirmed the high temperatures at the top of the open borehole and indicated that the borehole was essentially isothermal at 272°C (near the maximum measured in the vent field). Although we were forced to disturb the thermal structure of Hole 858G during hole cleaning operations, we were successful in re-instrumenting the hole with a 370-m-long thermistor string and pressure transducer and in setting a new CORK in the reentry funnel. A second CORK at Hole 857D, which had been damaged during a prior recovery attempt, was successfully retrieved. A 898-m-long thermistor string was installed along with a new CORK as part of a long-term ocean floor observatory.

DEAD DOG HYDROTHERMAL FIELD

The major objective of drilling at Dead Dog Mound within the DDVF was to investigate formation of the sediment-covered mounds that are the site of active hydrothermal venting. Drilling in the DDVF during Ocean Drilling Program (ODP) Leg 139 (e.g., Hole 858B) provided indications that the mounds may form by an “inflationary” process whereby precipitation of anhydrite and Mg-rich smectite occurs in a subsurface mixing zone between hydrothermal fluid and shallowly circulating bottom seawater entrained into the upper part of the hydrothermal upflow zone. Several of the holes drilled in the DDVF also encountered a hard layer at ~30 mbsf that could be interpreted as a cap rock that controlled the lateral flow of hydrothermal fluids beneath the vent field, as indicated by the presence of steep gradients of pore-water compositions at about the same depth. The hard layer was not recovered in any of the Leg 139 drill holes, so a drilling strategy was designed to determine if such a layer was present underneath the large Dead Dog Mound. Additionally, we planned to reoccupy the sites (Holes 858G and 857D) where CORKs had been installed in cased boreholes during Leg 139 to conduct water-sampling and hydrological experiments and to reinstrument and reseal these holes. Specific objectives of the drilling were as follows:

1. Determine the mechanism of the growth of hydrothermal mounds in the active vent fields.
2. Measure pore-fluid compositions and constrain the extent of lateral flow and fluid mixing in the shallow subsurface.
3. Establish the extent and importance of a suspected hydrological seal (cap rock) in focusing hydrothermal discharge.
4. Determine the extent of microbiological activity within the sealed boreholes and sediments in active hydrothermal fields.
5. Study organic matter maturation as a function of the present thermal regime and determine peak paleotemperatures recorded by organic matter.

In addition, several specific objectives were related to the CORKing operation:

1. Measure the temperature gradient and sample hydrothermal fluids in Holes 858G and 857D.
2. Deepen Hole 857D to recover deeper portions of the sill-sediment complex and to cool the hole sufficiently to induce downhole flow.
3. Log Hole 857D to determine changes in physical properties related to hydrothermal alteration.
4. Determine the structural effects of sill emplacement and tectonic controls on fluid flow.
5. Reinstrument and reseal Holes 858G and 857D to determine the in situ temperature and pore pressure.

6. Conduct a hole-to-hole experiment on hydraulic conductivity and induced seismicity.

Geological Setting and Hydrothermal Processes

Regional setting

The DDVF is located ~6 km east of the spreading axis of Middle Valley, and at about the same distance from the eastern valley-bounding normal faults (Figs. 1, 2). Based on the spreading rate (58 mm/yr) and the distance to the Brunhes/Matuyama magnetic boundary, the age of the underlying igneous crust is ~350 k.y. (Davis and Fisher, 1994). A syndimentary normal fault that offsets seismic reflectors interpreted to be igneous basement separates the site from the current structural axis of the rift where the sediment is up to 1 km thick (Rohr and Schmidt, 1994). This fault has produced a 250-m scarp in the basement (Davis and Villinger, 1992), but at the latitude of the vent field, the relief of the fault at the seafloor is only 50 m. The sediment thickness ranges from ~400 to 700 m on the eastern side of the fault. The DDVF has formed where the sediment cover is locally attenuated above a buried volcanic high that rises to within 250 m of the seafloor (Langseth and Becker, 1994). The hydrothermal discharge probably is controlled by this local basement topography and by a secondary fault slightly oblique to the near-axis normal fault (Fig. 3). The seismic layering that characterizes the foot-wall block of the fault is disrupted locally beneath the vent field (Fig. 4).

Hydrothermal Field

The active Dead Dog hydrothermal field (800 m × 400 m) is situated within an axis-parallel thermal anomaly (Davis and Villinger, 1992), where heat flow exceeds 0.8 W/m² in a 1-km-wide zone at ~1.2 km east of the near-axis normal fault (Fig. 5). Near the perimeter of the vent field, heat flow increases sharply above background values of 0.3 W/m² and can exceed 20 W/m² near hydrothermal vents. In contrast to the Bent Hill Massive Sulfide (BHMS) deposit, no magnetic anomaly is present over the Dead Dog hydrothermal field (Tivey, 1994). The vent field is located in an 8-m-deep depression (Shipboard Scientific Party, 1992b), where the rougher seafloor can be easily identified on sonar images (Fig. 6). In addition, it is underlain by bright seismic reflectors at 130 and 300 ms two-way travel-time (TWT) that are not resolved elsewhere and are interpreted as resulting from the alteration of the upper sediment (Rohr and Schmidt, 1994). At least 20 vent sites have been mapped (Fig. 1); most sites consist of a mound, 5–15 m high and 25–35 m in diameter, topped by one to five separate anhydrite chimneys, 0.7–1.2 m high. The top and sides of the mounds expose only sediment that is locally indurated and hydrothermally altered (Goodfellow and Franklin, 1995). Piston coring has revealed that the underlying sediment is also hydrothermally altered. The anhydrite chimneys contain very minor amounts of pyrite and Mg-rich smectites and trace amounts of chalcopyrite and sphalerite (Ames et al., 1993). The chimneys typically grow to a height of 1–2 m before collapsing. The areas surrounding the chimneys are covered with chimney fragments that disaggregate by anhydrite dissolution, leaving a residue enriched in pyrite and Mg-rich smectites (Turner et al., 1993).

Vent Fluid

Vent fluid temperatures range from 234° to 276°C. The pH of 5.4 suggests that the fluids have reacted with carbonate. Ca concentration in the end-member fluids is 80 mmol, but most components, especially transition metals, are lower than in fluids from sediment-free ridges. The low metal contents (lower than the concentrations reported for Guaymas Basin fluids) indicate that either the metalliferous components have precipitated in the subsurface or that the fluid never reached sufficient temperature or low enough pH to contain abundant metals. Isotopic data for C, O, and H indicate that CO₂ and CH₄ are

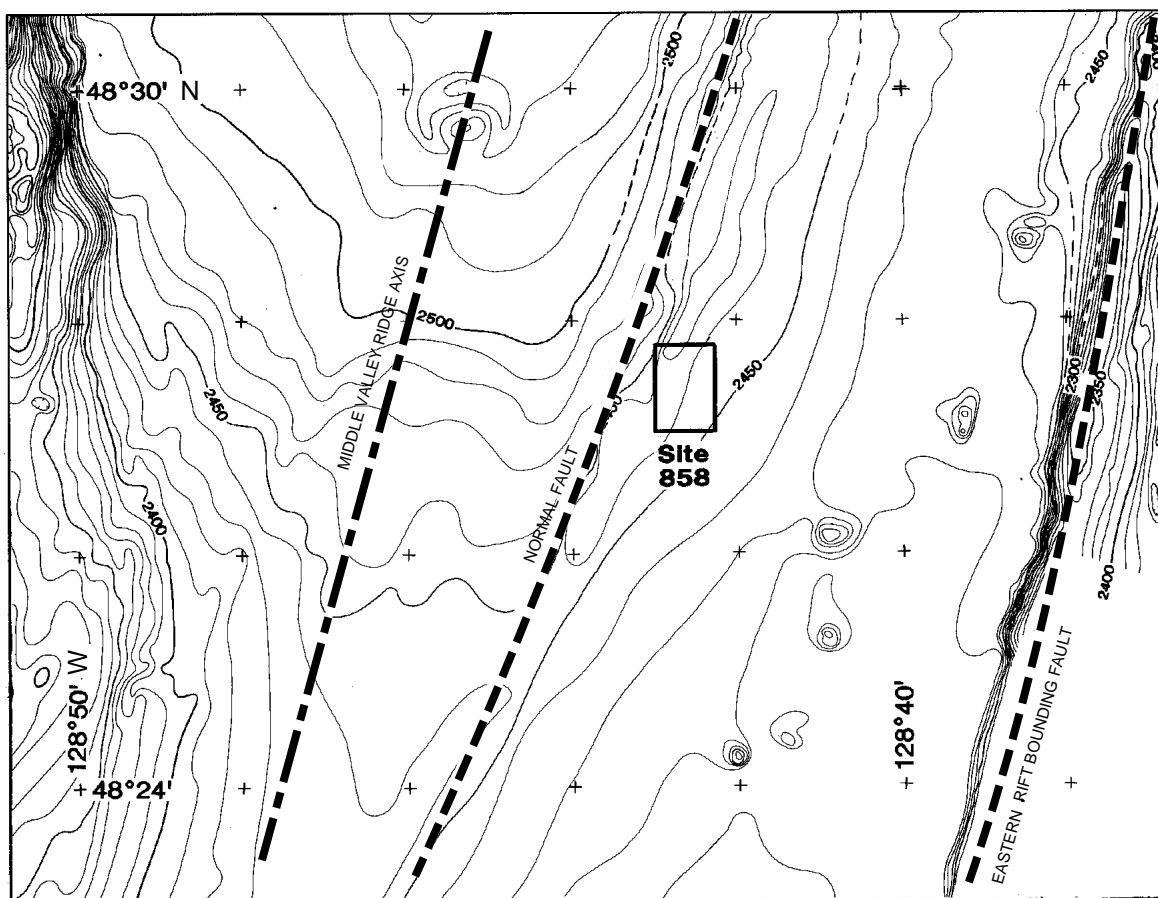


Figure 2. Seabeam bathymetry of Middle Valley. The location of the Dead Dog Vent Field (Site 858, Leg 139; Shipboard Scientific Party, 1992b) is outlined by the box.

generated by pyrolysis of organic material (Taylor, 1990). However, hydrothermal water collected from the vents show a strong influence of basalt-fluid interaction overprinted to some degree by reactions within the sediment column (Butterfield et al., 1994). For example, the Sr isotope ratio in the fluid (0.7043) is just slightly higher than the reported range for basalt-hosted mid-ocean ridge basalt (MORB) hydrothermal fluids (0.7028–0.7041; Palmer and Edmond, 1989; Von Damm, 1995) and is significantly lower than Sr ratios in bulk fresh sediment (>0.708) and hydrothermally altered sediment (>0.707 ; Goodfellow and Blaise, 1988). This indicates that little Sr, and by inference Ca, has been leached from the turbidites and hemipelagic sediment that hosts the hydrothermal deposits (Butterfield et al., 1994). Middle Valley vents appear to be relatively basalt-dominated fluids when compared with other sedimented MOR hydrothermal systems (Von Damm, et al., 1995). High Ca concentration and relatively low Na concentrations at Dead Dog suggest that albitization may be an important alteration process that may suggest a temperature lower than 325°C in the basaltic reaction zone (Butterfield et al., 1994). The lower Ca concentration at Bent Hill may indicate higher temperatures in the reaction zone, even though the vent fluid temperatures measured at the seafloor are similar to those in the DDVF.

The $^{87}\text{Sr}/^{86}\text{Sr}$ ratios in barite, gypsum, and calcite confirm that the hydrothermal fluid must have interacted with basalt (Goodfellow and Blaise, 1988; Goodfellow, et al., 1993). Sulfur isotope values in massive sulfide also indicate a mixture of basaltic sulfur and sulfur derived by reaction of seawater sulfate (Duckworth et al., 1994; Zierenberg, 1994). The relatively homogeneous sulfur isotope values ($\delta^{34}\text{S}$

average $\sim 6\text{‰}$, range about 1‰ – 10‰) of massive sulfide, hydrothermally altered sediment, and basalt indicates a complex, but consistent sulfur source.

Leg 139 Principal Results

Four advanced piston corer/extended core barrel (APC/XCB) holes (Holes 858A–858D) were drilled during Leg 139 in an array crossing the DDVF (Fig. 6) to document the local fluid flow, thermal regime, and sediment alteration beneath and around the vent field. The depth of these holes was respectively: Hole 858A, 339 m; Hole 858B, 39 m; Hole 858C, 93 m; and at Hole 858D, 41 m. Hole 858B was drilled ~ 20 m southeast of a 273°C vent and had a temperature of 197°C at 19.5 m depth. Hole 858D, drilled ~ 70 m north of this vent, had a temperature of 208°C at 21 mbsf. A rotary core barrel (RCB) exploratory hole (Hole 858F; total depth 297 mbsf) and a deep reentry hole (Hole 858G; total depth = 433 mbsf) were drilled approximately in the center of the field to characterize the deep hydrothermal and geologic structure in the upflow zone. However, basaltic flows were encountered at depths of 249 and 258 mbsf in Hole 858F and 858G, respectively, much shallower than the top of the sill-sediment complex drilled at Site 857, the top of which is at 470 mbsf. Hole 858G penetrated 184 m of pillow lavas and thin flows without further intersections of sedimentary rocks, indicating that basement had been reached. The elevation of these rocks compared to the regional basement suggests that the basalt may be part of an axial volcano or similar volcanic edifice. The composition of the somewhat

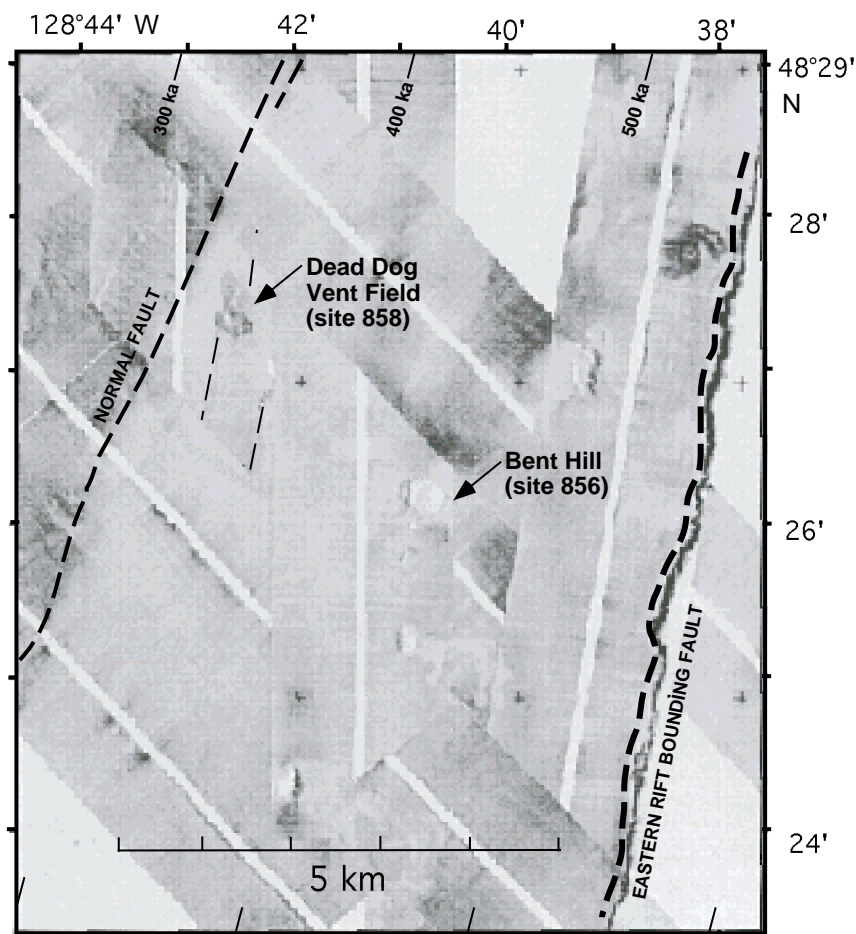


Figure 3. SeaMARC I (30 kHz) side-scan acoustic image mosaic of the southeastern part of Middle Valley showing Bent Hill and the Dead Dog Vent Field, Sites 856 and 858, respectively (Leg 139; Shipboard Scientific Party, 1992b).

evolved basalts from Site 858, compared to rocks from the sill-sediment complex, reflects either a different mantle source region or a lower degree of melting (Stakes and Franklin, 1994).

Hydrothermally altered sediments were recovered in all holes in the DDVF. The degree of alteration varies laterally and with depth and is consistent with the thermal structure. Conditions are thermally diffusive and chemically reactive in Holes 858A and 858C. Geothermal gradients are very steep in holes drilled in the vent field until temperatures near 270°C are reached, below which the section is nearly isothermal (Shipboard Scientific Party, 1992b). Temperatures in excess of 250°C are encountered at depths as shallow as a few tens of meters in the hydrothermal upflow zone that underlies the vent field. Extreme alteration may have resulted in the formation of a cap of indurated sediment at 30 mbsf in Holes 858B, 858C, 858D, and 858F, although very little of this material was recovered. Resistivity logs suggest a correlation between sedimentary units at Site 858 and Site 857, which is located 1.6 km to the south.

Based on the degree of alteration, the sulfide content and percentage of turbidites, five lithologic units were identified at Site 858: Unit I consists of fine-grained hemipelagic sediments of Holocene age that were probably deposited during the last highstand of sea level. Subunit IIA consists of interbedded hemipelagic and turbidic sediments. Subunit IIB consists of brecciated anhydrite and carbonate-rich, hemipelagic and turbiditic sediments. Subunit IIC consists of indurated interbedded hemipelagic and turbidite strata. Subunit IID consists

of silicified and hydrothermally altered hemipelagic and turbiditic strata. Unit III consists of oxidized metalliferous sediment, Unit IV consists of semi-massive sulfides, and Unit V consists of basaltic rocks (Shipboard Scientific Party, 1992b).

A general downcore decrease in organic carbon results from microbial and thermal degradation of organic carbon. Inorganic carbon varies inversely with organic carbon caused by the precipitation of diagenetic carbonate that is partly derived from organic sources (Baker and Cross, 1994).

Alteration

Density measured on sediment samples from the DDVF (Site 858) are as much as 0.5 g/cm³ higher than normal abyssal turbidites. The relatively high values are interpreted as being derived from the hydrothermal alteration of sediments (Rohr and Gröschel-Becker, 1994). Six distinct and concentric alteration zones are identified in the hemipelagic and turbiditic sediments (Fig. 7; Goodfellow and Peter, 1994; Leybourne and Goodfellow, 1994):

- Zone Ib: quartz-wairakite-epidote-pyrite-sphene;
- Zone IIB: quartz-epidote-chlorite-pyrite;
- Zone IIIb: albite-chlorite-illite-pyrite;
- Zone IVb: anhydrite-illite-pyrite;
- Zone Vb: calcite-illite-pyrite-barite; and

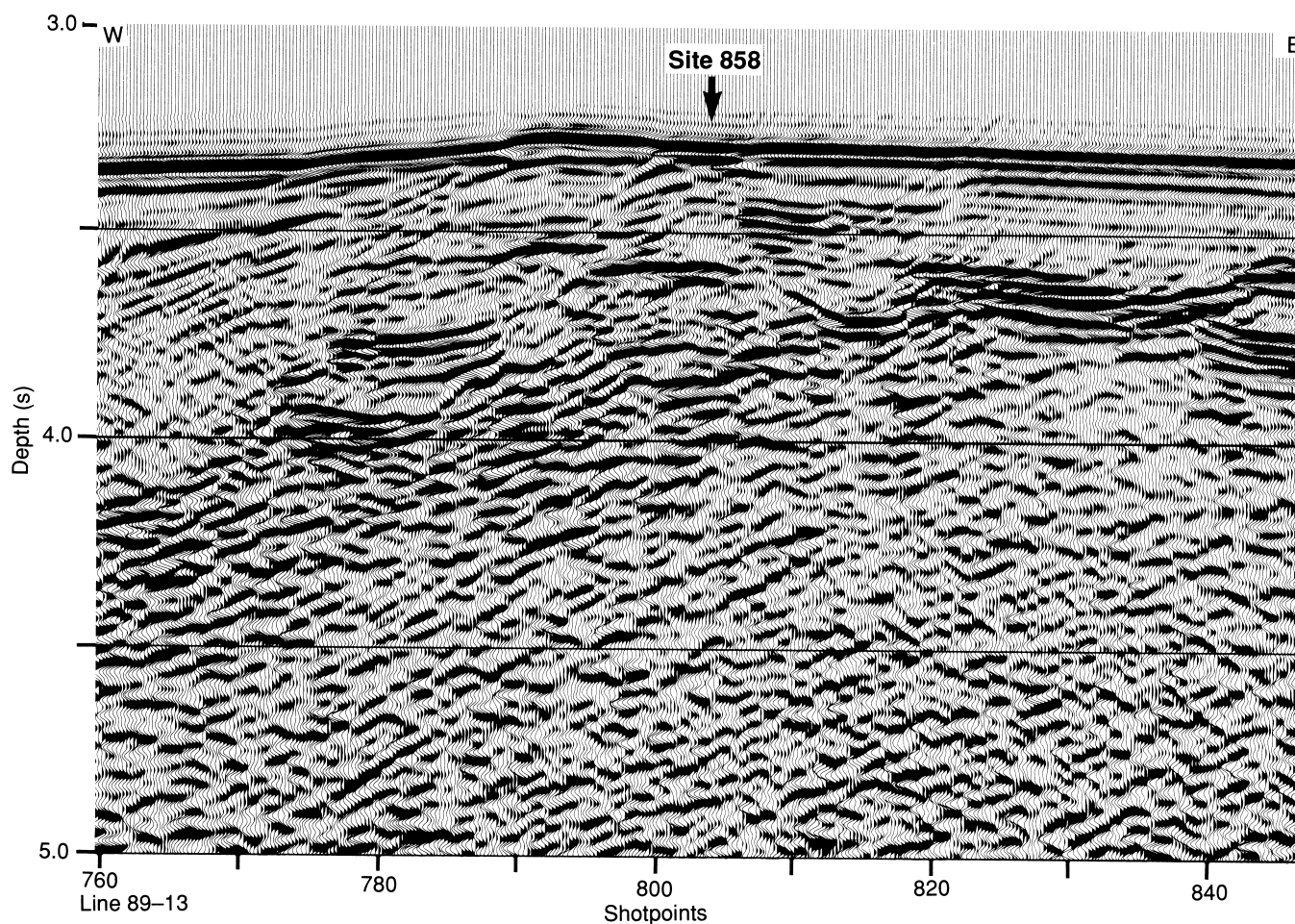


Figure 4. Migrated multichannel seismic section across Site 858 drilled during Leg 169 (Davis and Villinger, 1992).

Zone VI: saponite-talc-pyrite.

The zonal distribution of minerals reflects the gradient from high temperature near hydrothermal vents to lower temperature conditions at the margin of the vent field. Veins and mineral assemblages show little indication of very high temperature (>350°C) alteration, even though the basaltic flows drilled at the bottom of Hole 858G are highly altered. Heat-flow measurements indicate that temperatures at depth beneath the vent field are approximately isothermal at ~270°C (Shipboard Scientific Party, 1992b).

Mineral assemblages in the basaltic basement suggest alteration at subgreenschist to greenschist facies conditions (~200°–300°C; Shipboard Scientific Party, 1992b; Buatier et al., 1994; Goodfellow and Peter, 1994; Leybourne and Goodfellow, 1994). The mineralogical, geochemical, and thermal similarities between the central alteration zone at the venting area and the reaction zone at the base of sediment at Site 857 are consistent with the generation of hot fluids near the base of the Middle Valley sedimentary pile in the highly permeable sill-sediment complex. The section has probably been at close to its current temperature for >125 k.y. (Davis and Wang, 1994). This conclusion agrees with the observed levels of hydrocarbon maturation and the isotopic composition of authigenic minerals in the section.

Pore Water

The chemical composition of pore water changes downhole with increasing temperature, approaching the composition of the end-

member hydrothermal fluids discharging at 276°C in the vents. Minima and maxima in the chlorinity profile suggest that bottom seawater and hydrothermal water are both flowing laterally within the vent field. Mixing of these two solutions causes anhydrite to precipitate. Pore-water compositions show strong chemical gradients in the central part of the field because of the steep thermal gradient. The pore water from most cores shows a strong depletion in SO₄ and Mg with depth and a consistent increase in Ba.

Hydrothermal System

Injection tests showed that the basaltic sill complex is highly permeable compared to the overlying sediments. Davis and Wang (1994) have used temperature and permeability measurements to construct a two-part model of the hydrothermal system. The section of interbedded and fractured sills and sediment forms a permeable hydrothermal reservoir in which convective transport is highly efficient (Becker et al., 1994). This unit is overlain by a relatively low-permeability sediment section where vertical heat transport is conductive (Fisher et al. 1994; Davis and Fisher, 1994; Langseth and Becker, 1994). Although uniform heat flow with depth in Hole 857C indicates that vertical heat transport through the sedimentary layer is predominantly by conduction, significant horizontal heat transport by fluids flowing in more permeable sediment layers is likely (Langseth and Becker, 1994). Numerical simulation of convection also shows that it is possible that discrete zones of extremely high permeability are sufficiently well connected to substantially increase the large-

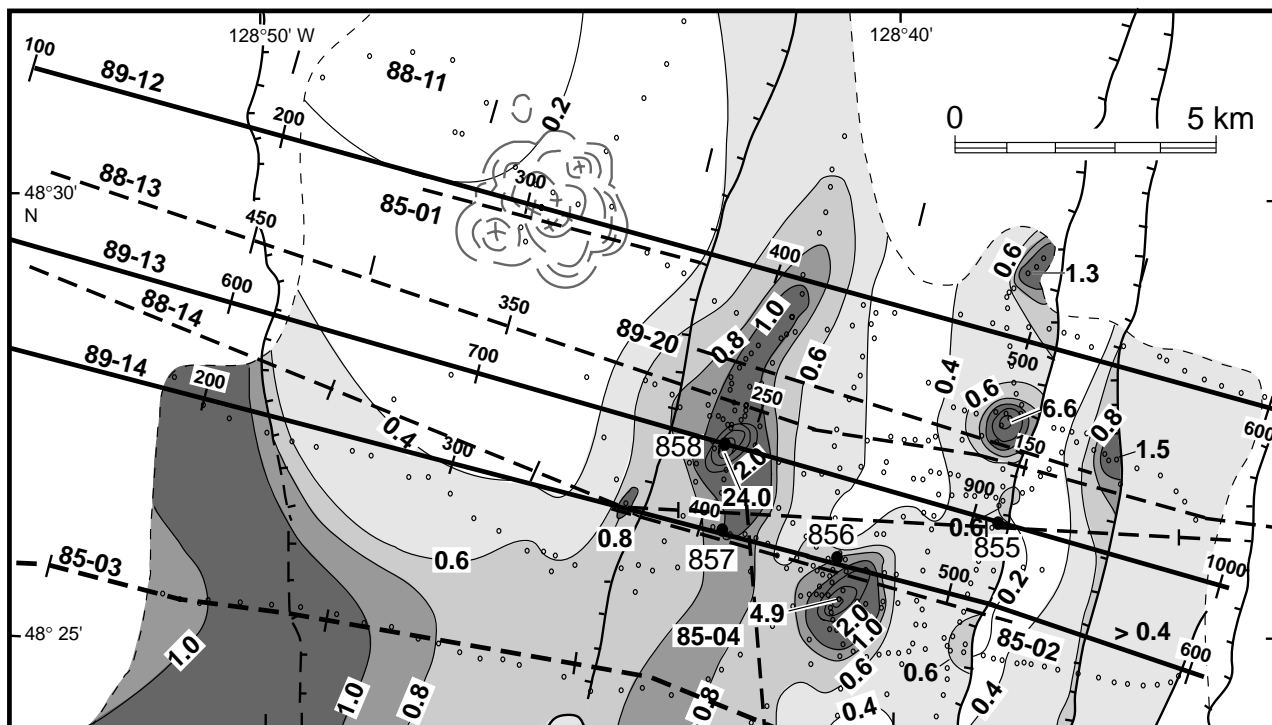


Figure 5. Location of multichannel (solid lines) and single-channel (dashed lines) seismic reflection profiles relative to heat-flow measurements (open circles) in Middle Valley (after Davis and Villinger, 1992; Rohr et al., 1993). Nominal line spacing is 2 km. Lines 85-01, 85-02, 85-03, and 88-13 were acquired with a single 0.65-L air gun and a single-channel receiving hydrophone array. Lines 89-12, 89-13 and 89-14 were acquired with a six-air gun array totaling 100 L and a 3600-m-long, 144-channel hydrophone array. Heat flow anomaly contours are at intervals of 0.2 W/m² in areas of relatively low heat flow and 2.0 W/m² where heat flow is higher. Major normal faults, with hachures on the downthrown side, shotpoint numbers, and Leg 139 drill sites (solid circles) also are shown (from Gröschel-Becker, 1996).

scale permeability of the sill and sediment sequence (Bessler et al., 1994).

Summary of Similarities and Differences Between Dead Dog and Bent Hill

Striking similarities exist between Sites 858 (Dead Dog) and 856 (Bent Hill). Lateral thermal, mineralogical, and chemical gradients are high. Thermal measurement in holes as close as 50 m away from discharge sites require only conductive heat transport, indicating that fluid flow is restricted to relative narrow zones (Davis and Fisher, 1994). Extremely sharp increases in thermal maturity of organic material at Sites 856 and 858 characterize past and present hydrothermal systems (Mao et al., 1994). A gradient of 10°C/m was determined by $\delta^{18}\text{O}$ studies of carbonates in sediment from the central part of the active zone (Baker et al., 1994). The dominant permeability control in the upflow zone is probably related to open fractures in the sediment. Only the hydrothermally altered sediment is likely to be sufficiently brittle to support open fractures. Both hydrofracturing and tectonic activity may be responsible for initiating cracking (Davis and Fisher, 1994).

A major difference between Dead Dog and Bent Hill is the end-member fluid temperature that was inferred from mineral assemblages and fluid inclusions, which have been as high as 400°C at Bent Hill. The current venting temperature (~275°C) is similar both at the DDVF and at the ODP Mound. These temperatures are close to those estimated in the reaction zone in the sill-sediment complex (280°C). Alteration mineralogy and fluid inclusions measured in rocks recovered from this zone also suggest temperatures ranging from 250° to 300°C (Peter et al., 1994). The persistence of uniform conditions with

time suggest that temperature in the reservoir is controlled by vigorous hydrothermal circulation. The alteration mineral assemblages at BHMS and DDVF are distinct and have clearly formed from fluids of different temperature and composition. The alteration assemblage at Bent Hill was produced by an Fe-rich and K-rich, high-temperature (300°–400°C), metal-rich fluid with low Ca concentration, whereas at Dead Dog, the fluid is the result of lower temperature reactions (270°–290°C). This, together with the absence of significant sulfide accumulation, indicates that the hydrothermal discharge at Dead Dog is not an exact analog of the fossil system at Site 856 (Davis and Fisher, 1994).

Drilling Strategy for Dead Dog Mound

Our strategy for investigating the formation of the hydrothermal mounds within the DDVF was to drill three, 50-m-deep holes separated by ~35 m each along a transect across the flank of one of the larger mounds, the Dead Dog Mound. The proposed transect includes drilling on the top, flank, and periphery of the mound, thus characterizing the sediment that occurs directly beneath and on the flanks of an active hydrothermal mound to test the seafloor inflation model for mound formation. The strategy included measuring pore-fluid and temperature gradients to evaluate the direction and magnitude of fluid flow in the shallow subsurface. A second objective of Leg 169 was to determine the presence, continuity, and nature of a suspected cap rock horizon underlying the vent field at ~30 mbsf. Drilling during Leg 139 suggested that such a layer may be controlling gradients in pore-fluid composition that appear to be maintained by lateral fluid flow at approximately this depth. The absence of such a layer, or permeable pathways through it, could also control the location of the in-

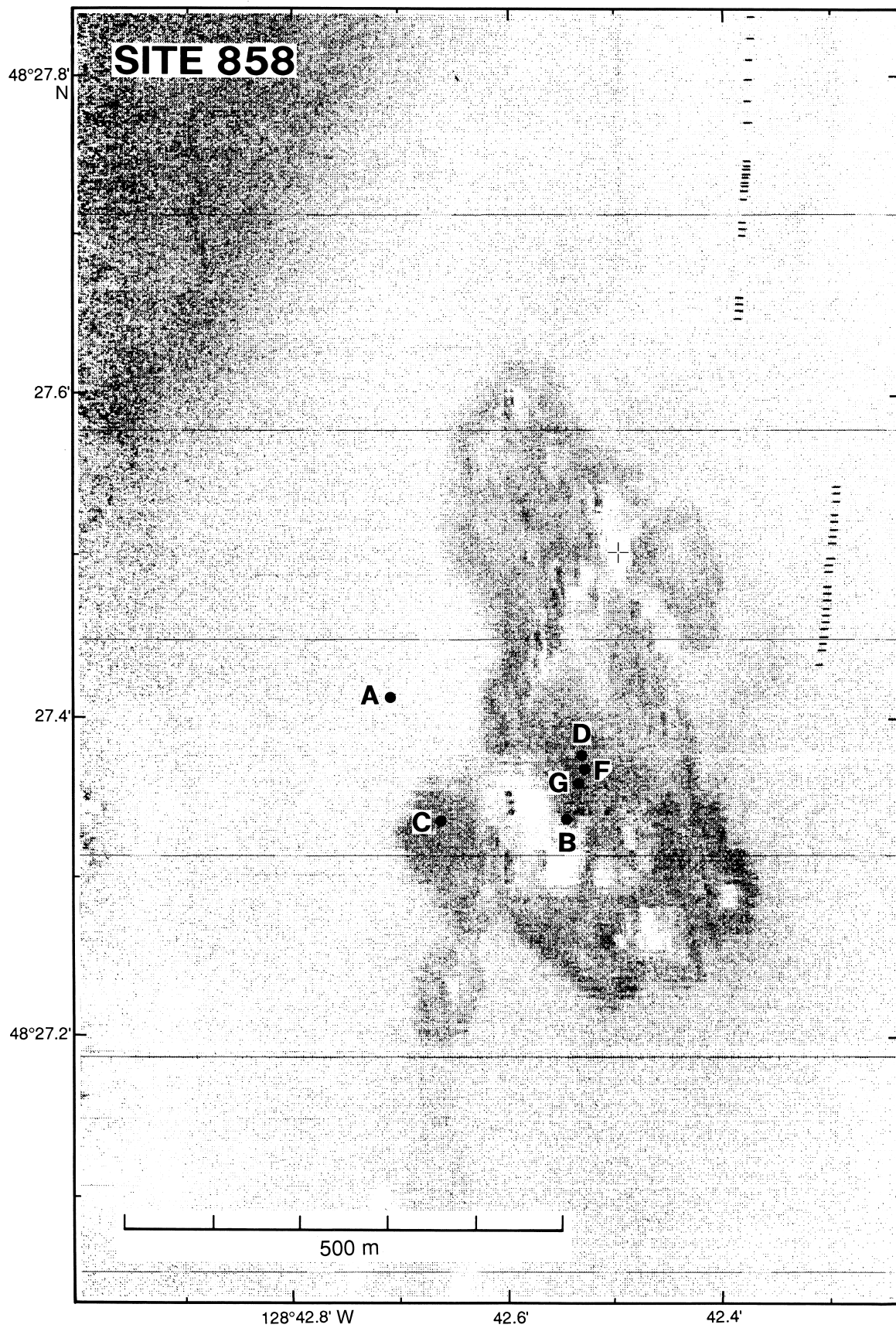


Figure 6. SeaMARC I (30 kHz) side-scan acoustic image mosaic of the Dead Dog Vent Field in the southeastern part of Middle Valley (Site 858; Shipboard Scientific Party, 1992b). Position of individual holes at Site 858 is shown.

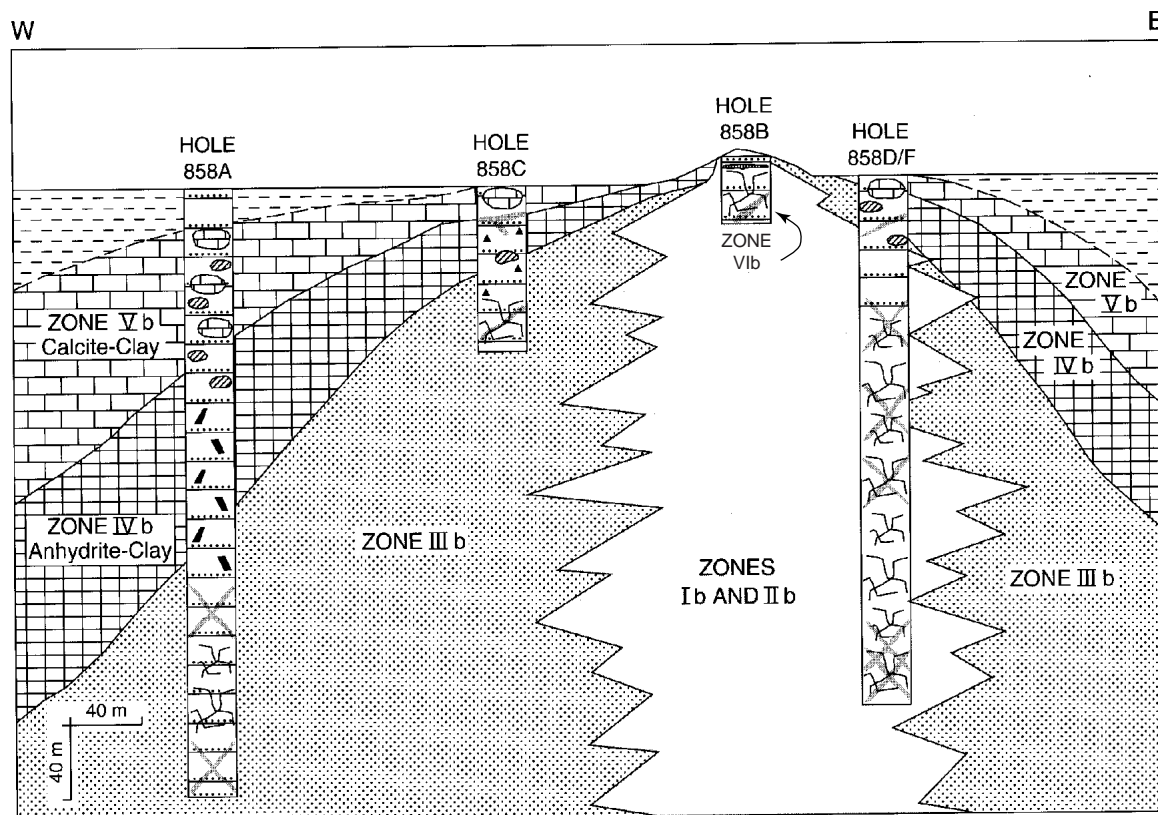


Figure 7. Geological cross section of the Dead Dog Vent Field showing the different hydrothermal alteration zones. Mineralogy of alteration zones is as follows: Zone Ib (quartz-wairakite-epidote-pyrite), Zone IIb (quartz-epidote-chlorite), Zone IIIb (albite-chlorite-illite-pyrite), Zone IVb (anhydrite-illite-pyrite), Zone Vb: (calcite-illite-pyrite), and Zone VIb (saponite-talc-pyrite). From Goodfellow and Peter (1994).

dividual vent sites. Authigenic cementation of the sediment by either carbonate or silica was thought to be the likely cause of this apparent hydrothermal cap rock. Hydrothermal cap rocks are an important component of near-surface fluid flow and the localization of ore deposition in ancient hydrothermal deposits, but it is difficult to unambiguously establish the time of formation or genetic importance of such features in ancient deposits. Recognition of this horizon (based primarily during Leg 139 drilling conditions and the rate of penetration) allowed us to target recovery of the rocks and to evaluate gradients in the pore-fluid composition at this potential barrier to hydrological flow.

OPERATIONS SUMMARY

Operations in the Dead Dog area included revisiting holes drilled during Leg 139, as well as completing a three-hole, southeast to northwest transect across the Dead Dog hydrothermal mound. During Leg 139, CORKs were installed in Holes 858G and 857D, and a summary of the Leg 169 replacement of these instruments can be found in the "Downhole Measurements" section (this chapter). For more details on operational parameters (drill string configurations, time expended on operations, drilling conditions, etc.), the reader is referred to the Operations Data Appendix on CD-ROM in the back pocket of this volume.

Hole 1036A

The first part of the coring operation at Dead Dog Mound consisted of a 2.25-hr Vibration-Isolated Television (VIT) survey to locate the top of the mound and to confirm that the site was free of visible

bottom-dwelling fauna. Hole 1036A (48°27.370'N, 128°42.585'W; water depth of 2407 meters below sea level [mbsl]) was spudded within 10 m of the active vent on top of the mound. APC Cores 169-1036A-1H through 4H were taken from 0 to 33.0 m (2452.0 meters below rig floor [mbrf]) with 103.8% recovery (see Table 1). XCB Cores 169-1036A-5X and 6X were taken from 33.0 to 38.5 m (2457.5 mbrf) with 10.0% recovery. We noted that the XCB shoe was excessively worn after recovering Core 169-1036A-6X in siltstone and silty claystone, and the hole was terminated.

Hole 1036B

The ship was moved ~37 m northwest in dynamic positioning (DP) mode to Hole 1036B (48°27.384'N, 128°42.607'W; water depth of 2414 mbsl). A 1.75-hr VIT survey found the edge of the Dead Dog Mound and confirmed that this site was also free of visible fauna. APC Cores 169-1036B-1H through 3H were taken from 0 to 27.7 m with 102.1% recovery (Table 1). XCB Cores 169-1036B-4X through 6X were taken from 27.7 to 52.3 m (2479.1 mbrf) with 75.0% recovery. We ended this hole when the target depth of 50 mbsf was reached.

Hole 1036C

The ship was again moved in DP mode ~40 m northwest to Hole 1036C (48°27.398'N, 128°42.631'W; water depth 2414 mbsl) just off the edge of Dead Dog Mound. APC Cores 169-1036C-1H through 4H were taken from 0 to 34.9 m with 101.2% recovery (Table 1). XCB Cores 169-1036C-5X and 6X were taken from 34.9 to 54.2 m (2479.3 mbrf) with 60.0% recovery. The XCB bit would not penetrate any further, and our drilling objective of 50 mbsf had been

Table 1. Coring summary, Dead Dog sites.

Core	Date (September 1996)	Time (UTC)	Depth (mbsf)	Length cored (m)	Length recovered (m)	Recovery (%)
169-857D-1M	07	1200	0.0–300.0	0		
Coring totals:						
169-858G-17W	04	0000	0.0–2.5			
18W	04	0000	0.0–2.5			
19W	04	1045	236.0–296.0	60.0	0.81	(wash core)
Coring totals:				0.0	0.00	
Washing totals:				60.0	.81	
Combined totals:				60.0	.81	
169-1036A-1H	16	0430	0.0–9.5	9.5	9.64	101.0
2H	16	0600	9.5–19.0	9.5	9.86	104.0
3H	16	0650	19.0–28.5	9.5	9.81	103.0
4H	16	0740	28.5–33.0	4.5	4.93	109.0
5X	16	1200	33.0–37.5	4.5	0.35	7.8
6X	16	1345	37.5–38.5	1.0	0.20	20.0
Coring totals:				38.5	34.79	90.4
169-1036B-1H	16	1700	0.0–8.7	8.7	8.69	99.9
2H	16	1825	8.7–18.2	9.5	9.93	104.0
3H	16	1910	18.2–27.7	9.5	9.65	101.0
4X	16	2110	27.7–37.3	9.6	8.90	92.7
5X	16	2220	37.3–45.2	7.9	7.48	94.7
6X	17	0050	45.2–52.3	7.1	2.07	29.1
Coring totals:				52.3	46.72	89.3
169-1036C-1H	17	0400	0.0–6.4	6.4	6.35	99.2
2H	17	0450	6.4–15.9	9.5	9.30	97.9
3H	17	0340	15.9–25.4	9.5	9.64	101.0
4H	17	0830	25.4–34.9	9.5	10.01	105.3
5X	17	1115	34.9–44.6	9.7	7.15	73.7
6X	17	1230	44.6–54.2	9.6	4.42	46.0
Coring totals:				54.2	46.87	86.5

Note: An expanded version of this coring summary table that includes lengths and depths of sections, location of whole-round samples, and comments on sampling disturbance is included on CD-ROM in the back pocket of this volume.

reached, so we pulled the pipe for the transit back to the Bent Hill area. The two PUPPIs deployed on 29 August were recovered, and operations at Dead Dog Mound for Leg 169 were completed.

LITHOSTRATIGRAPHY

Site 1036 is located in the Area of Active Venting (AAV) also known as the DDVF. The area occupied by the DDVF is defined by side-scan acoustic imaging (Figs. 1, 3). This region was previously

cored during Leg 139, and included Holes 858A through 858G. The AAV was revisited on the present leg with four primary objectives to (1) deduce the nature of fluid flow in the uppermost portion of the sediment column, (2) determine the effects of hydrothermal activity on the alteration of sediments in shallow upflow and recharge zones, (3) understand the mode of formation of one of the hydrothermal mounds and testing the subseafloor inflation model, and (4) determine the presence, continuity, and nature of a suspected cap rock horizon thought to exist at ~30 mbsf. To meet these objectives, three hydraulic piston core holes were sited along a northwest-southeast transect from the top, to the margin, to slightly away from the margin of the 7-m-high Dead Dog Mound.

Hole 1036A was located ~9 m west of an active vent that was discharging water at temperatures of 268°C when last measured (Butterfield et al., 1994). This hole was cored to a depth of 38.50 mbsf. Hole 1036B was offset ~37 m to the northwest of Hole 1036A and cored to a depth of 47.30 mbsf. Hole 1036C was offset another 40 m to the northwest of Hole 1036B and cored to a depth of 54.20 mbsf. Core recovery is shown in the coring summary at the beginning of this chapter.

Lithologic Units

Three lithologic units are recognized in the three holes. Following the nomenclature used for Site 1035, Units I (hemipelagic sediments with minor turbidites), II (interbedded turbidites and hemipelagic sediments), and IV (collapsed chimney-derived sediments) are present at Site 1036 (Table 2; Fig. 8; note that Unit III is not present at this site). Units I and II are differentiated (somewhat arbitrarily) by the presence of significant thicknesses of strata composed of silt or sand within Unit II. Units I and II are subdivided on the basis of the relative abundance of alteration minerals, specifically carbonates and anhydrite. Unit IV, as described below, is easily differentiated on the basis of its mineralogical composition and texture. Unit I overlies Unit II. Unit IV, present only in Hole 1036A, overlies Unit I.

Unit I

Lithologic Unit I is a gray (5Y 5/1), greenish gray (5GY 5/1), or dark greenish gray (5GY 4/1) silty clay. The transition to underlying Unit II was chosen at the first downcore appearance of fine sandy lamina. There is little variation in thickness of Unit I between holes (25.14 m at Hole 1036A, 25.60 m at Hole 1036B, and 26.70 m at Hole 1036C). The age of this unit is Holocene to late Pleistocene. In Hole 1036C, strata interpreted to be deposited during oxygen isotopic Stage 5 (the last interglacial stage; 125 ka) were tentatively identified in Section 169-1036C-3H-CC at 25.29 mbsf (see “Biostratigraphy” section, this chapter). The age of Unit I, therefore, is tentatively con-

Table 2. Lithologic units and subunits, Site 1036.

Unit	Subunit	Description	Interval	Top (mbsf)	Bottom (mbsf)	Thickness (m)
I	IA	Hemipelagic sediments with minor turbidites	1036A-1H-5, 10 cm, to 1H-7, 20 cm	6.10	9.20	3.10
		Unaltered, hemipelagic sediments with minor fine-grained turbidites	1036B-1H-1, 0 cm, to 1H-6, 70 cm	0.00	8.20	8.20
	IB	Silty clay with carbonate concretions and cements in abundance	1036C-1H-1, 0 cm, to 2H-4, 80 cm	0.00	11.70	11.70
IC	IC	Altered silty clay with anhydrite concretions and authigenic crystals	1036A-1H-7, 20 cm, to 1H-CC, 20 cm	9.20	10.04	0.84
			1036B-1H-6, 70 cm, to 3H-1, 35 cm	8.20	18.55	10.35
			1036C-2H-4, 80 cm, to 4H-1, 130 cm	11.70	26.70	15.00
II	IIB	Moderately altered muds, silts, and sands with carbonate concretions and cements	1036A-2H-1, 0 cm, to 4H-2, 70 cm	9.50	30.70	21.20
			1036B-3H-1, 35 cm, to 3H-5, 140 cm	18.55	25.60	7.05
			1036C-4H-1, 130 cm, to 5X-CC, 25 cm	26.70	42.20	15.50
IIC	IIC	Altered muds, silts, and sands with anhydrite concretions and authigenic crystals	1036A-4H-3, 0 cm, to 6X-CC, 20 cm	30.70	37.70	7.00
			1036B-3H-5, 140 cm, to 6X-CC, 36 cm	25.60	47.27	21.67
			1036C-5X-CC, 25 cm, to 6X-CC, 36 cm	42.20	49.02	6.82
IV		Collapsed chimney-derived sediments	1036A-1H-1, 0 cm, to 1H-5, 10 cm	0.00	6.10	6.10

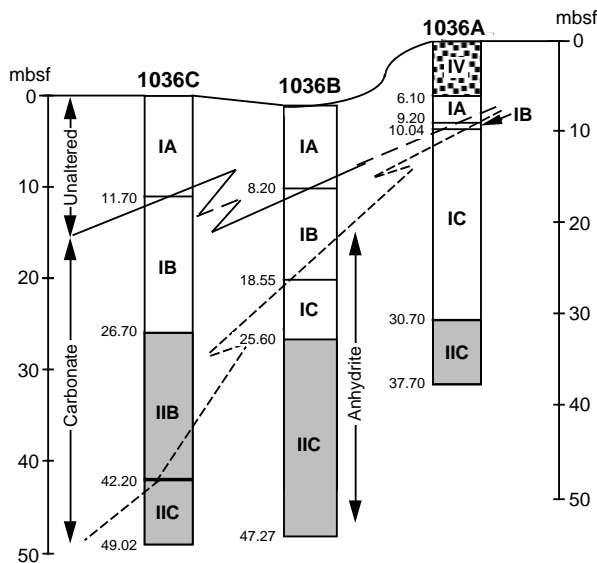


Figure 8. Hole-to-hole correlation of lithologic units and subunits at Site 1036. Also shown is bottom bathymetric relief. The carbonate and anhydrite depths of first appearances in each hole are connected by solid/dashed and dashed lines, respectively. Sub-bottom depths of unit and boundaries are shown to the left of each hole. Plain area = Unit I, shaded area = Unit II, and stippled area = Unit IV.

sidered to range from 0 to 125 ka. The first downcore appearance of significant fine sand turbidites predated Stage 5 and may coincide with the penultimate deglaciation.

Although trace fossils are not particularly well represented in the sediments at Site 1036, a distinctive *Zoophycus* horizon is present in interval 169-1036B-1H-5, 10–20 cm (Fig. 9). This horizon was described previously in Middle Valley by Davis, Mottl, and Fisher, et al. (1992) and by Goodfellow et al. (1993). The “*Zoophycus* marker horizon” (Davis, Mottl, and Fisher, et al., 1992) is usually ~40 cm thick and has a distinctive reddish gray color (5R 5/1). The top of the horizon was encountered at 6.49 mbsf in Hole 139-857A, 5.33 mbsf in Hole 139-858C, 6.70 mbsf in Hole 139-858D, and 6.07 mbsf in Hole 169-1036B. In previous studies, the age of the horizon was bracketed by ^{14}C dates between 13,900 and 21,000 BP (Goodfellow et al., 1993; i.e., latest Pleistocene).

Lithologic Unit I is interpreted to be largely a hemipelagic sequence. On the basis of earlier work (Goodfellow et al., 1993; Brunner, 1994), the Holocene portion of this sequence is known to have accumulated at rates of ~6 cm/k.y. This is substantially slower than the sedimentation rates of ~20 cm/k.y. for the lower portion of Unit I between Stage 5 (the last interglacial) and the Holocene/Pleistocene boundary.

Lithologic Unit I has been subdivided into three subunits on the basis of hydrothermal/diagenetic alteration. Subunit IA (unaltered, hemipelagic sediments with minor fine-grained turbidites) lacks distinctive hydrothermal or diagenetic products. Subunit IB (silty clay with carbonate concretions and cements in abundance) contains authigenic carbonate nodules and cements, and Subunit IC (altered silty clay with anhydrite concretions and authigenic crystals) contains authigenic anhydrite and little or no carbonate.

Subunit IA (Unaltered Hemipelagic Sediments with Minor Fine-Grained Turbidites: Holocene to Late Pleistocene, <125 ka)

Subunit IA consists of slightly altered, hemipelagic silty clay with several thin (0.1–10 cm thick) laminae and beds of silt. These silty units are composed of quartz, feldspar, mica, clay, and chlorite with trace amounts of calcite, hornblende, pyroxene, epidote, and pyrite.

In cores from Holes 1036B and 1036C, a 3- to 5-cm-thick, dark reddish brown (5YR 3/4) silty clay marks the oxidized top of this unit

and indicates at least partial recovery of the mudline. In Hole 1036A, chimney rubble (Unit IV) has buried the top of Subunit IA. The upper 55 cm of the chimney rubble is oxidized to a brown color (10YR 5/3). However, no oxidized layer exists at the top of Unit I in this hole (1036A-1H-5, 10 cm; 6.10 mbsf).

Subunit IB (Carbonate-Altered Hemipelagic Sediments with Minor Fine-Grained Turbidites: Late Pleistocene, <125 ka)

Subunit IB consists of slightly altered silty clay with thin beds and laminae of silt, the same protolith as Subunit IA. The major distinction between the two subunits is the presence of diagenetic carbonate in Subunit IB. Because much of this carbonate is known (on the basis of strontium, carbon, and oxygen isotopic composition) to be of hydrothermal origin (Baker et al., 1994) and because carbonate nodules are common in this part of Middle Valley only in sediments near modern or ancient vent systems, this subunit is considered to be a useful alteration facies indicative of moderate hydrothermal activity (Goodfellow et al., 1994).

Subunit IB contains both biogenic and diagenetic carbonate. Biogenic calcite is dominantly comprised of foraminifers with lesser quantities of nanofossil calcite. Within silt layers there are also rare bioclasts of undetermined (and possibly neritic) origin. Hole 1036A contains just a few dolomite nodules, apparently filling burrows. In Hole 1036B, numerous dolomite and calcite nodules are found in the interval from Section 169-1036B-2H-2 (10.20 mbsf) through 4X-3 (32.20 mbsf). Disseminated micrometer-sized dolomite rhombohedrons were found in Section 169-1036B-2H-3 (11.70–13.20 mbsf), and a bed of nearly pure, but uncemented, authigenic dolomicrite was found in interval 169-1036B-2H-4, 40–55 cm. A very distinctive sequence of calcite nodules with rough, pitted exterior surfaces and containing euhedral pyrite was found in interval 169-1036B-2H-5, 70–130 cm (15.40–16.00 mbsf; Fig. 10). The same sequence is found in interval 169-1036C-2H-6, 0–40 cm (13.90–14.30 mbsf). The pitted nature of these calcite nodules suggests that they may be a product of dedolomitization, or that they have been partially dissolved by circulating fluids. Underlying this zone of pitted nodules in both holes are distinctive large (~6–7 cm diameter) nodules of calcite (now brecciated) that contain a network of fine, white calcite veinlets (16.60 mbsf in Hole 1036B and 14.65 mbsf in Hole 1036C).

Core-catcher samples prepared for paleontological analysis were devoid of foraminifers below Section 169-1036A-1H-CC, 0 cm (9.49 mbsf), below Section 1036B-3H-CC, 0 cm (18.61 mbsf), and below Section 169-1036C-4H-CC, 0 cm (35.04 mbsf). Siliceous microfossils disappear at even shallower burial depths in all holes. Small, nearly pure patches of well-preserved sponge spicules are present in Sections 169-1036C-2H-1, 2H-2, 2H-CC, and 3H-2. In interval 169-1036C-2H-CC, 2–4 cm, a light brownish gray (2.5Y 6/2) calcimicrite nodule encloses a large number of well-preserved fossil diatoms and radiolarians.

Subunit IC (Anhydrite-Bearing Hemipelagic Sediments with Fine-Grained Turbidites: Late Pleistocene, <125 ka)

Subunit IC is developed in the same protolith as Subunit IA and is differentiated because it is a distinctive alteration facies of the hydrothermal system (Goodfellow et al., 1994). Subunit IC (and Subunit IIC, discussed below) is characterized by authigenic anhydrite that occurs as finely disseminated fine crystals, commonly associated with pyrite (Fig. 11). Anhydrite also forms nodules, clusters of crystals, and cements. Anhydrite contents in Hole 1036A are estimated at 40% in interval 169-1036A-2H-3, 90–150 cm; 30% in interval 2H-4, 0–44 cm; up to 30% in interval 2H-6, 25–31 cm, 68–74 cm, and 114–115 cm; 20% in interval 3H-1, 0–150 cm; and 20% in interval 3H-7, 0–46 cm. In Section 169-1036C-6X-1, anhydrite contents may be as high as 10% to 20%. Elsewhere in Hole 1036A, as well as in Holes 1036B and 1036C, anhydrite contents vary from 0% to 5%. This authigenic anhydrite may have formed at a mixing front between hot, calcium-rich hydrothermal fluids and cold, sulfate-bearing seawater or by the conductive heating of seawater. Experimental studies con-

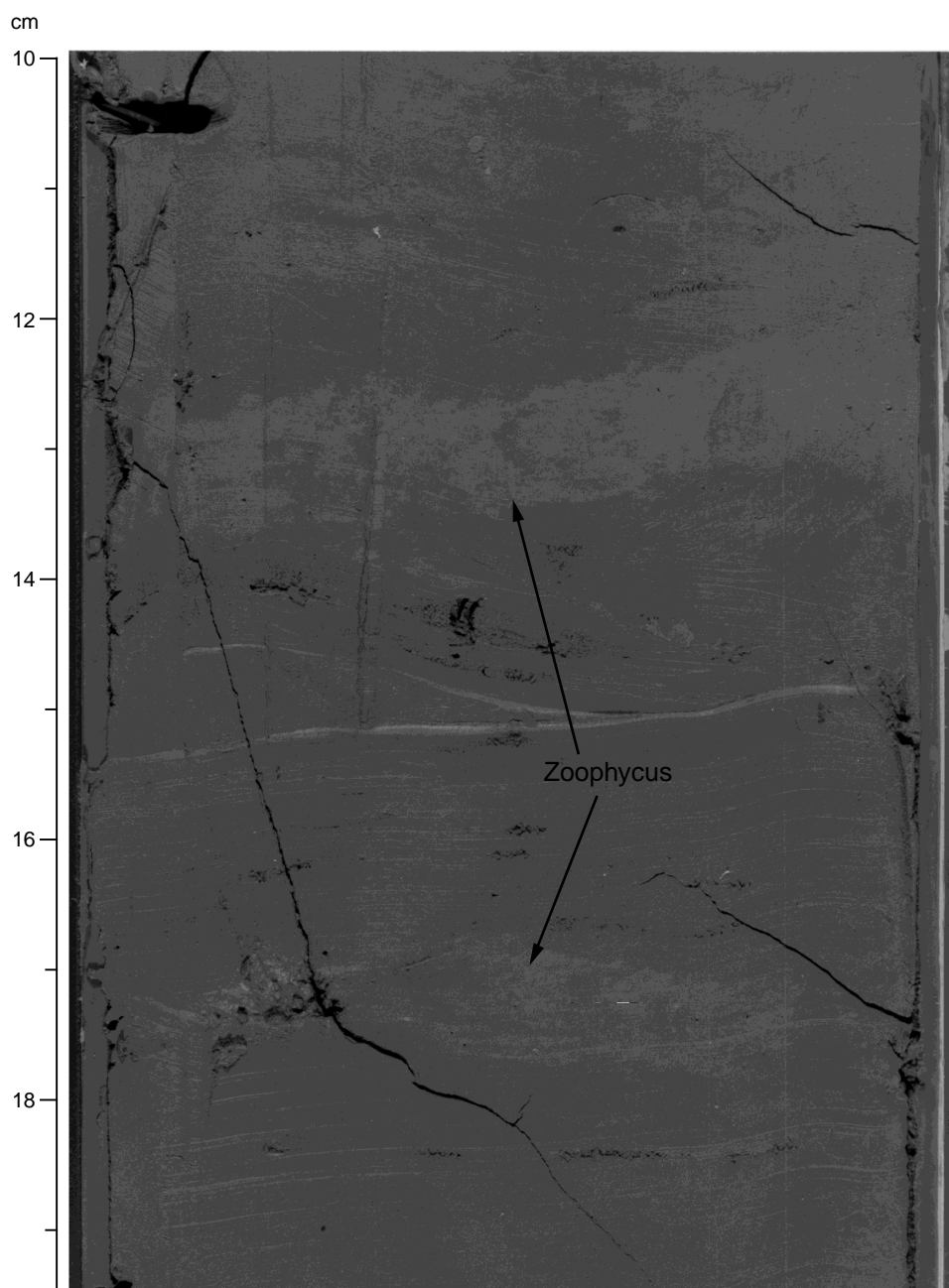


Figure 9. *Zoophycus* marker horizon in Subunit IA (interval 169-1036B-1H-5, 10–19.5 cm).

strain the temperature of anhydrite precipitation from seawater to 100°–150°C (Bischoff and Seyfried, 1978; Seyfried and Bischoff, 1979). The depth of the first appearance of anhydrite in these holes is equivalent to a crude isotherm. This boundary was found at 9.50 mbsf in Hole 1036A and at 18.55 mbsf in Hole 1036B. The first appearance of anhydrite in Hole 1036C (Subunit IIB) is at 42.20 mbsf (see Fig. 8). Below the depth of the first appearance of anhydrite, carbonate cements, grains, and nodules are rare, most likely because they are dissolved under conditions that lead to anhydrite formation. Carbon-nitrogen-sulfur (CNS) data (see “Inorganic Geochemistry” section, this chapter) confirm the lower inorganic carbon concentrations in this subunit.

An interesting and unique indurated mud-clast breccia within anhydrite-cemented claystone (Fig. 12) occurs in interval 169-1036A-3H-2, 81–88 cm. It has the form of a nodule, and one hypothesis for

its origin is formation by the decarbonation of a calcite or dolomite nodule followed by brecciation caused by solution collapse. Alternatively, this breccia may have formed from partially indurated muddy sediments slumping off of a nearby mound or fault scarp.

Pyrite is present throughout all three cores, generally in trace (<2%) amounts. Intervals containing higher pyrite contents include all of Unit IV in Hole 1036A and the previously mentioned sequence of pyrite-rich sediments interbedded with calcite nodules. Authigenic, magnetic, hexagonal-shaped grains of euhedral pyrrhotite (1–3 mm) also are found. The presence of this pyrrhotite in intervals 169-1036B-3H-6, 30–50 cm, and 80–100 cm, and in Sections 169-1036B-4X-2 through 4, is reflected by local high values of magnetic susceptibility in a zone where magnetic susceptibility is generally low, presumably because of the hydrothermal alteration of detrital magnetic phases (see “Physical Properties” section, this chapter).

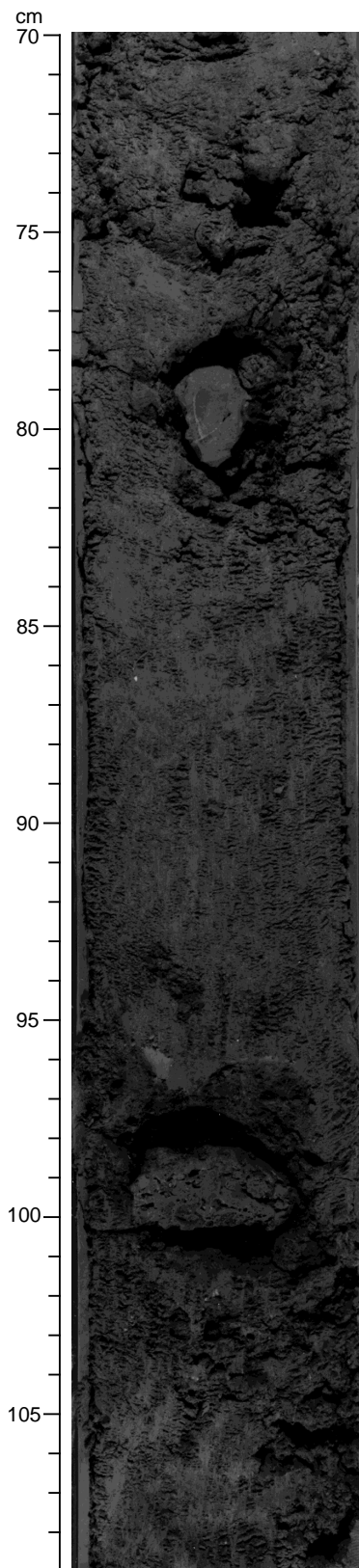


Figure 10. Pitted carbonate nodules in Subunit IIB (interval 169-1036B-2H-5, 70–109 cm).

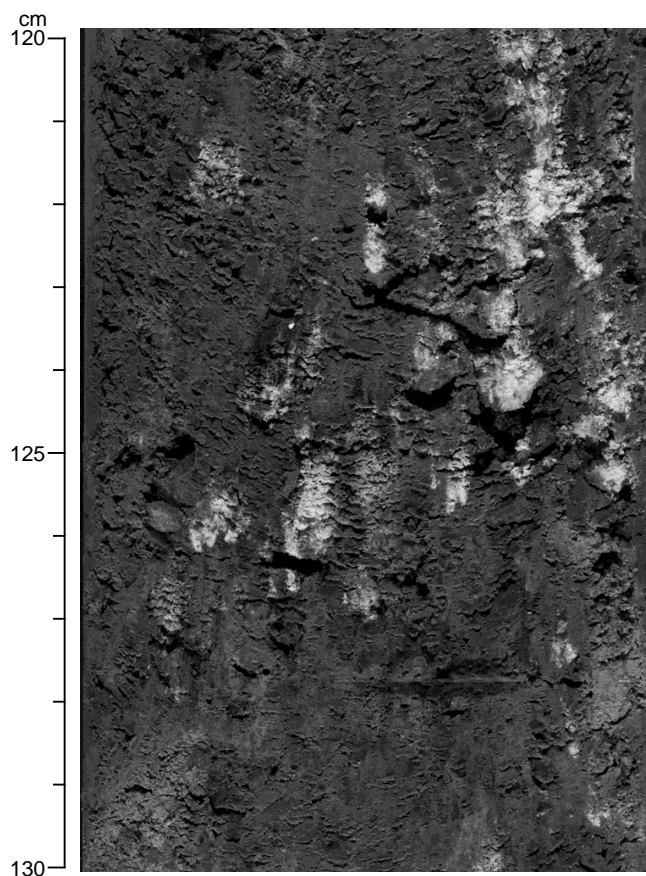


Figure 11. Anhydrite finely disseminated with pyrite in Subunit IIC (interval 169-1036A-3H-2, 120–130 cm).

Unit II

Unit II is characterized by hemipelagic silty clays interbedded with silt to fine sand turbidites. This unit is generally correlative throughout Middle Valley. Where least altered and best recognized (e.g., Core 169-1036C-4H, 25.40–35.41 mbsf), the hemipelagic portion of the unit is composed of nonindurated greenish gray (5GY 5/1) to dark greenish gray (5GY 4/1) to gray (N 5) silty clay. It contains variable quantities of fine-grained diagenetic framboidal pyrite. These hemipelagic sediments are intercalated with laminae and beds, up to 10 cm thick, of dark greenish gray (5GY 4/1) to dark gray (N4) silt and very fine to fine sand. The sand beds commonly have scoured basal contacts, parallel laminations, and fining-upward textures. Deeper in the section, sands are more common, and cross-laminae are present in a few intervals.

Unit II has been subdivided at Site 1036 into Subunits IIB (moderately altered muds, silts, and sands with carbonate concretions and cements) and IIC (altered muds, sands, and silts with anhydrite concretions and authigenic crystals). Subunit IIA (i.e., unaltered, interbedded hemipelagic and turbiditic sediments) is not present in Site 1036 cores. Subunit IIB contains authigenic carbonate cements and nodules, but no anhydrite. Subunit IIC contains authigenic anhydrite as disseminated crystals, nodules, or cements.

Subunit IIB (Carbonate-Altered Turbidites and Hemipelagites: Late Pleistocene, >125 ka)

Characteristic of this subunit is the occurrence of diagenetic carbonates within interbedded hemipelagic and turbiditic sediments. In other regards, the protolith is as previously described (Subunit IIA at

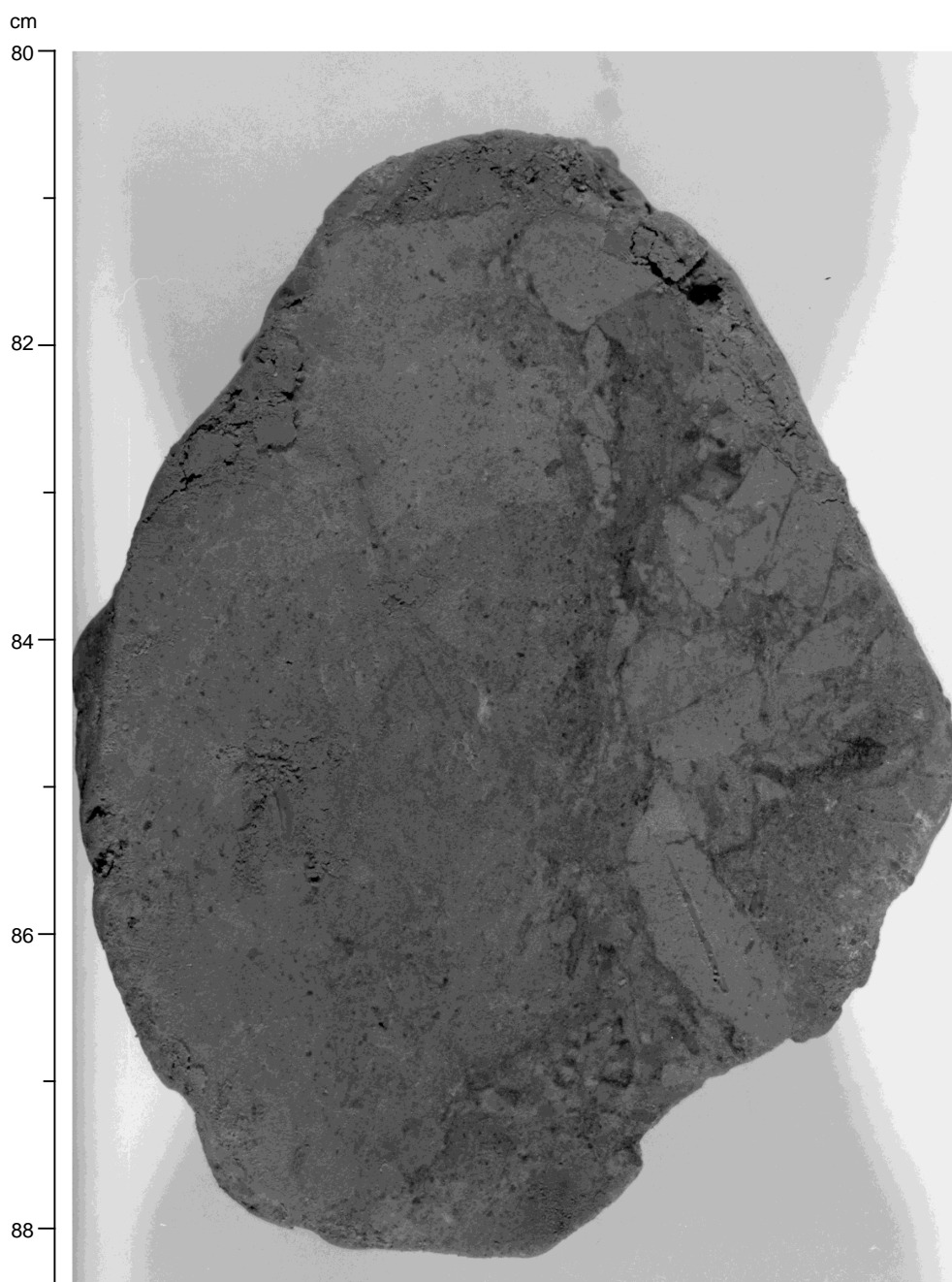


Figure 12. Mud-clast breccia from Subunit IC (interval 169-1036A-3H-2, 80–88.5 cm).

Site 1035). In carbonate-cemented intervals of Subunit IIB, cements occur selectively in the coarsest sediments at the base of turbidites (e.g., Sections 169-1036C-4H-2, 5X-1, 5X-2, and 5X-4).

Subunit IIC (Altered, Anhydrite-Bearing Turbidites and Hemipelagites: Late Pleistocene, >125 ka)

This subunit is distinguished by the presence of anhydrite cements and nodules in turbiditic and hemipelagic sediments that were originally similar to the unaltered protolith described above. The boundary between Subunit IIB and IIC (as for the IB/IC boundary) is characterized by the first downcore appearance of nonvein anhydrite. Carbonate grains and nodules disappear completely a few meters below this boundary. For example, Section 169-1036C-5X-4 (39.40–

40.90 mbsf) contains abundant calcite cement, Section 169-1036C-5X-5 (40.90–41.95 mbsf) contains neither calcite nor anhydrite, and Section 169-1036C-5X-CC (41.95–42.33 mbsf) contains anhydrite, but no calcite.

Unit IV

Unit IV, which consists of collapsed, chimney-derived, Holocene sediments, is a 6.10-m section which accounts for most of the 7-m bathymetric relief of the Dead Dog Mound. Unit IV (Fig. 13) is composed predominantly of three end-members: (1) white talc; (2) mostly monomineralic, very fine-grained pyrrhotite with subordinate quantities of pyrite and, possibly, sphalerite; and (3) greenish gray

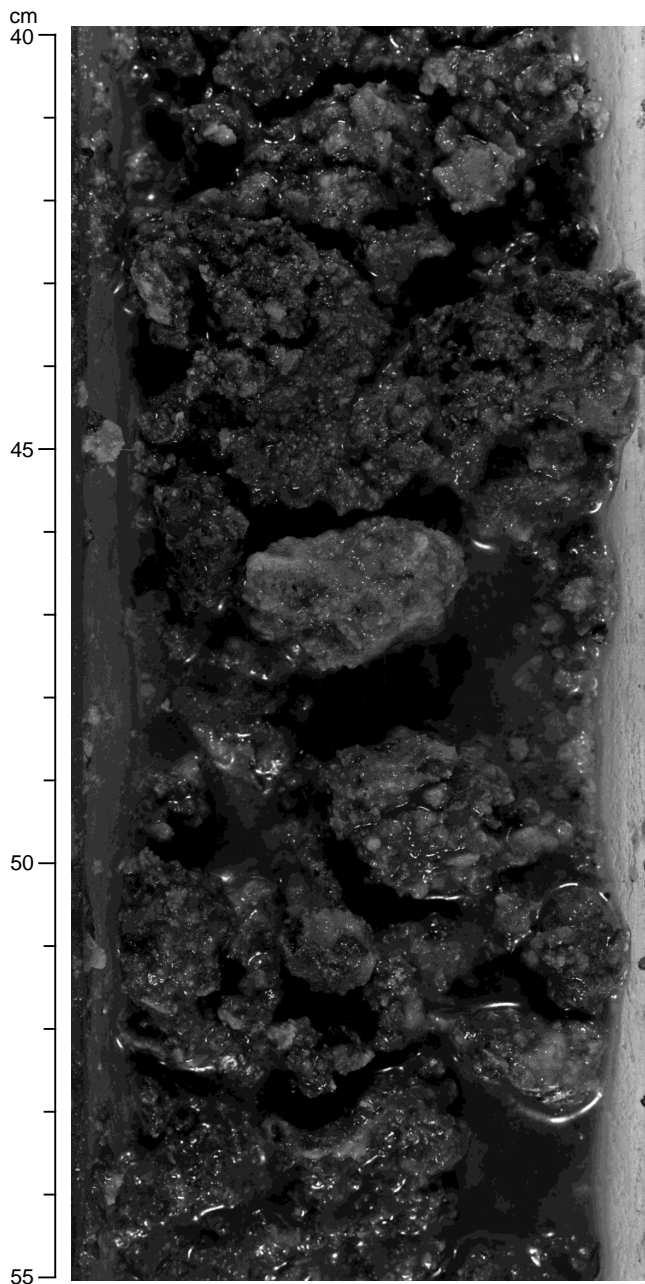


Figure 13. Unit IV collapsed chimney-derived sediments (interval 169-1036A-1H-1, 40–55 cm).

clay, probably an Mg-bearing smectite. There is no anhydrite or gypsum present in the X-ray diffraction samples that have been analyzed (Fig. 14; Table 3). Sand- to pebble-sized (up to 4 cm) sulfide and talc clasts and smectite are mixed in variable quantities downcore. About 30% of the clasts are greater than sand size. The upper 55 cm of this unit is a yellowish brown (10YR 5/3) color, indicating oxidation during exposure of this unit at the seafloor. Below this uppermost sequence, the overall color of Unit IV sediments is greenish gray (5GY 5/1), to dark greenish gray (5GY 4/1), to white (5YR 8/1), depending on the relative quantities of clay, sulfide, and talc. The lowermost 1.6 m of the sequence has a darker color, probably the result of a greater concentration of clay and sulfide.

Hole 1036A was drilled 9 m away from an active anhydrite chimney surrounded by an apron of anhydrite formed from collapsed chimneys. Unit IV is interpreted to be an accumulation of chimney

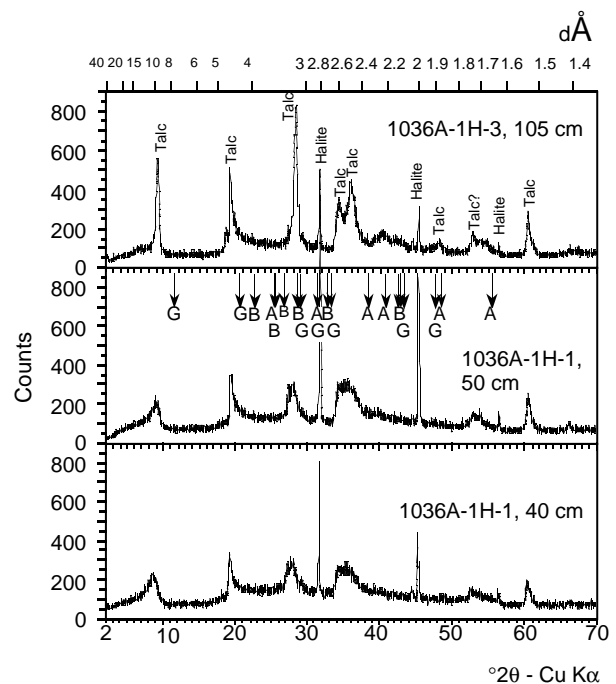


Figure 14. X-ray diffractograms of white minerals collected from the clastic chimney rubble (Unit IV) at the top of Hole 1036A. No common sulfate minerals are present. A = anhydrite, B = barite, and G = gypsum. Talc and halite are the only crystalline phases identified.

debris from which all of the anhydrite has been removed by seafloor dissolution. The angularity and size of the clasts, as well as the relief of the mound, suggest that these clasts are derived from the collapse of chimneys formed at vents on Dead Dog Mound. Unit IV is underlain by an unaltered, homogenous, silty clay that appears to be of hemipelagic origin. This sediment is assigned to Subunit IA.

Conclusions

To the limits of our resolution, the turbiditic and hemipelagic sedimentary sequences (Subunits IA and IIA) are flat-lying deposits and have not been significantly displaced since deposition (see Fig. 8). Furthermore, Unit I, consisting only of fine-grained hemipelagic sediments, ranges in age from Stage 5 (125 ka) to the present. There was little coarse-grained sediment deposited in this region during the last glacial stage, possibly a result of the tectonic isolation of Middle Valley from its sediment source. Second, the bathymetric relief of the Dead Dog Mound is close to the stratigraphic thickness of chimney rubble, hence the mound is a buildup of rubble, and its relief is not caused by authigenic hydrothermal mineral precipitation or tectonic uplift. The Dead Dog Mound is presumably a young feature as the thickness of Unit I is the same under the mound as away from the mound (although, again, our resolution is limited). Dating of the mound and immediately underlying sediments is required to refine this conclusion. Third, the upper boundaries of the carbonate and anhydrite alteration subunits deepen away from Dead Dog Mound, reflecting the decreasing geothermal gradients away from the mound. The first appearance of anhydrite is calculated to occur at $\sim 120^{\circ}\text{C}$, based upon equilibrium calculations using measured Ca and SO_4 concentrations in pore water (see “Inorganic Geochemistry” section, this chapter). Using this isotherm and the depths of anhydrite first occurrence, it is calculated that thermal gradients decrease from $\sim 12^{\circ}\text{C}/\text{m}$ to $6^{\circ}\text{C}/\text{m}$ to $3^{\circ}\text{C}/\text{m}$ from Hole 1036A to Hole 1036B to Hole 1036C, respectively (the measured temperature at 34.9 mbsf in Hole 1036C was 122.3°C , resulting in a slightly higher gradient than calculated). No evidence of the purported cap rock at ~ 30 mbsf (see “Dead Dog

Table 3. X-ray diffraction identifications of minerals, Site 1036.

Core, section, interval (cm)	Description	XRD mineralogy
169-1036A-		
1H-1, 40–40	Clastic sulfate (?)	(Halite), talc
1H-1, 50–50	Clastic sulfate (?)	(Halite), talc
1H-3, 105–105	Clastic sulfate (?)	(Halite), talc
3H-4, 71–71	Anhydrite	Anhydrite >> quartz > pyrite
3H-4, 124–126	Gypsum layer (?)	Quartz, minor chlorite/white mica
2H-4, 140–150	IW sample - sediment	Quartz, anhydrite, plagioclase, pyrite, chlorite, white mica
3H-4, 140–140	IW sample - sediment	Quartz, smectite > chlorite-mixed layer, with mica, minor anhydrite
4H-CC, 16–26	IW sample - sediment	Quartz, anhydrite, chlorite, pyrite, white mica, magnetite (?)

Hydrothermal Field” section, this chapter) was recovered during Leg 169 drilling.

BIOSTRATIGRAPHY

In general, foraminifer preservation at Site 1036 is poor in surficial sediment and at depth (see Table 4 on the back-pocket foldout, this volume), and carbonate microfossils are abundant and moderately preserved only in the near surface sediments. The core tops from Holes 1036A through 1036C are nearly barren of calcareous foraminifers and contain decreasing amounts of anhydrite relative to noncarbonate hemipelagic material between Holes 1036A and 1036C. Hole 1036A contains >6 m of sediment derived from anhydrite shed from adjacent chimneys. Hole 1036B contains a 5-cm-thick surface layer dominated by residue left after dissolution of anhydrite (see “Lithostratigraphy” section, this chapter) derived from broken hydrothermal chimneys along with abundant radiolarians and diatoms, few agglutinated benthic foraminifers, and very rare planktonic foraminifers. Hole 1036C contains a few centimeters of iron-stained anhydrite with siliceous microfossils and agglutinated foraminifers in a reddish brown oxidized sediment (also reported by Brunner, 1994, and Quintero, 1994). Beneath this unit, an assemblage of carbonate benthic and planktonic foraminifers is found in olive-gray distal turbidites interlayered with hemipelagic units. Planktonic foraminifers are abundant to common to 9.94, 18.61, and ~26 mbsf at Holes 1036A, 1036B, and 1036C, respectively. The depths where foraminifers completely disappear are just above the shallowest occurrences of weakly indurated sediments and authigenic anhydrite at all three holes.

Assemblage zones from both the Holocene and isotopic Stage 5e were observed at Site 1036. The base of the Holocene dextral coiling event in *Neogloboquadrina pachyderma* lies between 6.09 and 7.5 mbsf in Hole 1036A, 0.42; 1.48 mbsf in Hole 1036B; and 0.75 and 1.25 mbsf in Hole 1036C. This result is consistent with other reports of the boundary at Middle Valley (Fig. 15). The dextral coiling event of the penultimate interglacial period at ~125 ka occurs at 25.29 mbsf (+0.39, -9.75 m) in Hole 1036C (Fig. 16). Regional sedimentation rates to the 125 ka horizon range from 17 to 33 cm/k.y., which is surprisingly slow considering the young age of the basement and the thickness of sediment cored.

STRUCTURAL GEOLOGY

The structure of the Dead Dog Mound was studied with a northwest-southeast transect of three ~50 m-deep holes across the mound. A 6.10-m-thick unit of sulfide, sulfate, and clay clasts drilled only in Hole 1036A is underlain by hemipelagic and turbiditic sediments (see “Lithostratigraphy” section, this chapter). Although Hole 1036A is located ~9 m to the west of an active vent discharging hydrothermal fluids at temperatures between 261° and 268°C (Butterfield et al., 1994), no major hydrothermal vein network was intercepted. In addition, most sediments are still very soft (“Physical Properties”

section, this chapter), indicating that they have not been lithified by high-temperature fluids.

The only hydrothermal structures encountered in the core consist of a hydraulic breccia (interval 169-1036A-3H-2, 82–89 cm) and a few anhydrite veinlets. The hydraulic breccia consists of indurated, angular clasts up to 1 cm wide embedded in a black, fine-grained, less indurated clay (chlorite-smectite?) matrix. This piece is within a core of slightly indurated clays, which suggests that the breccia may be a clastic vein. The anhydrite veins are 1 to 2 mm thick, appear only in Section 169-1036A-4H-3 (Table 5; seven veins in 80 cm of core), and have a preferred subhorizontal orientation. Holes 1036B and 1036C showed no hydrothermal or tectonic features.

None of the holes penetrated a stockwork underlying the hydrothermal mound. This and evidence from Site 858 suggest that the Dead Dog Mound is a young and immature feature, consistent with the occurrence of collapsed chimney material overlying very young sediments (see “Lithostratigraphy” section, this chapter).

INORGANIC GEOCHEMISTRY

The chemical composition of fluid samples from Hole 858G, and pore-water samples from Site 1036, which are both located in the area of the DDVF, have been determined. Seven holes (Holes 858A through 858F) were drilled previously in this area during Leg 139.

Hole 858G was cased to basaltic basement and instrumented with a CORK and thermistor string during Leg 139 (Shipboard Scientific Party, 1992b). This hole is located ~30 m north of the 276°C Chowder Hill vent (Ames et al., 1993). Sampling of the fluid contained in this case hole was a key objective of Leg 169, to determine whether the hole contained formation fluid derived from the basement. Submersible observations of the hole showed that hydrothermal fluid was venting from the bottom of the reentry cone and flowing past the CORK data logger (Davis and Becker, 1994). The seals on the CORK failed, presumably because of high temperatures, 17 months after deployment (see “Downhole Measurements” section, this chapter).

A further objective of Leg 169 was to determine the fluid-flow regime in an active hydrothermal area. For this purpose, three short holes (Holes 1036A, 1036B, and 1036C) were drilled along a transect across the Dead Dog Mound. Samples of interstitial water were obtained from these holes, complementing data obtained previously from Holes 858A through 858F.

In this section, we first discuss the composition of fluids contained in Hole 858G and proceed to discuss the composition of pore fluids from Site 1036 and their implications for fluid flow in the DDVF. Details of the sampling procedures are given in the relevant site discussions; chemical analysis of the fluid samples was conducted following Gieskes et al. (1991).

Hole 858G

Three separate fluid samples were collected from Hole 858G after removal of the CORK. One sample (1M-01) was collected using the WSTP sampling tool at ~20 mbsf; the temperature at this depth ex-

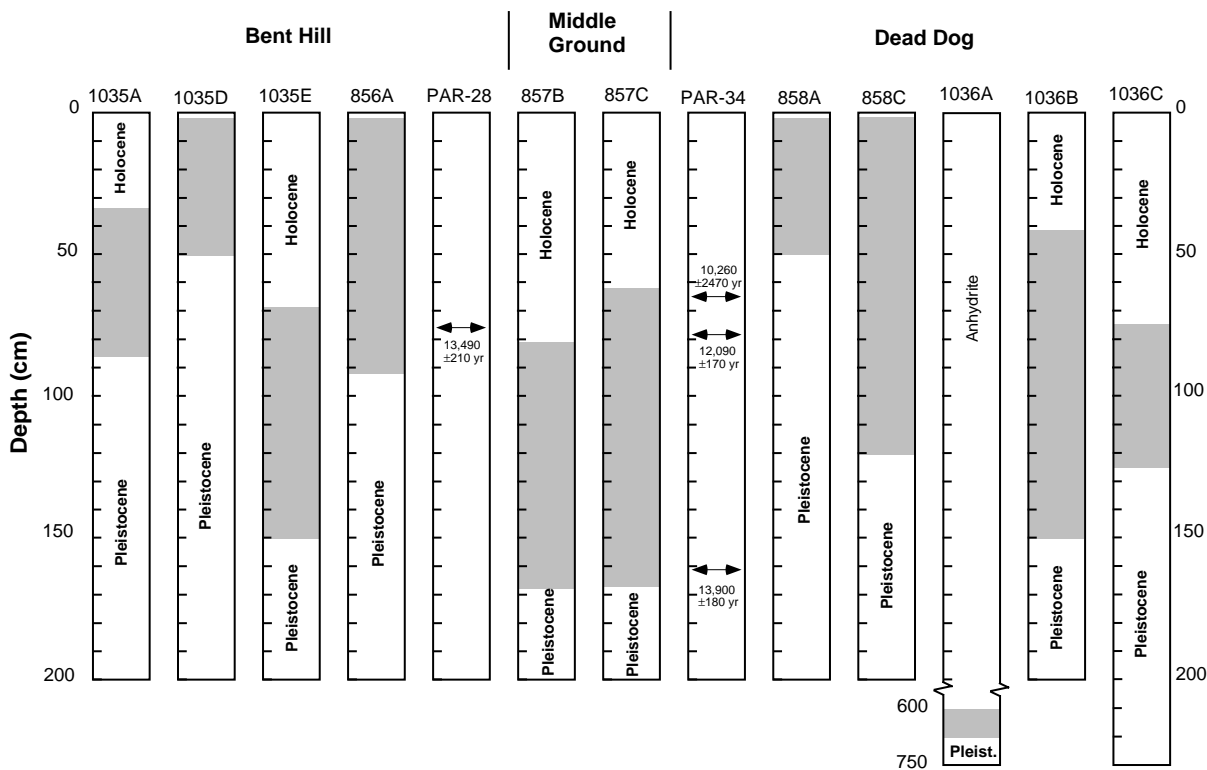


Figure 15. Depth of the Holocene/Pleistocene boundary in Middle Valley. Holocene sediment is found in thin layers a few centimeters thick at the tops of Holes 1035D, 856A, 858A, and 858C. The gray area delimits the stratigraphic error defined as the interval between the deepest Holocene sample and the shallowest Pleistocene sample examined. The boundary is based on the change in coiling of *N. pachyderma* from sinistral to dextral at the end of the last glacial stage. Site 856 and 857 data are from Brunner (1994); piston cores labeled PAR are described by Goodfellow et al. (1993).

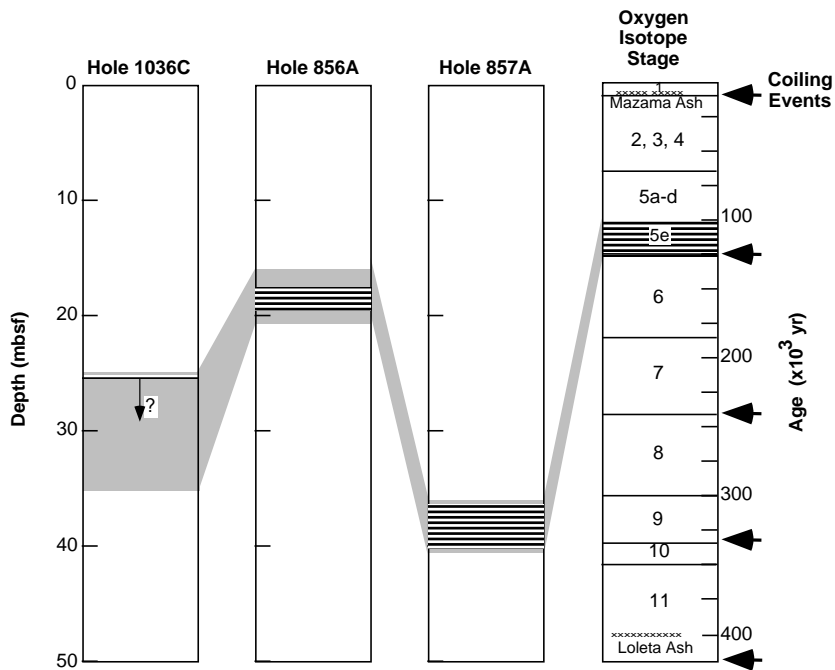


Figure 16. Depth of the Stage 5e interglacial assemblage zone at Hole 1036C and other nearby holes. Data from Sites 856 and 857 are from Brunner (1994).

Table 5. Summary of structural features, Hole 1036A.

Core, section	Depth (mbsf)	Feature		Position		Veins			Comments
		Oriented	Identifier	Top (cm)	Bottom (cm)	Mineralogy	Width (mm)	Wall rock	
169-1036A-									
4H-3	30.8	N	V1a	10	14	Anh	2	SED	Veins in Section 169-1036A-4H-3 occur in drilling-disturbed silt. The original vein orientations are lost, but the widths are accurate.
4H-3	30.99	N	V1b	29	31	Anh	1	SED	
4H-3	31.02	N	V1c	32	34	Anh	2	SED	
4H-3	31.09	N	V1d	39	41	Anh	2	SED	
4H-3	31.18	N	V1e	48	49	Anh	2	SED	
4H-3	31.25	N	V1f	55	59	Anh	1	SED	
4H-3	31.29	N	V1g	59	62	Anh	1	SED	
4H-3	31.35	N	V1h	65	68	Anh	2	SED	

Notes: N = not oriented; Anh = anhydrite; SED = sediment.

ceeded 220°C. A second sample (2M-01) was collected using the Los Alamos water sampler at ~100 mbsf. A log using the UHT-MSM temperature tool recorded a temperature of ~274°C at this depth. The third fluid sample is from a wash core recovered from an unlined core barrel that was drilled over the interval from 205 mbsf to the bottom of the hole at 387 mbsf. The wash core comprised loosely aggregated, fine-grained pyrrhotite and pyrite, with minor anhydrite. The water trapped by this plug was recovered and subsequently analyzed.

Results and Discussion

Results of the chemical analyses of these fluids are presented as a function of their Mg content in Figure 17; the raw data are given in Table 6. All samples show some degree of dilution with seawater. Mg is usually completely removed from solution during basalt-seawater experiments at high temperatures (e.g., Bischoff and Dickson, 1975) and, therefore, the Mg concentration of a hydrothermal fluid sample serves as a measure of its dilution with seawater.

With the exception of fluids collected using the Los Alamos sampler, the Cl data lie within error of the Dead Dog end-member vent fluid/seawater mixing line (Fig. 17A). Excluding the Los Alamos samples, the data extrapolate to 590 ± 8 mM Cl at zero Mg, which is essentially identical to the value calculated for the Dead Dog end-member hydrothermal fluid in 1990 (591 mM; Butterfield et al., 1994). Fluids collected using the Los Alamos sampler have Cl concentrations 9% lower than predicted by simple mixing. We believe that the failure of the seals in this sampler led to boiling of the fluid sample on retrieval, resulting in dilution of the sample with a recondensed vapor of low salinity and intruded seawater. Concentrations of H_4SiO_4 , NH_4 , B, and K in the Los Alamos sampler fluids are also ~9% lower than predicted by simple mixing. This is again consistent with dilution of these samples by a low salinity, and hence low-cation component. It is, therefore, appropriate to apply a correction to the Los Alamos sampler fluid data by increasing the concentration of cations as dictated by the Cl loss; a correction of this type reduces the scatter about the mixing line. Figure 18 demonstrates this for K.

The Cl-corrected Li, K, B, NH_4 , and H_4SiO_4 data extrapolate to values at zero Mg comparable to those calculated for the Dead Dog vent fluid end-member (Table 7). This strongly suggests that Hole 858G contains a hydrothermal fluid similar to that sampled from the Dead Dog vents in 1990 (Butterfield et al., 1994). This implies that the chemical composition of the Dead Dog vent fluids has remained stable over the 6-yr sampling interval; such stability has also been observed in other vent fluids with Cl values near seawater, including 21°N East Pacific Rise (EPR; Campbell et al., 1988), the Guaymas Basin (Campbell et al., 1988; Gieskes et al., 1988) and the TAG hydrothermal site, 26°N Mid-Atlantic Ridge (MAR; Edmond et al., 1995). Too few data for pH and alkalinity were collected for meaningful interpretation.

SO_4 , Ca, and Sr data exhibit considerable scatter about the vent fluid/seawater mixing line, and it is difficult to calculate a vent fluid end-member from the borehole data. The concentration of these ele-

ments in the sample collected using the WSTP Ti tool and in the wash core sample are higher than predicted by simple mixing, whereas the concentration of SO_4 in the WSTP overflow and Los Alamos samples is lower than predicted. There is some evidence that the dissolution of anhydrite has contributed to the SO_4 , Ca, and Sr content of the wash core and WSTP Ti samples. The material collected in the wash core contained a component of anhydrite, and a great quantity of anhydrite was also observed in the CORK recovered from the mouth of the borehole. Because the WSTP sample was taken from only 20 mbsf, suspended anhydrite may have contaminated the sample collected in the WSTP Ti sampler. Although we have no direct evidence, the data suggest that precipitation of anhydrite has lowered the SO_4 , Ca, and Sr content of the WSTP overflow and Los Alamos samples. A correction to the Ca data for anhydrite dissolution or precipitation (as determined from the SO_4 data; see Fig. 19) has been applied in Figure 20. This results in a reduction in the scatter about the mixing line and gives an end-member value for the vent fluid from the borehole data of 79 ± 3.2 mM, in agreement with that calculated for the Dead Dog vent fluids in 1990 (83 mM; Butterfield et al., 1994). The Sr/Ca precipitation/dissolution value of the borehole fluids is in the range $1.1\text{--}6.1 \times 10^{-3}$, which is within the range determined experimentally by Berndt et al. (1988) and in anhydrite samples from the TAG hydrothermal mound (Teagle et al., in press). This agreement supports our correction. The range in the distribution coefficient of Sr in anhydrite makes it difficult to correct the borehole Sr data for the effects of anhydrite dissolution and precipitation.

Conclusions

The Li, K, B, NH_4 , and H_4SiO_4 data for the borehole fluids are best described as representing a high-temperature hydrothermal fluid with an end-member composition similar to fluid sampled from the nearby Dead Dog vent in 1990. The Cl concentration of the fluid collected using the Los Alamos sampling tool is 9% lower than predicted; this may result from the fluid boiling during retrieval of the tool. Concentrations of SO_4 , Ca, and Sr are both higher and lower than predicted by simple vent fluid/seawater mixing, consistent with the dissolution and precipitation of anhydrite, respectively. The Sr/Ca precipitation/dissolution value lies between $1.1\text{--}6.1 \times 10^{-3}$, in agreement with the ratio determined for anhydrite (e.g., Berndt et al., 1988; Teagle et al., in press). More important, the B and NH_4 contents of the borehole fluids agree with those of the vent fluids at Dead Dog. Hole 858G is cased through the sediment section and, if the casing is intact, can only derive its hydrothermal fluid from the basaltic basement. Because the B and NH_4 components are interpreted to be derived from sediments, this would imply that the fluids have obtained this signature during the recharge process.

Site 1036

Pore fluids were collected from three holes (Holes 1036A, 1036B, and 1036C) forming a transect across the Dead Dog Mound, one of

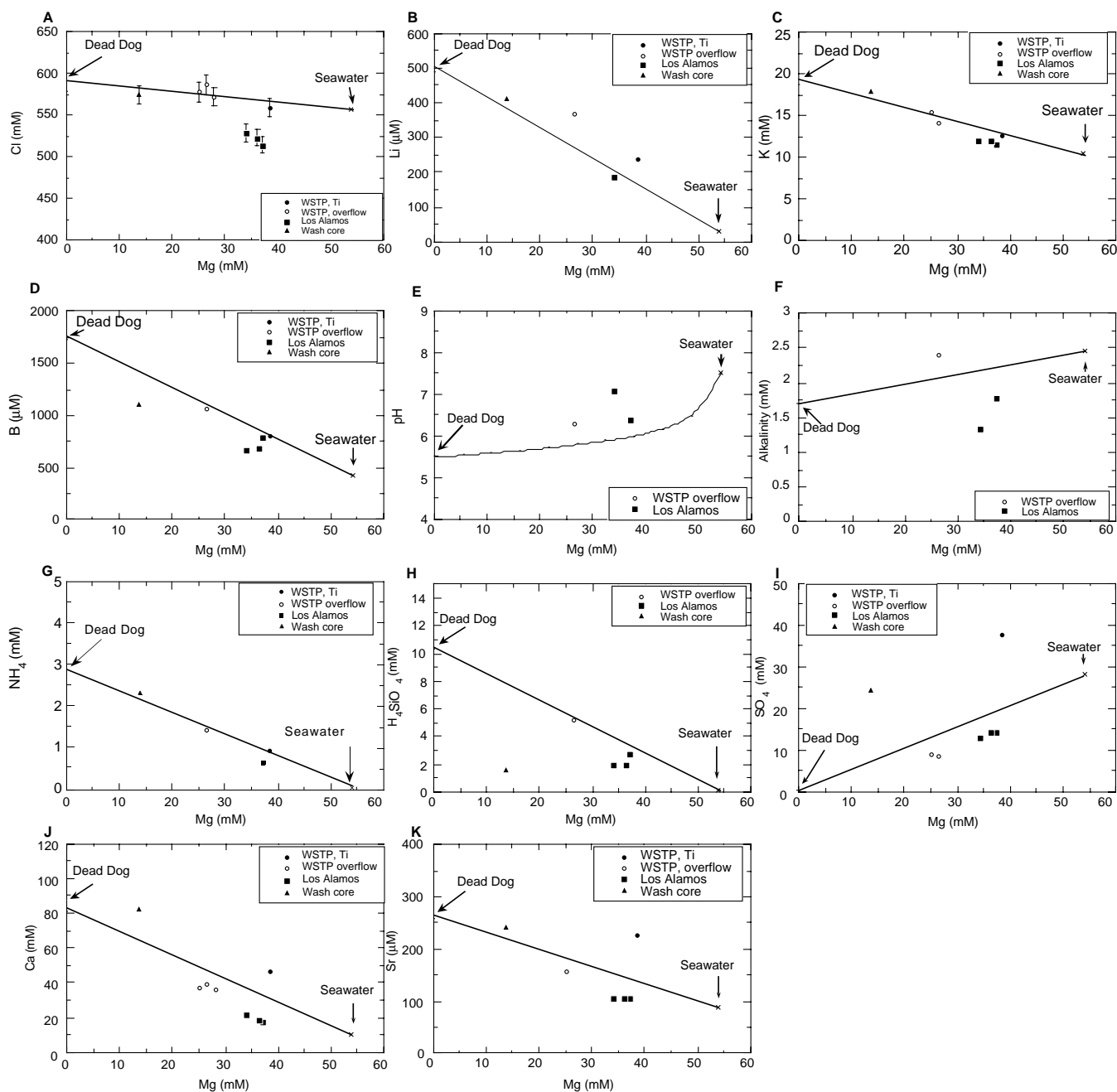


Figure 17. Concentration in borehole fluids plotted as a function of Mg vs. (A) Cl, (B) Li, (C) K, (D) B, (E) pH, (F) alkalinity, (G) NH₄, (H) H₄SiO₄, (I) SO₄, (J) Ca, and (K) Sr. The solid black line denotes simple mixing between seawater and high-temperature hydrothermal fluid from the Dead Dog Mound (Butterfield et al., 1994).

several active mounds in the DDVF. This set of holes was designed to provide a transect between an active hydrothermal mound (Dead Dog Mound) and Hole 858A located at the western edge of the active hydrothermal vent field. Hole 1036A was located at the top of the mound and 9 m away from an active vent that was discharging water at temperatures of 268°C (Ames et al., 1993). Hole 1036B is located 37 m to the northwest of Hole 1036A, which is on the side of the mound. Hole 1036C was offset another 34 m to the northwest of Hole 1036B. Hole 1036A was drilled to 38.5 mbsf, Hole 1036B to 52.3 mbsf, and Hole 1036C to 54.2 mbsf.

Samples of interstitial water were obtained by squeezing sediment from whole-round samples immediately upon retrieval of the cores. Before squeezing, the outermost layer of the sample was removed to

prevent contamination with seawater. Two samples of interstitial water were also obtained in situ at Hole 1036C using the WSTP.

Results of shipboard analyses of the pore fluids are reported in Table 8. The variations in the chemical composition of the fluids with depth is shown in Figure 21. For comparison, results of the analysis of pore fluids from Hole 858A above 60 mbsf (Shipboard Scientific Party, 1992b; Wheat and Mottl, 1994) are also given in Figure 21.

Hole 1036A

Above 20 mbsf, the chemical composition of the pore fluids from Hole 1036A is quite similar to that of seawater. This strongly suggests that the sediments are rapidly recharged with seawater. Vigor-

Table 6. Composition of borehole fluids, Hole 858G.

Sample	Depth (mbsf)	Temp (°C)	Ca (mM)	Mg (mM)	Cl (mM)	NH ₄ (mM)	H ₄ SiO ₄ (mM)	B (μM)	Sr (μM)	Li (μM)	SO ₄ (mM)	K (mM)	Alkalinity (mM)	pH
169-858G-														
1M-1 (Ti sampler)	~20	>220	46.7	38.4	559	0.9	—	809	226	240	37.9	12.7	—	—
1M-1 (overflow replicate 1)	~20	>220	39.3	26.4	587	1.41	5.26	1072	—	370	8.6	14.2	2.4	6.3
1M-1 (overflow replicate 2)	~20	>220	37.8	25.1	578	—	—	—	156	—	9.2	15.7	—	—
1M-1 (overflow replicate 3)	~20	>220	36	28	572	—	—	—	—	—	—	—	—	—
2M-1 (replicate 1)	~100	~274	18	37.2	514	0.6	2.8	790	104	—	14.5	11.6	1.78	6.39
2M-1 (replicate 2)	~100	~274	22.2	34.1	528	—	1.94	669	105	184	13.1	11.9	1.33	7.06
2M-1 (replicate 3)	~100	~274	18.8	36.2	523	—	1.95	682	107	—	14.5	11.9	—	—
Wash core:	205–387	—	82.2	13.8	574	2.3	1.53	1101	241	410	24.3	17.9	—	—
Seawater:	—	~2	10.5	54	557	0	0.16	420	87	27	28	10.4	2.45	7.8
Dead Dog end-member:	—	~276	83	0	591	2.9	10.5	1770	263	501	0.4	19.1	1.7	5.5

Notes: Dead Dog end-member analyses are from Butterfield et al. (1994). Seawater analyses have been performed as part of this study. — = no data.

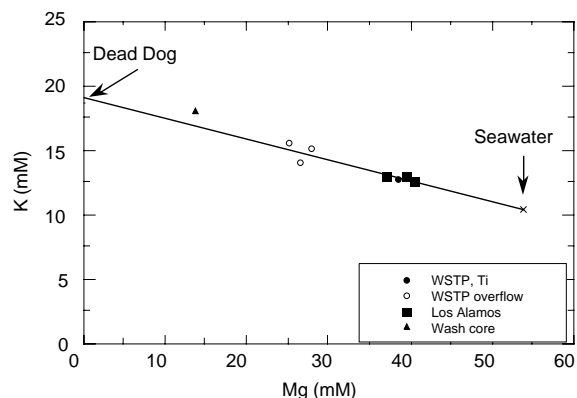


Figure 18. Concentration of K in borehole fluids as a function of Mg following correction of the data for boiling of the fluid. The solid line denotes ideal mixing between seawater and a high-temperature vent fluid from the Dead Dog Mound.

ous upflow of venting fluids in the vicinity of this hole could induce a pressure gradient forcing seawater entrainment to these depths (Schultz et al., 1992).

The anomalous high SO₄ concentration in the sample from 22 mbsf is attributed to the effect of anhydrite dissolution, as it is accompanied by an increase in Sr concentration. Although it is difficult to judge whether dissolution occurs in situ or as an artifact of sampling, we can correct this effect based on the relationship between Ca, Sr, and SO₄ concentrations during anhydrite dissolution (see “Inorganic Geochemistry” section, “Middle Valley: Bent Hill Area” chapter, this volume). Applying this correction suggests that the original Ca concentration of this sample is <5 mM, which is consistent with the remainder of the Ca profile at this hole.

Between 20 and 30 mbsf, there is a marked increase in the concentrations of Mg and Cl (by ~50 mM and ~40 mM, respectively) accompanied by marked depletions in the Na and Ca concentrations (by 30–50 mM, and 5 mM, respectively). This drastic change in pore-fluid chemistry suggests the substitution of Na and Ca by Mg as a consequence of hydrothermal alteration of detrital minerals in the sediment. Removal of Mg from sediments close to active hydrothermal vents has previously been reported in short push cores in the Guaymas Basin (Magenheim and Gieskes, 1992). Upward flow of

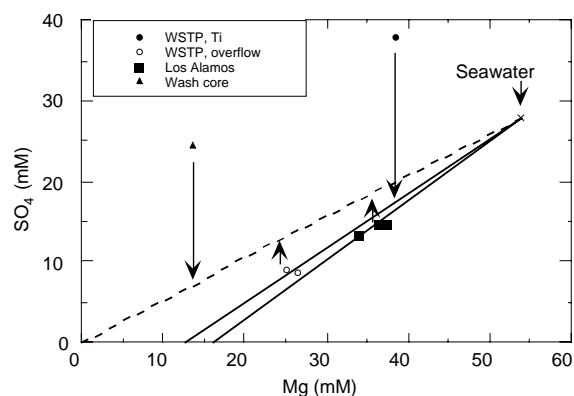


Figure 19. Scheme for correction of the SO₄ data for the effects of anhydrite precipitation and dissolution. The SO₄ concentration of the borehole fluids is increased or reduced such that the data fall on a mixing line between an end-member vent fluid (that contains zero SO₄; e.g., Von Damm et al., 1985) and seawater. The Los Alamos tool samples have been corrected for the effects of boiling. The SO₄ content of the WSTP Ti sample has a corrected fit on a mixing line between a fluid containing zero SO₄ and 13 mM Mg (as determined by the remainder of the borehole fluid data; anhydrite precipitation in the borehole results in a non-zero intercept in the fluid Mg content), and seawater.

hydrothermal fluid is interpreted to provide the heat that drives these alteration reactions. Although we have no direct measurement of temperature in this hole, there are several lines of evidence supporting a temperature of >200°C at 20–30 mbsf. First, the lack of calcite concretions and the abundance of anhydrite, even at shallow depths (below 10 mbsf), suggest that the thermal gradient in this hole is very high (see “Lithostratigraphy” section, this chapter). Second, oil components found in the sediment at depths of 12 to 17 mbsf indicate that high-temperature degradation of organic carbon and upward migration occur. The absence of oil components within the layer between 20 and 30 mbsf strongly suggests temperatures in excess of 200°C (see “Organic Geochemistry” section, this chapter).

Within the 20–30 mbsf interval, all the species show fairly uniform concentrations, implying lateral pore-fluid flow. Preliminary X-ray diffraction (XRD) analysis of sediments showed the presence of smectite in this layer (Section 169-1036A-3H-4) that is absent in the layers immediately above (Section 169-1036A-2H-4) and below

Table 7. Compositions of hydrothermal fluids, Bent Hill area.

	Cl (mM)	Li (μM)	K (mM)	B (μM)	Alkalinity (mM)	NH ₄ (mM)	Silica (mM)
Dead Dog	591	501	19.1	1770	1.7	2.9	10.5
Hole 858G borehole fluids	590 ± 8	620 ± 50	20.0 ± 0.51	1660 ± 100	1.6 ± 1	2.9 ± 0.3	9.6 ± 1

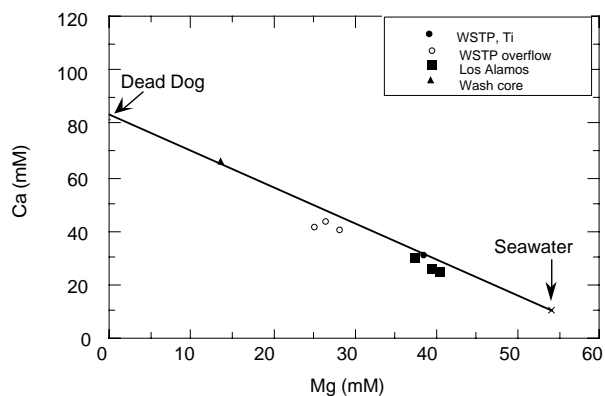


Figure 20. Concentration of Ca in the borehole fluids vs. Mg following the correction for the effects of anhydrite precipitation or dissolution as determined from the SO₄ data. The solid line denotes simple mixing between seawater and a high-temperature vent fluid from the Dead Dog Mound.

(Section 169-1036A-4X-CC). This supports the hypothesis of intense flow of the pore fluids, resulting in alteration of the sediments. During Leg 139, lateral flow of pore fluids was identified between 5 and 20 mbsf in Hole 858B, which was also drilled very close to an active hydrothermal vent (Shipboard Scientific Party, 1992b).

The pore fluids at a depth of 33 mbsf show a different composition from those in the 20 to 30 mbsf interval. A drastic decrease in sediment porosity below 30 mbsf would prevent downflow of the fluid

(see “Physical Properties” section, this chapter). A marked increase in the concentrations of NH₄, K, and B implies some contribution from a hydrothermal component.

Hole 1036B

From 0 to 40 mbsf, pore fluids from Hole 1036B show an overall decrease downhole in the concentrations of Mg and SO₄, as well as increases in the concentrations of K, Ca, Li, Sr, NH₄, and Cl. Fluctuations in the profiles of Cl and Na could be attributed to evaporation during sample handling; some cores were steaming upon retrieval. The consistency in the Na/Cl value supports this. The effects of anhydrite dissolution appear in Ca, Sr, and SO₄ profiles for several samples.

A decrease in Mg and SO₄, accompanied by an increase in Ca, is observed below 15 mbsf, and the concentration gradients increase significantly below 30 mbsf. This signature is consistent with the modification of entrained seawater as a result of thermally enhanced diagenesis (Gieskes et al., 1982). Several hydrothermal experiments reacting seawater with sediment confirm this alteration process (e.g., Thornton and Seyfried, 1987). Mg is removed from the fluid by formation of Mg-rich clay minerals. This is associated with the dissolution of plagioclase feldspar and a subsequent increase in the Ca (and K) concentration of pore fluids. Slight increases in the concentrations of Li and Sr are attributed to the same process. In addition to this cation exchange, anhydrite precipitation occurs at temperatures >150°C. The abundance of anhydrite in sediments below 18.6 mbsf (see “Lithostratigraphy” section, this chapter) is consistent with the pore-water profiles. The occurrence of Mg-rich clay minerals in sediments

Table 8. Composition of pore water in sediment, Site 1036.

Sample	Core, section, interval (cm)	Depth (mbsf)	Salinity	Cl (mM)	pH	Alkalinity (mM)	SO ₄ (mM)	NH ₄ (μM)	Ca (mM)	Mg (mM)	Sr (μM)	Li (μM)	K (mM)	Na (mM)	B (μM)	H ₄ SiO ₄ (μM)
Seawater:			0.00	35	557	2.45	28	0	10.6	54	87	27	10.4	480	420	170
169-1036A-																
IW-1	1H-3, 140-150	3.45	36	554	7.68	2.90	28.8	1	10.7	52.4	85	27	10.4	478	460	310
IW-2	1H-5, 140-150	5.45	32	556	7.53	4.62	28.7	83	12.1	55.4	92	29	8	475	357	952
IW-3	2H-2, 140-150	12.5	33	564	6.97	2.85	26.9	41	12.7	54.2	88	34	8.2	478	367	841
IW-4	2H-4, 140-150	15.4	34	561	7.40	2.43	24.3	107	12.4	51.5	89	48	8.6	476	372	1132
IW-5	2H-5, 140-150	18.5	36	561	6.83	2.29	30.1	78	12.8	62.3	91	44	9	465	281	1053
IW-6	3H-2, 140-150	22	39	583			45.0	16	15.3	99.1	121	32	8.1	436	123	377
IW-7	3H-4, 140-150	25	37	583	7.06	1.87	27.3	8	5.9	97.1	75	29	8.1	426	245	1134
IW-8	3H-6, 140-150	28	38	592			27.7	43	4.3	94.2	51	29	9.1	441	285	1571
IW-9	4H-CC, 16-26	33	33	574	6.66	2.30	20.9	774	14.9	60.8	52	48	13	454	685	2540
169-1036B-																
IW-1	1H-2, 140-150	3	35	566	7.69	3.45	29.5	48	11	54.0	90	27	10.2	488	439	546
IW-2	1H-4, 140-150	6	36	568	7.29	4.27	30.2	75	12.9	55.1	97	36	8.5	488	375	557
IW-3	1H-5, 140-150	7	36	577	7.52	4.79	30.1	107	15.2	53.7	104	46	8.2	497	382	635
IW-4	2H-2, 140-150	11.7	37	596	7.52	3.80	29.0	167	27.4	44.2	145	69	7.7	508	325	605
IW-5	2H-4, 140-150	14.7	36	560	7.47	4.80	23.9	230	32.1	33.7	143	95	7.8	474	356	681
IW-6	2H-6, 140-150	17.7	38	588	6.66	6.58	14.1	248	31.5	27.8	126	112	7.6	497	433	883
IW-7	3H-2, 140-150	21.2	38	561	7.60	5.20	17.0	215	27.9	30.5	117	93	7.6	477	391	671
IW-8	3H-4, 140-150	24.2	38	595	7.55	6.64	7.6	345	28.9	23.1	112	128	9.2	505	414	972
IW-9	3H-6, 140-150	27.2	37	581	7.56	8.74	3.4	512	36.9	9.2	106	128	14.1	491	414	1396
IW-10	4X-2, 140-150	30.7	36	588	7.52	11.38	4.1	618	45.9	6.4	116	151	13.8	490	331	1343
IW-11	4X-5, 140-150	35.2	37	586	7.52	9.05	10.8	775	54.6	5.9	134	164	16.1	481	407	1608
IW-12	5X-1, 140-150	38.8	34	576	7.26	7.17	2.0	1014	39.2	4.1	116	163	19	482	510	1958
IW-13	5X-3, 140-150	41.8	35	572	7.43	10.00	2.8	1546	59.8	8.3	182	328	17.7	434	914	1753
IW-14	6X-1, 90-100	50	35	591		10.00	1.7	1619	74	5.4	222	380	15.1	431	1083	1362
169-1036C-																
IW-1	1H-2, 140-150	3	36	558	7.72	3.49	27.9	21	10.6	52.9	87	27	11	480	517	554
IW-2	1H-4, 140-150	6	38	559	7.58	4.04	30.7	74	11.4	54.4	90	26	10	483	458	799
IW-3	2H-2, 140-150	9.4	38	563	7.48	5.27	27.6	144	13.4	54.6	96	34	8.8	478	407	1025
IW-4	2H-4, 140-150	12.4	38	562	7.60	5.43	27.9	208	16.4	52.7	98	49	8.2	477	352	736
IW-5	2H-5, 140-150	13.9	38	561	7.56	6.22	27.6	253	15.9	54.3	98	57	8.2	474	337	1521
BC-6	WSTP-5	15.9		557			27.3	240	16	52.8	94	68	7.6	480	287	1312
IW-7	3H-2, 140-150	18.9	38	565	7.20	7.48	27.4	346	17.2	51.8	100	67	9.3	480	333	1918
IW-8	3H-4, 140-150	21.9	38	565	6.97	7.26	28.5	382	19.5	51.5	104	75	8.7	479	364	849
IW-9	3H-6, 140-150	24.9	38	568	7.12	6.78	27.2	409	23	47.7	110	86	8.4	479	364	500
IW-10	4H-3, 140-150	29.9	36	564	6.53	4.62	16.9	501	27.1	31.0	106	105	8.5	478	375	667
IW-11	4H-6, 140-150	32.9	36	563	6.73	6.24	11.5	572	28.5	24.4	108	113	10.1	477	489	881
BC-12	WSTP-6	34.9		568			9.5	741	26.2	19.8	111	117	14	562	1435	
IW-13	5X-3, 140-150	39.4	37	565	6.78	7.80	9.3	577	32.4	18.6	113	119	11.4	478	482	1153
IW-14	5X-4, 140-150	42.4	36	565	6.69	7.38	17.6	565	38.3	18.2	126	115	11.3	484	497	1276
IW-15	6X-2, 140-150	47.6	34	565	6.63	9.76	14.0	523	29.8	24.6	93	86	14.1	480	482	1554

has been identified in samples collected from Hole 858B, which was drilled very close to an active hydrothermal mound. (Goodfellow and Peter, 1994).

There is a sudden change in the pore-fluid profiles of Na, Ca, Li, Sr, and B at a depth of 40 mbsf. The chemical composition of the pore fluids below this depth is similar to the Dead Dog vent fluid end-member composition, which is indicated by an arrow in Figure 21. This suggests upward penetration of a hydrothermal component through the sediment at this hole. To confirm the presence of a hydrothermal component, chemical compositions of the pore fluids collected from holes around the Dead Dog Mound are compiled in Figure 22. K, Ca, Li, and Cl compositions of the deepest samples in each hole are clearly explained by mixing of the hydrothermal fluid end-member with seawater. This agreement is also evident for Na, Sr, and SO_4 . However, the NH_4 and B concentrations of these samples are systematically lower than predicted by the mixing line. We observed a similar discrepancy in the pore fluids from Site 1035 (see "Inorganic Geochemistry" section, "Middle Valley: Bent Hill Area" chapter, this volume). This discrepancy may be attributed to the adsorption of these species in sediments, either in situ, on retrieval, or during the squeezing process.

Hole 1036C

The composition of pore fluids from Hole 1036C is generally similar to seawater in the upper 20 m. A slight decrease in Mg and SO_4 is observed below 30 mbsf, which also coincides with an increase in the abundance of anhydrite concretions in the sediment (see "Lithostratigraphy" section, this chapter). However, the pore-fluid chemistry is less modified than observed at Hole 1036B. The effects of hydrothermal alteration are much weaker in Hole 1036C, reflecting the decreasing hydrothermal gradient with distance from the active mound.

Two samples were collected in this hole using the WSTP tool. The chemical composition of these samples, with the exception of K, B, H_4SiO_4 , and NH_4 , agrees within analytical error with that determined from squeezed fluids (Fig. 21). The discrepancy in K, B, H_4SiO_4 , and NH_4 concentrations may be attributed to adsorption, either in clay-rich sediments, in situ, on retrieval, or during the squeezing procedure. Adsorption of B from pore fluids onto clay-rich sediments has been demonstrated in several previous studies (e.g., You et al., 1996).

There is no evidence for the penetration of a hydrothermal component above the drilling depth (50 mbsf) in Hole 1036C. At Hole 858A, which lies ~100 m to the northwest of Hole 1036C (~170 m from the active mound), evidence for a hydrothermal component in the pore fluids was observed below 220 mbsf, based on the drastic change in the Na concentration (Shipboard Scientific Party, 1992b). Hence, it is likely that the depth of hydrothermal penetration at Hole 1036C lies below the drilling depth.

Conclusions

The pore fluids from Hole 1036A have a composition that is distinct from that of other holes. Above 20 mbsf, the composition is similar to that of seawater, suggesting a vigorous recharge of seawater. Between 20 and 30 mbsf, a significant modification of the pore-water composition occurs, indicated by an increase in the Mg concentrations and decrease in the Ca and Na concentrations. This implies high-temperature (>200°C) alteration in the vicinity of the venting fluid conduit, caused by heat supplied from upflowing hydrothermal fluid. This alteration process would involve entrained seawater that is transported laterally through this section.

In Holes 1036B and 1036C, pore fluids are modified by thermally enhanced diagenesis (moderate hydrothermal alteration) of clay minerals and anhydrite precipitation. Below 40 mbsf in Hole 1036B, pore fluids contain a significant hydrothermal component similar in composition to the Dead Dog fluid end-member. The upper boundary of the hydrothermal penetration was not observed in Hole 1036C, but

was previously identified at ~220 mbsf in Hole 858A. These results suggest decreasing hydrothermal penetration with distance from the active mound.

Overall Conclusions

The chemical composition of the fluid contained in the cased hole (Hole 858G) at the Dead Dog vent site is similar to the composition of fluids sampled from the active Dead Dog vents in 1990 (Butterfield et al., 1994). This implies that the composition of the vent fluids has remained stable over the 6-yr sampling interval. In particular, the B and NH_4 contents of the fluids contained in Hole 858G are identical to those in the Dead Dog vent fluid; providing that the hole casing is intact to basement, this implies that the B and NH_4 components (which are interpreted to be derived from sediments) have been obtained during the recharge process.

Pore fluids collected below 40 mbsf in Hole 1036B contain a significant hydrothermal component with a composition similar to the Dead Dog vent fluid end-member. There is no evidence for a hydrothermal component in pore fluids above the drilling depth (50 mbsf) at Hole 1036C. The upper boundary of hydrothermal penetration at Hole 858A lies at ~220 mbsf; these results imply decreasing hydrothermal penetration with distance from the active mound. Pore fluids from Hole 1036A, which is located ~9 m away from an active vent, show evidence for vigorous entrainment of seawater, and, in addition, for intense lateral flow in the interval 20 to 30 mbsf, resulting in alteration of the sediments within this layer.

ORGANIC GEOCHEMISTRY

Shipboard gas analyses were carried out on the headspace gas of sediments recovered from Site 1036, from the water sampling tools, and from clamped-off sections of the 300-m-long tygon tube recovered while unCORKing Hole 857D. Analyses of solvent extracts of bitumen from sediments of Site 1036, from the hydrothermal precipitates in the body of the CORK housing recovered from Hole 858G, and from sulfide recovered in the wash core from Hole 858G were also conducted. Routine elemental analyses were performed on sediments for total C, N, and S, and carbonate C.

Volatile Gases

Hole 857D

The plastic tubing recovered from Hole 857D was sampled for fluid and gas by cutting out clamped off sections (~2 m long each) near the middle and bottom. The water was black (suspended sulfides and possibly carbonaceous soot) near the middle and almost clear near the bottom end. This is also reflected in the gas content. Gas was sampled by syringe through the wall of the tubing and put into vials for analysis by gas chromatography (GC; both methods were used and the results were averaged; see "Explanatory Notes" chapter, this volume). The data, corrected for air, are given in Table 9. The major component was air with significant and equal amounts of CH_4 and CO_2 and traces of C_2 – C_5 hydrocarbons. The intermittent presence of ethylene is troublesome. It could originate from thermal cracking of the plastic polymer of the tube or from breakdown of the Teflon fluoridated ethylene propylene (FEP) thermistor cable. Ethylene is not found in hydrothermal hydrocarbon gas, but has been detected in laboratory hydrous pyrolysis experiments on sediments. The C_1/C_2 ratios range from 31 to 63, with an average of 47. This narrow range indicates a common source for the gas and a high temperature of formation. The gas concentrations are higher in the black water (sulfidic) zone than at the bottom end of the tube. This indicates that the gas was introduced with hydrothermal fluid or was generated by microbial activity in the upper portion of the tube.

The WSTP was deployed at 620 mbsf of Hole 857D, where the temperature was ~2.5°C above ambient bottom water. Most of the

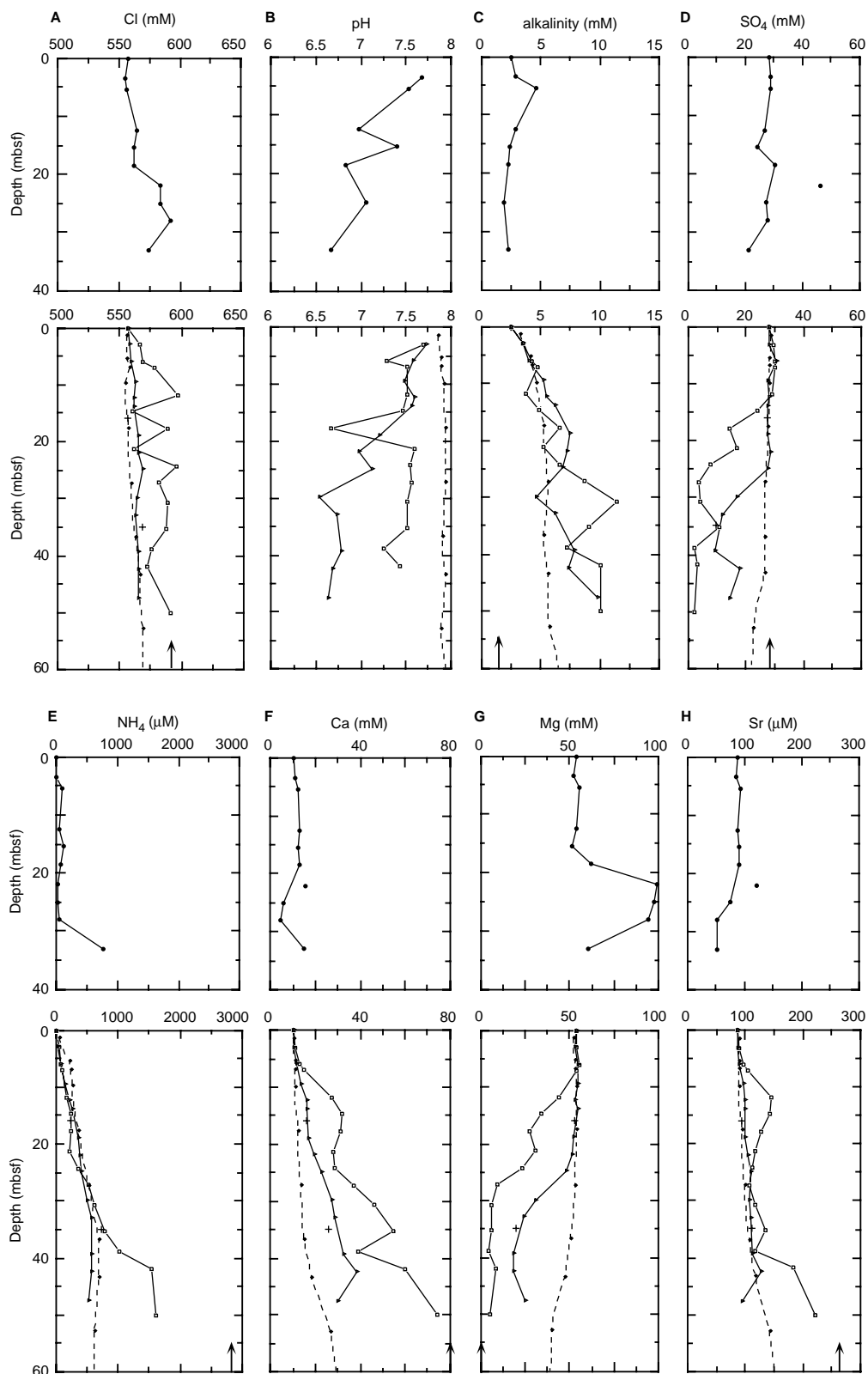


Figure 21. Profiles of pore-water composition at Site 1036. **A.** Cl. **B.** pH. **C.** alkalinity. **D.** SO₄. **E.** NH₄. **F.** Ca. **G.** Mg. **H.** Sr. **I.** Li. **J.** K. **K.** Na. **L.** Na/Cl value. **M.** B. **N.** H₄SiO₄. Solid circles = Hole 1036A, squares = Hole 1036B, triangles = Hole 1036C, + = WSTP samples from Hole 1036C, and diamonds = Hole 858A (data from Shipboard Scientific Party, 1992b, and Wheat and Mottl, 1994, after unit conversion). Arrow = the composition of Dead Dog Mound end-member hydrothermal fluid (data from Butterfield et al., 1994, after unit conversion). Solid lines = data from Leg 169, and dashed lines = connection to data from Leg 139.

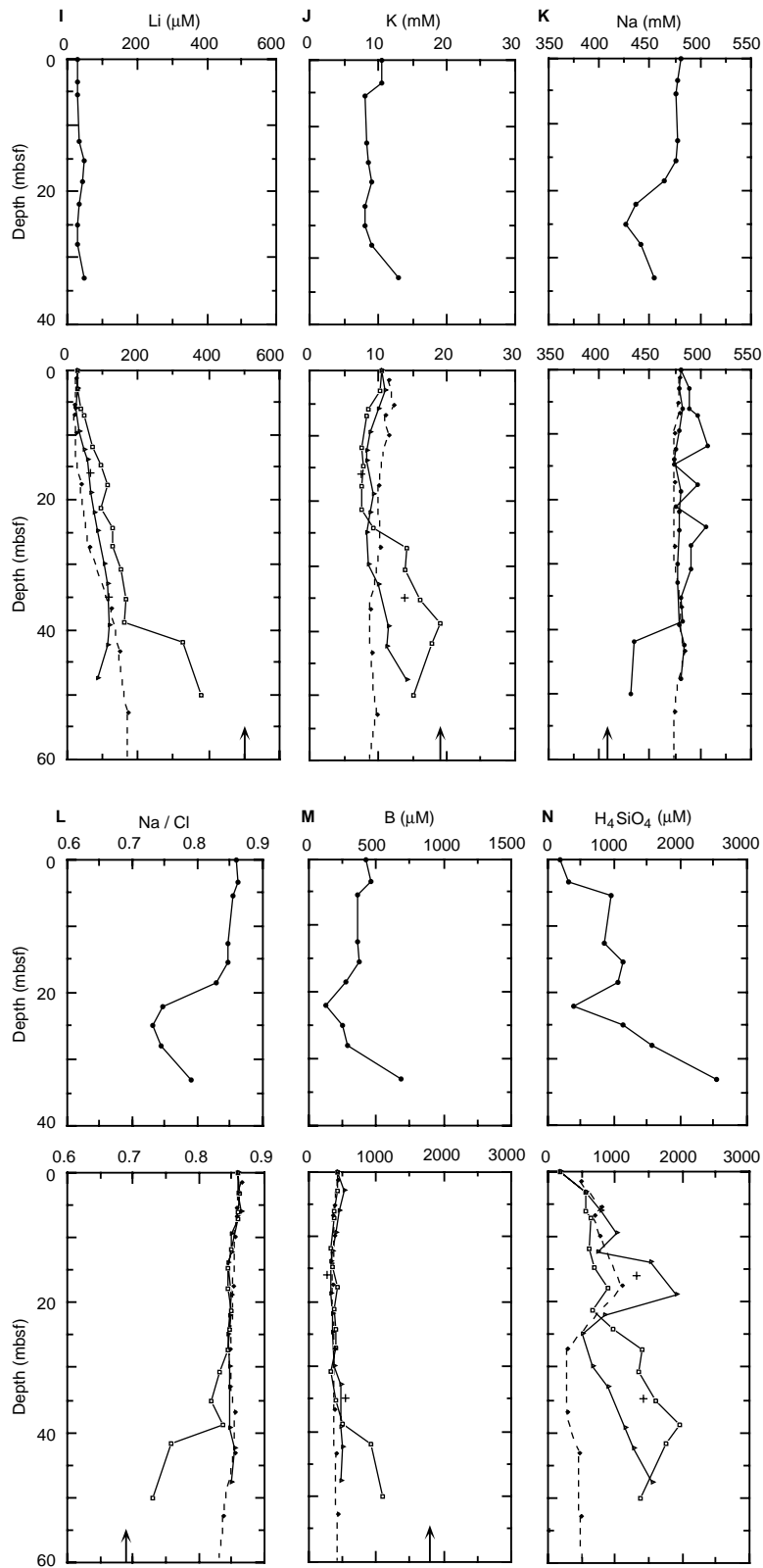


Figure 21 (continued).

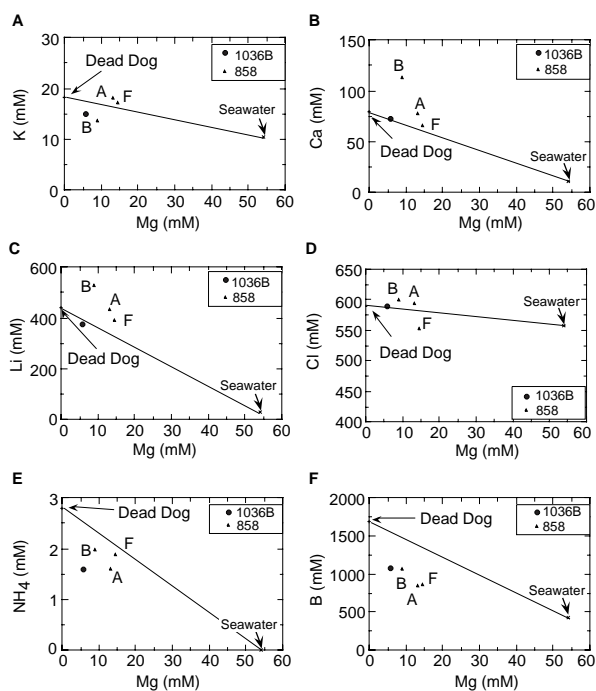


Figure 22. Concentration in pore fluids as a function of Mg vs. (A) K, (B) Ca, (C) Li, (D) Cl, (E) NH_4 , and (F) B. Solid circles = 1036B, triangles = Holes 858A, 858B, and 858F (data from Shipboard Scientific Party, 1992b; Wheat and Mottl, 1994; after unit conversion; Dead Dog Mound end-member fluids data from Butterfield et al., 1994, after unit conversion). The solid line denotes mixing between seawater and the vent fluid end-member.

gas sampled was air from leakage; however, the traces of CH_4 and CO_2 above air background (Table 9) indicate intermixing of hydrothermal fluid with the downwelling water in the bottom of the hole.

Hole 858G

Volatile gases (hydrocarbons, CO_2 , H_2S , and N_2) were measured on headspace gas from the WSTP (both early and later bleed gas) and on gas stripped (by shaking in a vacutainer) from the water collected with the Los Alamos sampler. The results are listed in Table 9. The early gas sample from the WSTP that was deployed at 20 mbsf in Hole 858G contained a major amount of air with C_1 – C_4 hydrocarbons and CO_2 , whereas the later gas sample consisted of only ~5% air (the data reported are normalized after correction for air) and hydrocarbons from C_1 to C_5 , CO_2 , and excess N_2 . The bulk gas composition was ~5% air, 37% N_2 , 28% CO_2 , and 29% hydrocarbons. H_2S was not detectable (the gases also had no H_2S odor). The C_1/C_2 ratios for the early and late bleed gas samples are 80 and 76, respectively, well within the window for a thermogenic origin from rapid organic matter maturation. The upper limit for thermogenic gas is generally taken as 100 (Bernard et al., 1976). The gas from the water in the Los Alamos sampler, taken at 90 mbsf in Hole 858G, also contained C_1 – C_3 hydrocarbons and CO_2 . The CO_2 was present at a greater concentration than CH_4 , and H_2S was not detectable. The C_1/C_2 ratio is 57, also within the window for a high temperature origin.

Site 1036

The headspace gas composition monitored for sediment samples from Site 1036 is given in Table 9. The methane concentrations vary from 10 to 3500 ppm and generally increase with depth because of

increased temperature, except for samples from Hole 1036C, where the CH_4 concentration decreases with depth. The C_1 – C_3 hydrocarbon profile is superimposable on the trends described for Site 858, and the concentrations are low, similar to those reported for that site (Shipboard Scientific Party, 1992b). The C_1/C_2 ratios are typically <100, consistent with thermogenic methane formation in these geothermally heated sediments. The current measured temperature in Hole 1036C is 71°C at 16.5 mbsf and 122.3°C at 34.9 mbsf (see “Down-hole Measurements” section, this chapter). Carbon dioxide occurs at similar concentrations as reported before (Shipboard Scientific Party, 1992b; Taylor, 1990), and H_2S was not detectable.

Bitumen Fluorescence and Analysis

Hole 858G

Both the minerals/solids from the wash core at the bottom of Hole 858G and the hydrothermal minerals scraped from the interior of the CORK body had an odor like scorched oil. The in situ temperature in Hole 858G was measured at 274°C. Small samples were extracted with methanol/hexane (2:1). The hexane phase had a white fluorescence indicating the presence of aromatic hydrocarbons derived from high-temperature organic matter alteration. The extracts were concentrated and analyzed by high-resolution GC. All GC traces were similar (see the example in Fig. 23), showing an unresolved complex mixture (UCM) of branched and cyclic material typical of oil and n-alkanes ranging from C_{10} – C_{30} . The major resolved peaks in the GC retention range of C_{22} – C_{30} may be mixtures of n-alkanes with unknown components (possibly alkenes from cracking), because coinjection of standard alkanes broadened these peaks. The GC pattern does not match that of pipe dope or any other grease used aboard ship; however, the thermal alteration products of the various lubricants used aboard ship, especially pipe dope, could have such a composition.

Site 1036

Extracts from the near-surface sediments at Site 1036 were colorless, except for discrete horizons in Cores 169-1036A-2H (12–17 mbsf), 169-1036B-3H and 4X (24–35 mbsf), and 169-1036C-4H (32–35 mbsf), which showed a strong yellow-white fluorescence. The yellow fluorescence is interpreted as a result of the thermal maturation of bitumen to the mature stage (i.e., bitumen generated from sedimentary organic matter at temperatures of at least 50°–100°C or even higher temperatures for brief contact periods during hydrothermal alteration). Overmature bitumen, as described from Site 858, was not found here (Shipboard Scientific Party, 1992b). The presence of discrete horizons with fluorescence indicates hydrothermal generation and a limited migration of petroleum, consistent with a flow of high-temperature fluids through these sediments. This yellow-white fluorescence is a diagnostic indicator of lower thermal maturities, which is interpreted in these holes as limited upward migration away from the heat front and the accumulation of hydrothermal petroleum in narrow intervals. These extracts were analyzed by high-resolution GC for further interpretation.

Black Soot

Black soot (carbonaceous/mineral particulate matter) occurs in the hydrothermally altered intervals of this site, as was reported earlier for Site 858 (Shipboard Scientific Party, 1992b). Black soot was present in both soft and lithified sediments, but microscopic examination was inconclusive about its constitution. However, an association of black opaque particles with clay and other minerals was evident from microscopy, which explains the relatively low organic carbon content of the black particulate matter (2% for a sample from 43 mbsf in Core 139-858A-6H; Shipboard Scientific Party, 1992b).

Table 9. Composition of gas derived from Holes 857D and 858G and Site 1036.

Sample	Type	Depth (mbsf)	C ₁ (ppm)	CO ₂ (ppm)	C ₂ (ppm)	C ₂ H ₄ (ppm)	C ₃ (ppm)	C ₁ /C ₂	N ₂ (ppm)
169-857D:									
Tubing 1	V	150.00	8,054	7,431	127	1.1	23	63	
Tubing 2	V	150.00	11,748	10,619	219		59	54	
Tubing 3	V	150.00	5,191	6,312	94	2	16	55	
Tubing 4	V	300.00	1,075	1,023	32		8	34	
Tubing 5	V	300.00	1,906	1,916	62	0.6	14	31	
WSTP-3	V	620.00	31	560					
Lab air	V		<1	320	0				
169-858G:									
WSTP-2 early gas	V	20.00	38,500	25,500	484		140	80	
WSTP-2 later gas	V	20.00	288,900	285,000	3,800		1,060	76	367,700
Los Alamos water gas	V	90.00	13,000	23,500	230		60	57	
169-1036A-									
1H-7, 44-49	HS	9.46	2.7						
2H-7, 0-5	HS	18.53	437	1,364	5.5			80	
3H-2, 0-5	HS	20.53	121	828	1.6			76	
3H-6, 0-5	HS	26.53	111	709	1.2			93	
4H-2, 0-3	HS	30.02	347		5				
4H-CC	HS	33.00	1,164	1,497	11		2	106	
169-1036B-									
1H-3, 0-5	HS	3.03	123		1.7			72	
1H-6, 0-5	HS	7.53	47		0.6			78	
2H-7, 120-125	HS	18.93	40	1,602					
3H-2, 0-5	HS	19.73	22	1,118					
3H-5, 0-5	HS	24.23	13	2,300					
4X-2, 135-140	HS	30.58	11	4,786					
4X-5, 135-140	HS	35.08	9	4,000					
5X-2, 145-150	HS	40.28	1,615	5,219	18		3	90	
5X-3, 135-140	HS	41.68	3,707	3,652	54		8	67	
6X-1, 85-90	HS	46.07	3,482	1,691	54		4	64	
169-1036C-									
1H-2, 135-140	HS	2.88	935	595	11		1	85	
1H-4, 135-140	HS	5.88	513		6			86	
2H-4, 135-140	HS	12.28	354	518	4			86	
3H-4, 0-5	HS	20.43	37						
4H-4, 0-5	HS	29.93	34	3,670					
5X-4, 0-5	HS	39.43	29	2,980					
6X-2, 0-5	HS	46.13	15	4,092					

Notes: HS = headspace; V = vacutainer; N₂ = nitrogen in excess of air. Gas from Hole 857D was derived from the tygon water sampling tube connected to the CORK that was emplaced on Leg 139. For Hole 858G, gas was derived from the WSTP and Los Alamos water samplers and for Site 1036, from the sediment headspace samples.

Black particulate matter was separable from material of the following depths to the bottom of each hole: Hole 169-1036A, 12 mbsf; Hole 169-1036B, 21 mbsf; and Hole 169-1036C, 25 mbsf. These depths are also similar to the intervals of the onset of yellow fluorescence. The black soot is interpreted to represent, in part, the kerogen carbon residue after expulsion of the hydrothermally generated petroleum.

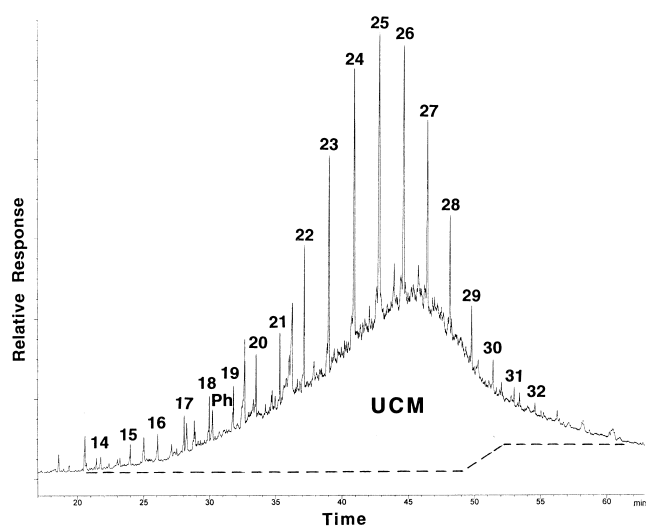


Figure 23. Gas chromatogram of the total extract from the minerals in the Hole 858G wash core. Numbers refer to the carbon chain length of the *n*-alkanes. UCM = unresolved complex mixture of branched and cyclic compounds, and Ph = phytane.

Bitumen Analyses

The supernatant (hexane) layers from the hexane/methanol extracts of the sediment samples prepared for fluorescence evaluation or subsamples of freeze-dried sediments were concentrated under a stream of nitrogen to ~10–100 μ L. These concentrates were analyzed by high-resolution GC, and typical traces are shown in Figures 24–26. The bitumen parameters for maturation and organic matter sources are listed in Table 10. Pristane (Pr) to *n*-C₁₇ and phytane (Ph) to *n*-C₁₈ ratios are not given because of the low concentrations of these compounds in many samples, although Pr/Ph is reported. Also, the U_K'₃₇ index (Davis, Mottl, Fisher, et al., 1992) could not be determined for these samples because the C₃₇ alkenones also had low concentrations and coeluting compounds interfered in the GC analyses.

In the relatively unaltered sediments, the *n*-alkanes > C₂₆ have a strong predominance of odd carbon numbered homologs (carbon preference index, CPI, >1.0) and a carbon number maximum (C_{max}) at C₂₉ or C₃₁ (e.g., Fig. 24A or 25A). This is typical for immature hydrocarbons with an origin from terrestrial higher plants (epicuticular plant waxes; Simoneit, 1977, 1978). Immature microbial lipid residues from autochthonous sources as reported earlier for other sediment samples from Middle Valley (Davis, Mottl, Fisher, et al., 1992) were not found.

Hydrothermal petroleums are products from rapid diagenetic/catagenetic alteration of sedimentary organic matter and have alkane distributions analogous to those of conventional crude oils (Simoneit and Lonsdale, 1982; Simoneit, 1985, 1990). As reported earlier for this area (Davis, Mottl, Fisher, et al., 1992; Simoneit, 1994; Simoneit et al., 1992), hydrothermal petroleums are also present in these sediments. The carbon number distributions and other geochemical parameters of these petroleums can be utilized to infer the source organ-

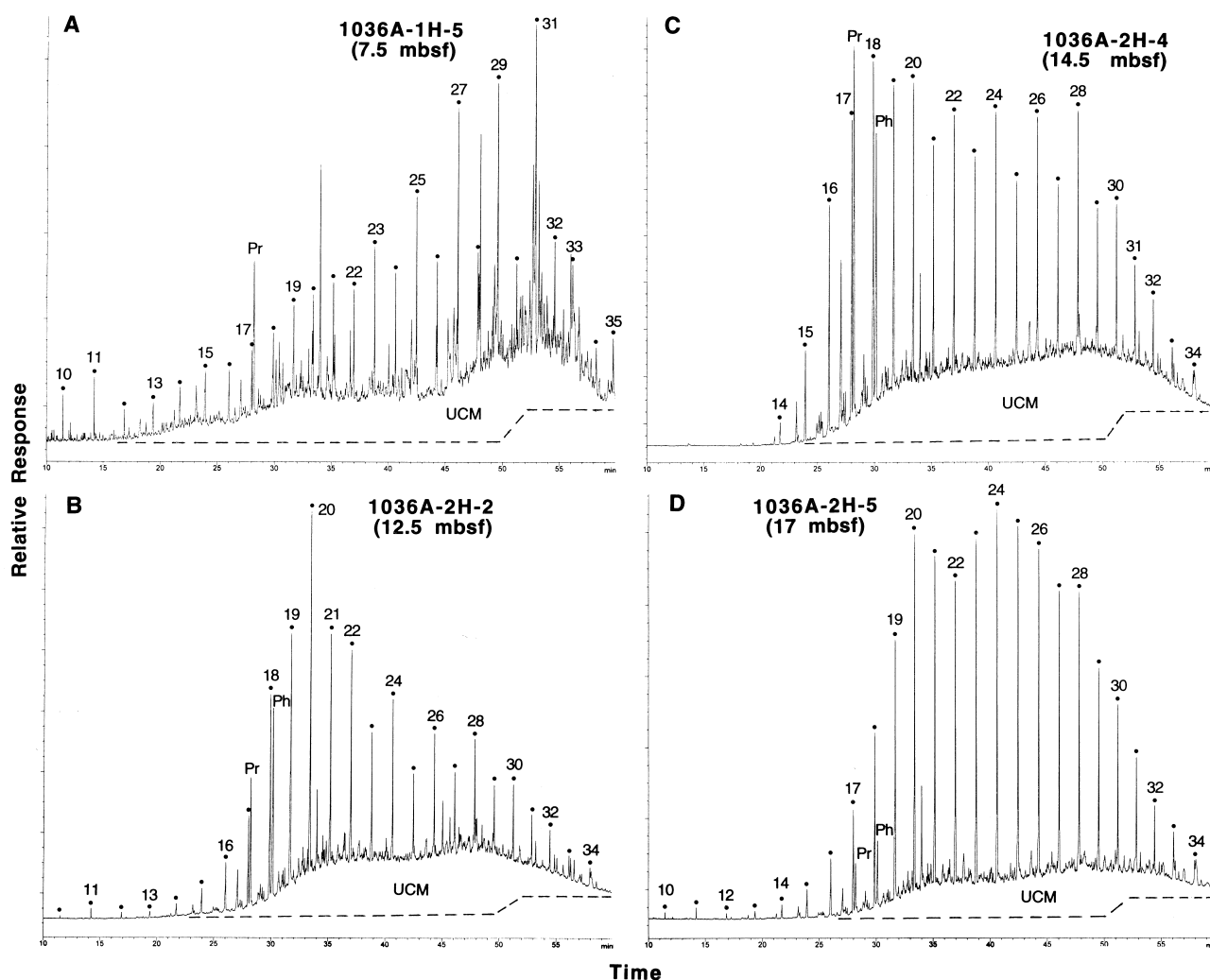


Figure 24. Typical gas chromatograms for total bitumen extracts from sediments of Hole 1036A. **A.** Section 169-1036A-1H-5 (7.5 mbsf). **B.** Section 169-1036A-2H-2 (12.5 mbsf). **C.** Section 169-1036A-2H-4 (14.5 mbsf). **D.** Section 169-1036A-2H-5 (17 mbsf). Dots and numbers refer to the carbon chain length of the homologous *n*-alkanes. Pr = pristane, Ph = phytane, and UCM = unresolved complex mixture.

ic matter and the degree of thermal alteration or maturity (Kawka and Simoneit, 1987; Kvenvolden et al., 1986; Simoneit and Lonsdale, 1982; Simoneit, 1985, 1990, 1994).

The alkane compositions of samples from the hydrothermal petroleum horizons in cores from Holes 1036A, 1036B, and 1036C are diverse just as was reported for Site 858 (Shipboard Scientific Party, 1992b). For example, relatively immature samples were extracted from Sections 169-1036B-2H-6 and 2H-6 (Figs. 25B, 26A), and full maturity is evident for the other samples whose GC patterns are shown (Figs. 24B–24D, 25C, D, and 26B–D). No overmature examples were found, probably because these petroleum products are able to migrate upward or laterally as the heat front advances through the sediment. Contamination from extraneous sources has been minimized, and thus the low carbon number range can also be considered. Many of these samples have been stripped in situ of the volatile components ($<C_{15}$), but if present, the volatile alkanes have a C_{max} at *n*- C_{11} or *n*- C_{12} and range down to $<C_8$ (Table 10; Figs. 25B, D, and 26D). The sedimentary precursor organic matter has a significant terrigenous component, and, therefore, the hydrothermal petroleum products have low contents of gas and volatiles compared to those formed from the more aliphatic marine organic matter in Guaymas Basin, Gulf of California (Simoneit et al., 1988; Kvenvolden and Simoneit, 1990). The alkane distributions and relative amounts of the envelopes

of the unresolved complex mixture (UCM) of branched and cyclic hydrocarbons are typical for hydrothermal petroleum products (examples in Figs. 24B–D, 25C, and 26C). Section 169-1036B-4X-5 (Fig. 25D) is a paraffin wax representing a preferential concentration of *n*-alkanes over isoprenoids and UCM probably by high temperature solution. Sections 169-1036B-2H-6, 4H-6, and 5X-4 (Figs. 25B and 26B, D) are enigmatic and require further analysis by GC mass spectrometry to elucidate the biomarker parameters.

CPI (range C_{24} – C_{33}) values are near 1 in the hydrothermal petroleum horizons and in all other samples at greater depth from Site 1036 (Fig. 27; note the petroleum horizons are designated by solid data points for samples with high extract yields). This indicates full maturity and is caused by high thermal stress that generates additional alkanes from the kerogen (bulk organic carbon). The CPI <1 in various intervals with the strong even carbon number predominance from *n*- C_{16} to *n*- C_{34} (e.g., Fig. 24B–D) should be pointed out. This was reported earlier for Middle Valley (Davis, Mottl, Fisher, et al., 1992; Simoneit, 1994) and for other geographic areas (e.g., Simoneit, 1977; Grimalt and Albaiges, 1987). It seems to be a characteristic of these hydrothermal petroleum products. Thermal maturation of petroleum products generally does not produce CPI values <1 , so that the low CPI for these holes must be partially source related. Because hydrothermal alteration in these sediments commences with immature organic mat-

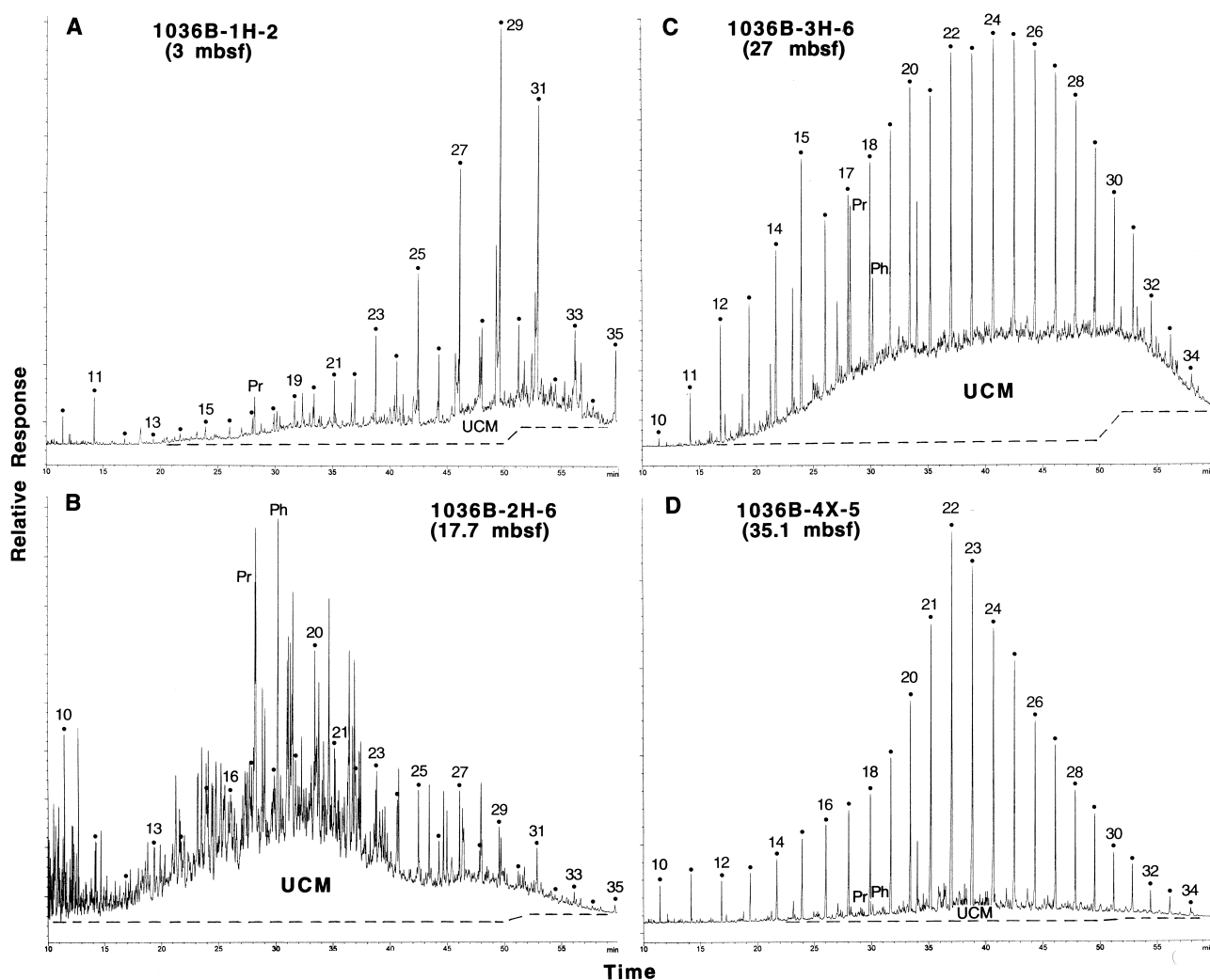


Figure 25. Typical gas chromatograms for total bitumen extracts from sediments of Hole 1036B. **A.** Section 169-1036B-1H-2 (3 mbsf). **B.** Section 169-1036B-2H-6 (17.7 mbsf). **C.** Section 169-1036B-3H-6 (27 mbsf). **D.** Section 169-1036B-4X-5 (35.1 mbsf). Abbreviations and homologous *n*-alkanes are the same as in Figure 24.

ter that has not completed diagenesis, lipids (e.g., *n*-alkanols and *n*-alkanoic acids) from terrestrial plant waxes and various biopolymers may be the sources of the even-chain alkanes. This would require reductive alteration as is observed in hydrothermal systems (Simoneit, 1990, 1994). The variability of the CPI values for bitumen in shallow intervals reflects the different source inputs of marine and terrestrial organic matter.

The isoprenoid alkane (Pr/Ph) ratios show severe variation vs. depth for these cores (Fig. 28). This ratio is generally influenced by both source and maturation. The Pr/Ph approaches low values at intermittent intervals in shallower horizons of these cores as well as at depth. This may be a reflection of primary organic matter sources at the shallower depths and full maturation at depth.

The intervals with hydrothermal petroleum are found progressively deeper along the transect from Holes 1036A through 1036C (Hole 1036A, 12–17 mbsf; Hole 1036B, 24–35 mbsf; and Hole 1036C, 32–35 mbsf), in concert with the inferred heat flow from the area (see “Downhole Measurements” section, this chapter). In situ temperature measurements in Hole 1036C at 34.9 mbsf indicated a present temperature of 122.3°C (Fig. 27). This, coupled with earlier temperature data for Site 858 (Shipboard Scientific Party, 1992b), indicates that hydrothermal petroleum was generated deeper in the sediments and accumulated in these discrete intervals within a contemporary tem-

perature window of 100°–150°C. This is corroborated further by the pore-fluid chemistry from Hole 1036A, where, for example, high concentrations of magnesium are found from 20 to 30 mbsf (see “Inorganic Geochemistry” section, this chapter), just below the petroleum horizon. The Mg anomaly is interpreted as a high-temperature (>200°C) transient fluid-flow zone with the petroleum residing above at 12–17 mbsf. The generation temperatures for these hydrothermal petroleum are estimated to be between 250° and 330°C, based on a comparison with laboratory simulation experiments and the following assumption (Kvenvolden et al., 1994; Leif et al., 1991; Simoneit, 1992). Simulation pyrolysis experiments are usually conducted for 2 days at 330°C for optimum yield. Fluid contact in the natural system is probably longer (weeks to decades), so that the temperature window for oil generation should be lower (i.e., approaching 250°C).

Elemental Analyses

The downhole profiles for weight percentages in sediments of C, N, and S, total organic (TOC), inorganic carbon (TIC), and the C/N ratio for all Site 1036 holes are listed in Table 11 and plotted in Figures 29–31. Total carbon ranges from 6.4% to 0.1% and decreases from variable contents to background levels at depth in sediments from Holes 1036A and 1036B. Total carbon in Hole 1036C decreases

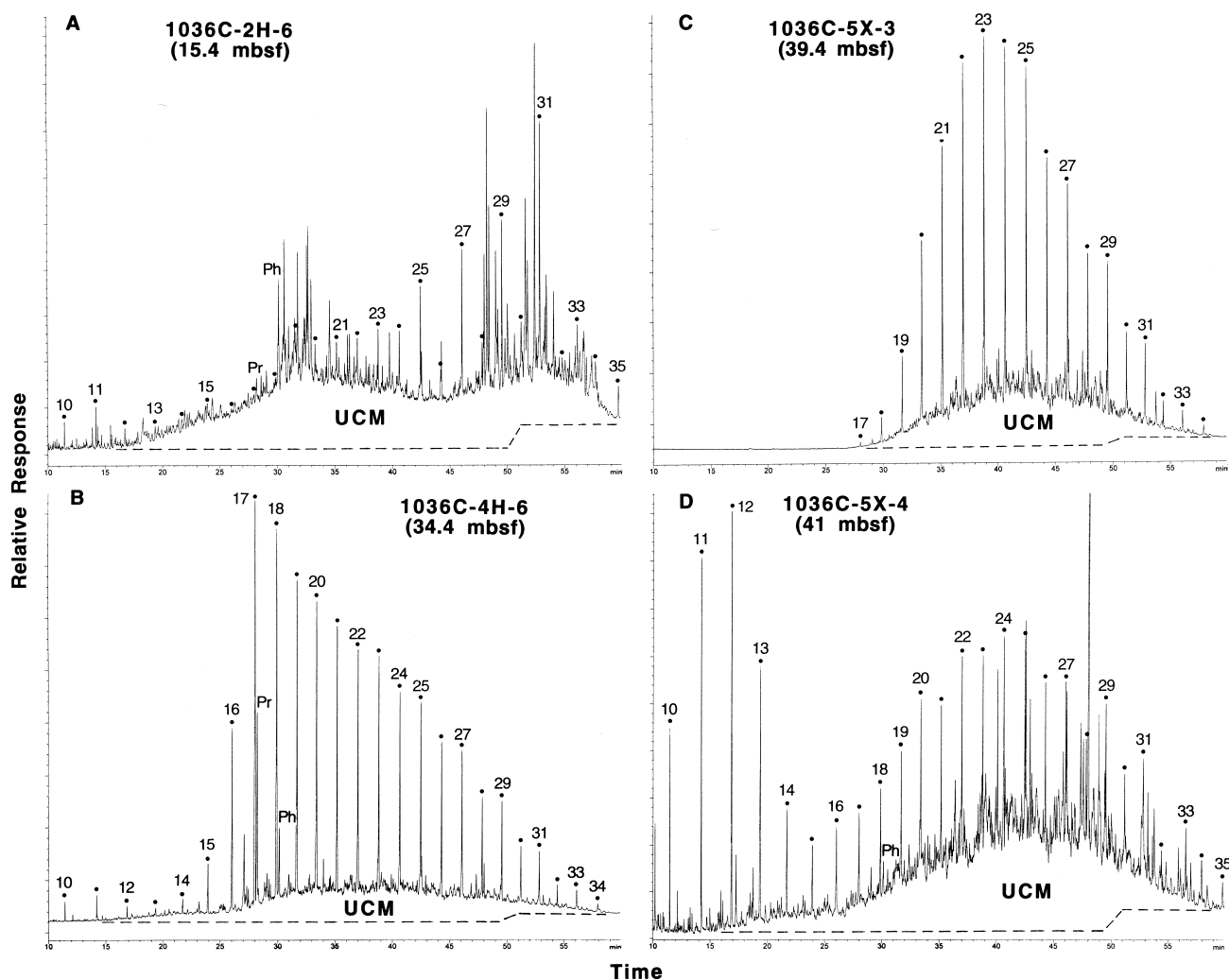


Figure 26. Typical gas chromatograms for total bitumen extracts from sediments of Hole 1036C. **A.** Section 160-1036C-2H-6 (15.4 mbsf). **B.** Section 169-1036C-4H-6 (34.4 mbsf). **C.** Section 169-1036C-5X-3 (39.4 mbsf). **D.** Section 169-1036C-5X-4 (41 mbsf). Abbreviations and homologous *n*-alkanes are the same as in Figure 24.

to low levels at shallow depths, with a high value for a carbonate at ~32 mbsf and then an increase to 1% below 45 mbsf. The TOC is low and erratic vs. depth, except for samples from Hole 1036A that show a decrease from 1.2% at the surface to a background below 19 mbsf. These trends and values are similar as reported for the previous Middle Valley sites (Shipboard Scientific Party, 1992b). The increase in N at depth also corresponds to an enhanced content of NH_3 in the interstitial water from that interval (see "Inorganic Geochemistry" section, this chapter). The maxima in the S depth profiles reflect the sedimentary sulfide contents. The depth profiles of C/N and C/S do not show any significant trends for these short holes.

Conclusions

The tygon water sampling tubing from Hole 857D contained water with gas. The gas composition indicates a probable origin from hydrothermal fluid that entered the tube above the midpoint or possibly a source from in situ microbial production. The WSTP sample taken at 620 mbsf in Hole 857D contained a trace of gas interpreted to be from entrained hydrothermal water in the downwelled seawater. The fluids sampled by the WSTP and Los Alamos samplers in Hole 858G contained methane and higher molecular weight hydrocarbons derived from the high-temperature alteration of organic matter. They

also had concentrations of CO_2 similar to CH_4 . The scorched oil odor of solids from the CORK body and from the wash core in Hole 858G was caused by low levels of extractable bitumen comprised of a series of *n*-alkanes and UCM. The source of this hydrocarbon mixture remains unclear.

Hydrothermal petroleum is found in discrete horizons in the sediments of Site 1036, namely at 12–17 mbsf of Hole 1036A (Sections 169-1035A-2H-2 through 2H-5), 24–35 mbsf of Hole 1036B (Sections 160-1035B-3H-4 through 4X-5), and 32–35 mbsf of Hole 1036C (Sections 169-4H-5 through 4H-6), progressively deeper along the transect. This is based on fluorescence and GC fingerprints of bitumen extracts, coupled with the occurrence of black particulate matter (soot) representing the residual organic C after hydrothermal petroleum expulsion. This petroleum has migrated only a short distance ahead of the heat front and resides at an in situ temperature of 100°–150°C. The gas concentration is low and consists mainly of CH_4 and CO_2 . There is no correlation between the CH_4 concentration and the onset of the oil zones, because these sediments are not gas prone "source rocks." However, CO_2 does increase near the oil horizons.

The elemental analyses for C, N, TIC, and TOC are generally low, and S is variable, being high in sulfide zones. The TOC shows a decreasing trend vs. depth for Hole 1036A and an increase at depth in

Table 10. Various parameters for the solvent soluble organic matter in sediments from Holes 1036A, 1036B, and 1036C (Dead Dog Vent Field).

Core, section, interval (cm)	Depth (mbsf)	C _{max} *	C _n range	CPI**	Pr/Ph
169-1036A-					
1H-1, 80-90	0.85	12, 29	8-35	2.05	1.10
1H-3, 145	4.45	12, 31	8-35	1.21	0.53
1H-5, 145	7.45	31, Pr	8-35	2.49	3.17
2H-2, 145	12.45	20	10-37	0.54	0.67
2H-3, 100	13.50	22	15-38	0.51	0.58
2H-4, 145	14.45	Pr, 28	14-38	0.65	1.41
2H-5, 145	16.95	24	8-38	0.84	0.75
3H-2, 145	21.95	24	16-35	0.86	0.25
3H-4, 145	24.95	17	15-35	1.04	1.25
3H-6, 145	27.95	25	16-35	1.02	0.45
4H-CC	32.90	25	16-35	1.11	0.13
169-1036B-					
1H-2, 145	2.95	29	14-35	3.87	2.70
1H-4, 145	5.95	31	15-35	1.97	0.63
1H-5, 145	7.45	31	15-35	2.77	1.22
2H-2, 145	11.65	29	17-35	3.07	0.10
2H-4, 145	14.65	31	17-35	2.45	0.25
2H-6, 145	17.65	Ph, 27	8-35	1.77	0.96
3H-2, 145	21.15	Pr, 27	8-35	1.66	1.21
3H-4, 145	24.15	Pr, 27	8-35	1.15	1.80
3H-6, 145	26.85	24, 15	10-35	0.88	1.88
4X-2, 145	30.65	11, 17	8-38	0.84	2.54
4X-5, 145	35.15	22	8-38	0.84	0.74
5X-1, 145	38.75	11, 24	8-35	0.86	0.94
5X-3, 145	41.75	11, 27	8-35	0.85	0.67
6X-1, 145	46.65	29	17-38	1.05	0.65
169-1036C-					
1H-4, 145	5.95	31	14-35	2.94	0.75
2H-2, 145	9.35	31	14-35	4.24	2.00
2H-4, 145	12.35	31	15-35	2.95	1.80
2H-6, 145	15.35	31	17-35	2.95	0.22
3H-2, 145	18.85	31	11-35	3.68	1.15
3H-4, 145	21.85	Ph, 27	10-35	3.93	0.75
3H-6, 145	24.85	22, 29	16-35	1.98	1.00
4H-3, 145	29.85	Pr, 20	14-35	1.32	2.60
4H-5, 99-100	32.40	23	14-35	1.13	3.30
4H-5, 109-110	32.50	Pr, 23	10-37	1.08	2.70
4H-6, 145	34.35	17	14-35	1.01	2.77
5X-3, 145	39.35	23	17-37	0.91	1.20
5X-4, 145	40.85	12, 24	8-37	1.09	0.25
6X-2, 145	47.55	11, 27	8-38	1.05	0.24

Notes: * = major homologs are listed in decreasing order of concentration (C_{max}). ** = carbon preference index calculated from *n*-C₂₄ to *n*-C₃₃; Pr = Pristane; Ph = phytane.

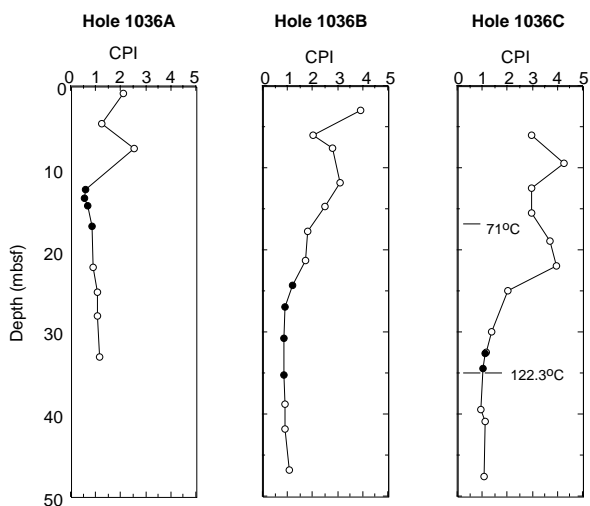


Figure 27. CPI depth profiles for sediments from Site 1036. Solid circles = hydrothermal petroleum.

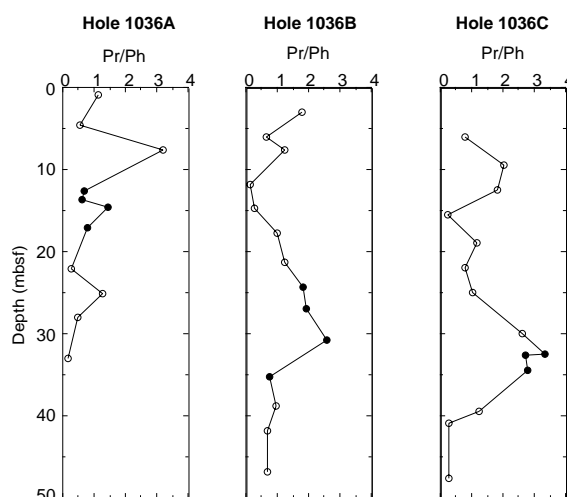


Figure 28. Pr/Ph ratio for bitumen extracts vs. depth for sediments from Site 1036. Solid circles = hydrothermal petroleum.

Hole 1036C. The total N of Hole 1036A is high at the bottom, as is the NH₃ in the pore water.

MICROBIOLOGY

The major objective of the microbiological work during Leg 169 was to examine the microbial community within the DDVF, a hydrothermal upflow zone. Preserved sediment samples from Leg 139 showed that microbes were present in hot sediments to depths of 70 mbsf and to temperatures estimated as high as 170°C (Cragg and Parkes, 1994); the goal for this leg was to confirm this result at a similar site and further characterize the high-temperature microbial communities through culture and DNA analysis. Aboard ship, special attention was given to cultures of thermophilic (growth at 50–90°C) and hyperthermophilic (growth above 90°C) anaerobic microorganisms. Samples also were taken for shore-based microbial counts and electron microscopy. Other opportunities for microbiological sampling presented themselves during the CORK operations at Holes 858G and 857D. The leaking CORK at Hole 858G had previously shown evidence of surficial microbial colonization (K. Becker, pers. comm., 1996); the thermistor strings below the CORKs were also prime substrates for growth of high temperature microbes as they had bathed for >4 yr in borehole fluids with a hydrothermal component.

Holes 1036A through 1036C

Section-top plugs and whole-round cores were taken from Holes 1036A through 1036C as described previously (see “Explanatory Notes” chapter, this volume). Inspection of selected samples by epifluorescent microscopy showed that microbes were present in the hot sediments. At the mudline at Hole 1036C, there are ~10⁷ microorganisms/cm³, comparable to bacterial abundances in other deep ocean sediments (Parkes et al., 1994); microbial abundance drops to 10⁶ microbes/cm³ by 3 mbsf in the same hole. With the exception of the “mudline” at Hole 1036A (rubble derived from anhydrite chimneys from a nearby vent), where microorganisms were present at levels <10⁵/cm³, other samples examined from 0 to 20 mbsf in Holes 1036A–1036C indicate microbial abundances in the range of 5 × 10⁵–10⁶/cm³. These values are close to those reported at similar depths by Cragg and Parkes (1994), although variations in fluid chemistry and thermal gradients between Holes 858A and 858D and Holes 1036A and 1036C make depth-based comparisons tenuous. Samples will be processed in more detail during shore-based studies

Table 11. Weight percent for Holes 1036A, 1036B, and 1036C (Dead Dog Vent Field).

Core, section, interval (cm)	Depth (mbsf)	TC (%)	TS (%)	TN (%)	C/N*	C/S*	TIC (%)	TOC (%)
169-1036A-								
1H-1, 80–90	0.85	2.14	0.03	0.12	17.8	71.30	0.99	1.15
1H-3, 39–40	3.40	1.10	0.00	0.04	27.5	—	0.58	0.52
1H-5, 90–91	6.90	1.49	0.00	0.06	24.8	—	0.80	0.69
1H-6, 39–40	7.90	0.77	0.00	0.04	19.3	—	0.40	0.37
1H-6, 99–100	8.50	1.20	0.00	0.04	30.0	—	0.87	0.33
2H-2, 36–37	11.36	1.83	1.29	0.02	91.5	1.40	1.61	0.22
2H-5, 98–99	16.48	0.28	2.81	0.04	7.0	0.10	0.03	0.25
2H-7, 0–5	18.53	0.10	2.06	0.02	5.0	0.05	0.03	0.07
3H-2, 140–150	21.95	0.10	4.58	0.01	10.0	0.02	0.04	0.06
3H-4, 140–150	24.95	0.16	1.15	0.01	16.0	0.14	0.08	0.08
3H-6, 140–150	27.95	0.15	0.52	0.00	—	0.29	0.06	0.09
4H-CC, 140–150	32.95	0.18	3.06	0.01	18.0	0.06	0.07	0.11
6X-CC, 2–3	38.58	0.16	0.06	0.06	2.7	2.70	0.05	0.11
169-1036B-								
1H-2, 140–150	2.95	0.62	0.00	0.02	31.0	—	0.99	–0.40
2H-2, 49–50	11.70	1.28	0.23	0.04	32.0	5.60	0.83	0.45
2H-4, 140–150	14.65	1.21	0.00	0.04	30.2	—	0.92	0.29
2H-5, 80–81	15.50	0.93	7.21	0.05	18.6	0.13	0.67	0.26
2H-7, 30–31	18.01	0.50	0.44	0.04	12.5	1.10	0.11	0.39
3H-2, 100–101	20.70	0.83	0.71	0.03	27.7	1.20	0.61	0.22
3H-5, 0–5	24.23	0.52	0.75	0.04	13.0	0.70	0.35	0.17
3H-5, 41–42	24.62	0.86	0.05	0.05	17.2	17.20	0.45	0.41
3H-5, 140–150	25.65	2.27	0.00	0.07	32.4	—	1.54	0.73
4X-2, 110–111	30.30	0.39	1.10	0.05	7.8	0.35	0.07	0.32
4X-2, 135–140	30.58	0.98	3.94	0.05	19.6	0.25	0.92	0.06
4X-5, 135–140	35.08	0.27	0.75	0.04	6.8	0.36	0.03	0.24
4X-6, 86–87	36.06	0.26	0.00	0.03	8.7	—	0.03	0.23
5X-3, 74–75	41.05	0.08	1.47	0.01	8.0	0.05	0.04	0.04
5X-5, 79–80	44.10	0.20	1.24	0.01	20.0	0.16	0.02	0.18
6X-2, 33–34	47.04	0.22	0.71	0.01	22.0	0.31	0.05	0.17
169-1036C-								
1H-2, 140–150	2.95	1.01	0.00	0.04	25.3	—	0.70	0.31
2H-2, 60–61	8.50	1.88	0.31	0.05	37.6	6.10	1.36	0.52
2H-4, 121–122	12.12	0.49	1.21	0.03	16.3	0.40	0.20	0.29
2H-4, 140–150	12.35	0.88	0.00	0.04	22.0	—	0.58	0.30
2H-5, 102–103	13.42	0.38	13.27	0.05	7.6	0.03	0.04	0.34
2H-CC, 9–10	15.80	0.52	1.72	0.03	17.3	0.30	0.18	0.34
3H-2, 80–81	18.20	0.47	0.05	0.03	15.7	9.40	0.08	0.39
3H-5, 89–90	22.80	0.63	0.23	0.05	12.6	2.70	0.13	0.50
3H-CC, 9–10	24.30	0.83	0.00	0.04	20.8	—	0.58	0.25
4H-1, 109–110	26.50	0.62	0.00	0.04	15.5	—	0.29	0.33
4H-4, 0–5	29.93	0.61	0.11	0.04	15.3	5.50	0.05	0.56
4H-5, 99–100	32.40	6.41	0.00	0.03	214.0	—	6.26	0.15
4H-5, 109–110	32.50	0.49	0.00	0.05	9.8	—	0.03	0.46
5X-1, 48–50	35.39	0.82	1.93	0.03	27.3	0.42	0.70	0.12
5X-1, 61–63	35.52	0.53	1.22	0.02	26.5	0.43	0.49	0.04
5X-3, 80–81	38.70	0.66	0.41	0.04	16.5	1.61	0.52	0.14
5X-4, 6–7	39.46	0.66	2.59	0.04	16.5	0.25	0.49	0.17
6X-1, 24–25	44.85	0.15	7.87	0.03	5.0	0.02	0.03	0.12
6X-1, 44–46	45.05	0.84	1.16	0.03	28.0	0.72	0.08	0.76
6X-3, 73–84	48.38	1.03	0.45	0.03	34.3	2.30	0.08	0.96

Notes: * = calculated as percentage ratios, and — = no data. TC = total carbon, TS = total sulfur, TN = total nitrogen, TIC = total inorganic carbon, and TOC = total organic carbon.

to determine the variation in microbial abundance with depth, fluid flow, fluid chemistry, temperature, and the relationship to microbial abundances from Leg 139.

High-temperature anaerobic culture was attempted from 26 samples distributed over the three cores, spanning a temperature range estimated to be 50°–150°C. Unfortunately, no direct temperature measurements were available for Holes 1036A and 1036B. Recovered cores were warm to the touch, however, and geochemical evidence supports temperatures of >200°C and >150°C at 20–30 mbsf in Holes 1036A and 1036B, respectively (see “Inorganic Geochemistry” and “Lithostratigraphy” sections, this chapter). None of these attempted enrichment cultures yielded microorganisms. The microbes for which enrichment was attempted included all groups of high-temperature microbes found at deep-sea hydrothermal vents to date (heterotrophic sulfur and sulfate reducers, autotrophic sulfate reducers, and methanogens; Baross and Deming [1995]), but none was observed to grow in culture.

In general, the inability to culture microorganisms is not a good indicator of the presence or absence of microbes, but certain groups of microorganisms grow reliably in culture, and negative culturing results can be meaningful in these instances. The death of thermo-

philic vent-associated microbes in a temperature range that would appear to be hospitable reflects the effect of fluid flow and fluid chemistry on the composition of the microbial community. Microorganisms that are easily cultured from bare-rock submarine hydrothermal environments thrive in high-temperature (50°–150°C) areas of mixing between vent fluid and seawater. The pore-fluid chemistry conducted during Leg 139 and this leg suggests that such regimes are rare in the seafloor within sedimented hydrothermal systems. Although the fluid-flow pattern in the AAV shows a few regions of focused upflow, it is dominated by recharge in the temperature range of 50°–150°C, which can be seen in the fluid chemistry (see “Inorganic Geochemistry” section, this chapter) and inferred from pore-pressure measurements in surface sediments (see “Pore Pressure Measurements Using PUPPIs” section, this chapter).

High-temperature, vent-associated microorganisms require not only a conducive thermal environment but the correct chemistry for growth. Sediments in the 50°–150°C temperature range drilled at Site 1036 may be relatively oxidizing compared with the normal habitats of these microbes (Baross and Deming, 1995), as indicated by the lack of hydrogen sulfide (see “Organic Geochemistry” section, this chapter). Consequently, the lack of any evidence for thermophilic,

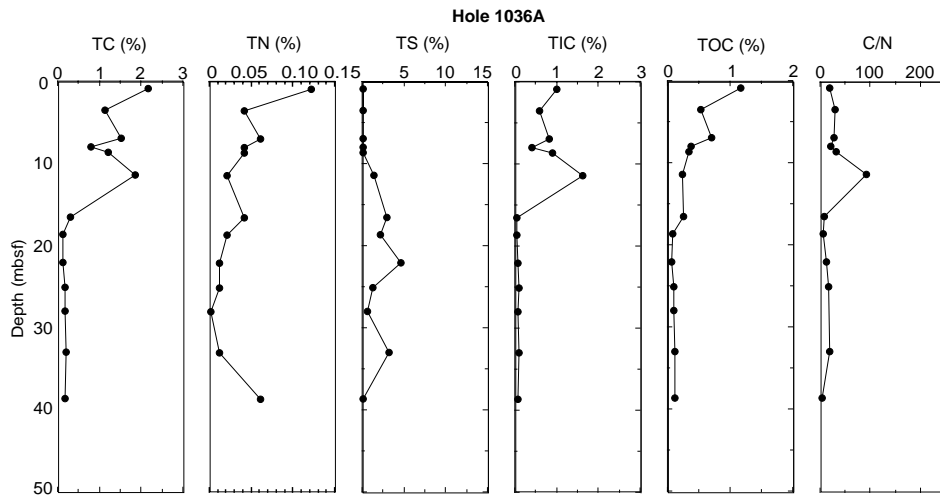


Figure 29. Percentages of total C, N, S, inorganic C, and organic C, and C/N ratio vs. depth for sediments from Hole 1036A.

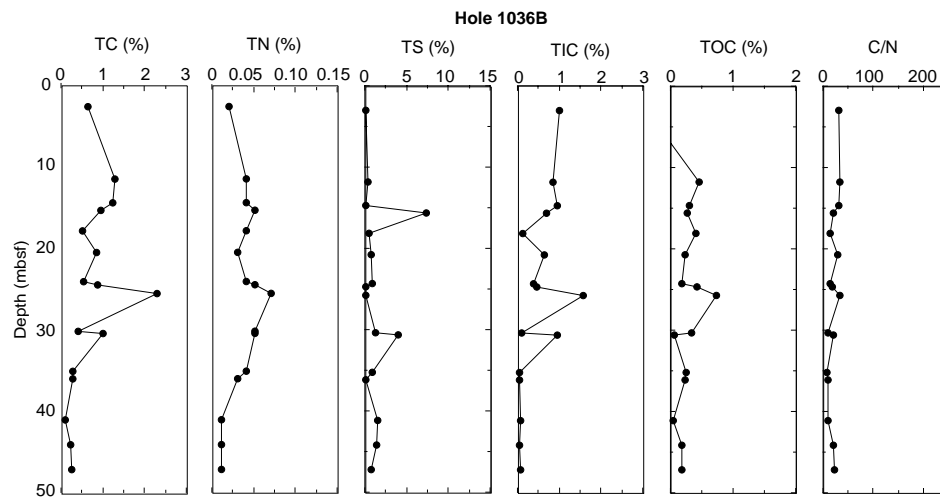


Figure 30. Percentages of total C, N, S, inorganic C, and organic C, and C/N ratio vs. depth for sediments from Hole 1036B.

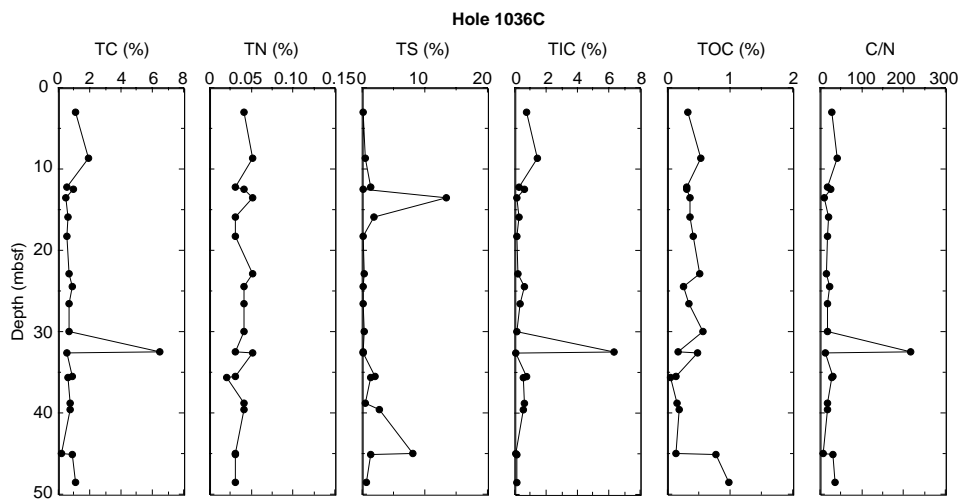


Figure 31. Percentages of total C, N, S, inorganic C, and organic C, and C/N ratio vs. depth for sediments from Hole 1036C.

anaerobic microorganisms in these sediments is consistent with the observed chemistry and our understanding of the biological processes involved.

Hole 858G CORK

A camera survey of the CORK at Hole 858G before retrieval showed that the bacterial mat that was observed coating the exterior of the data logger in 1993 (*Alvin* dive 2665, K. Becker, pers. comm., 1996) was no longer present. When the CORK was retrieved (see "Downhole Measurements" section, this chapter), the associated animal community (limpets and bamboo worms) indicated that the fluids coming into contact with the submersible landing platform were cold and probably depleted in hydrogen sulfide. A small clump of vestimentiferan worm tubes was found on the interior rim of the base of the submersible platform, but it had been uninhabited for some time; the low-temperature, sulfide-rich diffuse venting that the worms thrive on had ceased. The animals were preserved in 4% borax-buffered formalin in artificial seawater.

A high-temperature anaerobic culture was attempted from sulfides at the base of the submersible landing platform from homogenized limpets and other scrapings from the platform; all cultures were negative. Limpets, though not able to live at thermophilic or hyperthermophilic temperatures, often concentrate high-temperature microbes in their guts. This result implies that there was no suitable environment for thermophiles or hyperthermophiles near enough to the CORK for limpets to collect them.

We planned to sample the thermistor string for microbes, as it had been incubating in hydrothermal fluid, but the thermistor string was not recovered from this CORK. The pipe below the CORK was covered in hydrothermal precipitate, which was scraped off and preserved, and samples were also taken from the CORK-hosted sulfide chimney. No high-temperature microorganisms consented to grow from any of these samples. The pipe hanging below the CORK was likely at too high a temperature for standard vent microorganisms to grow; the explanation for the lack of growth from the chimney samples is probably similar. Temperatures around the top of the CORK had been lower at one point, as another clump of vestimentiferan worm tubes (heavily blackened from temperature or sulfide precipitation) was at the top of the retrieved CORK.

Both the WSTP and Los Alamos water samples from this hole consisted of extremely hot fluids (temperatures above 220°C; see "Downhole Measurements" section, this chapter), and these were preserved for later DNA extraction and microbial enumeration. High-temperature microbial enrichment cultures were negative from these samples.

Hole 857D CORK

Sampling for biology from the CORK at Hole 857D was restricted to the thermistor cable and associated water samples, as the body of this CORK contained no hydrothermal sulfide or animals. The animal community on the submersible landing platform would have been interesting for comparison with the samples taken from the platform at Hole 858G, but the landing platform was left on the bottom to avoid tripping pipe. When the thermistor string was fished out of the hole, it was sampled for microbiology at four locations distributed from the top to the bottom of the recovered portion of the string. The Kevlar braid was removed from the cable and preserved for microscopic examination and potential DNA extraction; high-temperature enrichments were also attempted, and two of the 55°C enrichments contained microorganisms.

Fluid was removed from the Teflon fluid sampling tube at three sites along the string between the middle and the bottom, preserved for counts, concentrated for DNA extraction, and used to inoculate high-temperature culture tubes. Enrichment cultures at 55°C from the

water sample near the middle of the string contained thin, 2- μ m rods. The water sample taken from this hole with the WSTP contained cold bottom seawater (see "Inorganic Geochemistry" section, this chapter) and was preserved as a reference. No high-temperature microorganisms were present in cultures inoculated with this sample.

PHYSICAL PROPERTIES

Data from the Multisensor Track (MST) and index properties measurements are reported with supplementary high-resolution information being provided from the Multisensor Split Core Logger (MSSCL) where appropriate. The material analyzed consisted of hydrothermally altered hemipelagic silty clay with interbedded fine sand and altered siltstones and mudstones. In addition, some clastic sulfate sediments (lithologic Unit IV) derived from hydrothermal chimneys were recovered from the top of Hole 1036A (adjacent to the DDV).

The MST logs for Holes 1036B and 1036C show similar profiles of natural gamma and gamma density in the upper 25 m (Figs. 32, 33). These profiles are also very similar to those measured in Hole 858A drilled during Leg 139, which can be considered to be a reference hole for the Dead Dog area (Shipboard Scientific Party, 1992b).

The gamma density logs and the index properties (IP) wet bulk density (WBD) measurements (see Table 12) follow similar patterns, but most WBD measurements are slightly lower than the density measurements from the MST (Fig. 33). This discrepancy can be attributed to the fact that the gamma density data from the MST are not "water corrected" (see "Physical Properties" section, "Explanatory Notes" chapter, this volume). Both measures of bulk density indicate a general increase in all three holes with increasing depth, as would be expected for unconsolidated sediments. This is paralleled by decreases in porosity with depth (Fig. 34), from >70% near the seafloor to 60% or less at 40 mbsf. The greatest decrease in porosity is observed in Hole 1036A, in which porosity drops abruptly from near 60% to <40% at ~30 mbsf, near the contact between lithologic Units I and II.

An interval of relatively high wet bulk density, up to 2.5 g/cm³ on the gamma logs, occurs within lithologic Unit I, at depths of ~20 mbsf in Hole 1036A, near 15 mbsf in Hole 1036B, and ~14 mbsf in Hole 1036C. These depths correspond to similar absolute elevations relative to sea level. One index properties sample from Hole 1036B (Sample 169-1036B-2H-4, 75–77 cm) also had a high porosity (Fig. 34) and a high grain density (Fig. 35) within this zone. This zone contains nodules in all three holes, consisting of pyrite and anhydrite in Hole 1036A, pyrite and carbonate in Hole 1036B, and sulfide, carbonate, and dolomite in Hole 1036C. Other intervals with high gamma density also generally contain nodules.

A natural gamma maximum occurs in Hole 1036C between 27 and 35 mbsf and in Hole 1036B at ~26 mbsf (Fig. 32). These maxima are located near the contact between lithologic Units I and II. No natural gamma high is apparent near the contact between lithologic Units I and II in Hole 1036A (Fig. 32), presumably because core recovery and, hence, MST log data, are limited in this interval. However, a natural gamma maximum appears in this hole at ~12 mbsf, where a few 1–3 cm dolomite nodules were found. The zone of relatively high natural gamma in Hole 1036A is quite close in elevation to the more subtle highs in Holes 1036B and 1036C between 2 and 4 mbsf. Calcite concretions were observed within this interval in Hole 1036C.

Grain densities determined for index properties samples (Fig. 35) generally cluster around values of 2.8 g/cm³ with a very slight trend of increasing density with increasing depth.

Thermal conductivity measurements (see Table 13) in all three holes fluctuate ~1 W/(m·K), with slight increases with depth in Holes 1036B and 1036C (Fig. 36). Two relatively high values of thermal

conductivity, over 1.5 W/(m·K), were measured ~25 mbsf in Hole 1036A, in a zone of relatively low porosity.

The most striking aspect of the MST logs is the distinct character of the magnetic susceptibility record, including the very low values below ~10 mbsf in Holes 1036A and 1036B and below 27 mbsf in Hole 1036C (Fig. 37). The magnetic susceptibility profile of the upper 35 m of Hole 1036C is similar in character to the profile for Hole 858A (also shown in Fig. 37), with two major zones of high magnetic susceptibility, each underlain by a zone of lower magnetic susceptibility.

The magnetic susceptibility profiles may reflect both an initial sedimentary signature and subsequent thermal alteration. Low values of magnetic susceptibility (MS wipeout zones) in the profiles at Site

1036, relative to those of Hole 858A for the same lithostratigraphic intervals, become shallower in cores taken closer to the vent, which may be consistent with the shallowing of isotherms near the vent. Taking the top of the wipeout zone to be at ~9 and 18 mbsf in Holes 1036A and 1036B, respectively, consistent with results from ship-board measurements of the remanent magnetization (see “Paleomagnetism” section, this chapter), the boundary of this alteration zone is parallel to but slightly shallower than the top of the anhydrite zone described in the “Lithostratigraphy” section (this chapter). Projection of the wipeout zone boundary to Hole 1036C would also explain the persistent low values of magnetic susceptibility below 35 mbsf, in contrast to the reference profile from Hole 858A, in which a zone of high magnetic susceptibility was found in lithologic unit II between 36 and 44 mbsf. The positions of the two narrow zones of magnetic susceptibility peaks in the deeper portions of Holes 1036A and 1036B also appear to parallel the top of the anhydrite zone, which is interpreted as an approximate isotherm (see “Lithostratigraphy” section, this chapter). This could be the result of magnetic mineral precipitation that is at least partially controlled by temperature. Similar peaks, if they occur at the location of Hole 1036C, would be at the base of or below the interval sampled during drilling.

It is probable that although the decrease in magnetic susceptibility amplitude is caused by hydrothermal alteration effects, the changes in character could provide additional useful information. The decrease in magnetic susceptibility probably reflects the alteration of

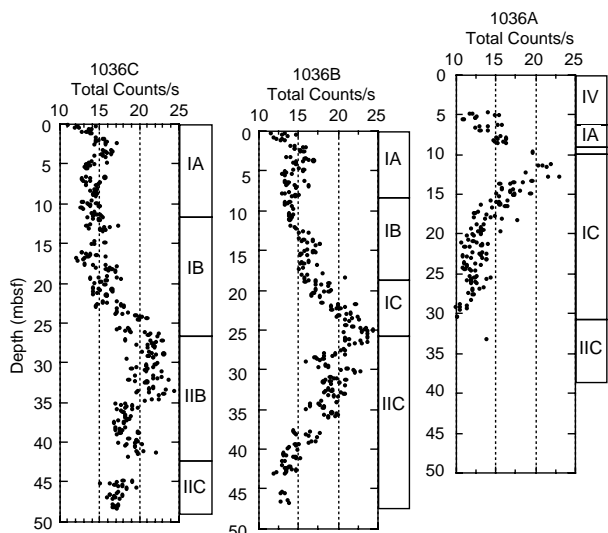


Figure 32. MST natural gamma measurements for Holes 1036A, 1036B, and 1036C plotted vs. depth below seafloor. Measurements are reported in total counts per second. Relative elevations of the holes shown on the figure correspond to absolute elevations relative to sea level. Lithologic unit numbers are also shown to the right of the profile for reference.

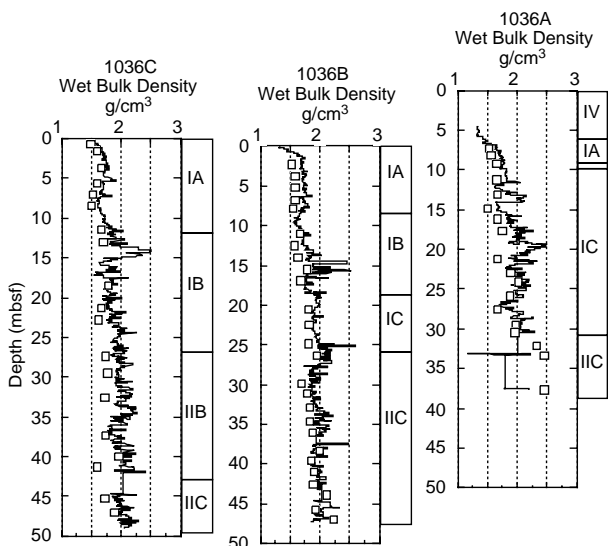


Figure 33. MST gamma density (solid lines) and index property wet bulk density (open squares) for Holes 1036A, 1036B, and 1036C plotted vs. depth below seafloor. Relative elevations of the holes shown on the figure correspond to absolute elevations relative to sea level. Lithologic unit numbers are also shown to the right of the profile for reference.

Table 12. Index properties measurements, Holes 1036A, 1036B, and 1036C.

Core, section, interval (cm)	Depth (mbsf)	Porosity (%)	Wet bulk density (g/cm ³)	Grain density (g/cm ³)	Wet water content (%)	Void ratio
169-1036A-						
1H-5, 119-121	7.19	76	1.51	2.80	33	2.9
1H-6, 60-62	8.10	76	1.55	2.78	33	2.7
1H-7, 15-17	9.15	70	1.65	2.83	30	2.1
2H-2, 20-22	11.20	64	1.64	2.86	27	1.8
2H-3, 58-60	13.08	72	1.66	2.91	31	2.3
2H-4, 80-82	14.80	73	1.49	2.76	33	2.7
2H-5, 62-64	16.12	71	1.65	2.83	30	2.2
2H-6, 60-62	17.60	66	1.74	2.84	27	1.8
3H-2, 60-62	21.10	72	1.66	2.83	30	2.2
3H-3, 92-94	22.92	60	1.88	2.84	21	1.3

Only part of this table is produced here. The entire table appears on CD-ROM.

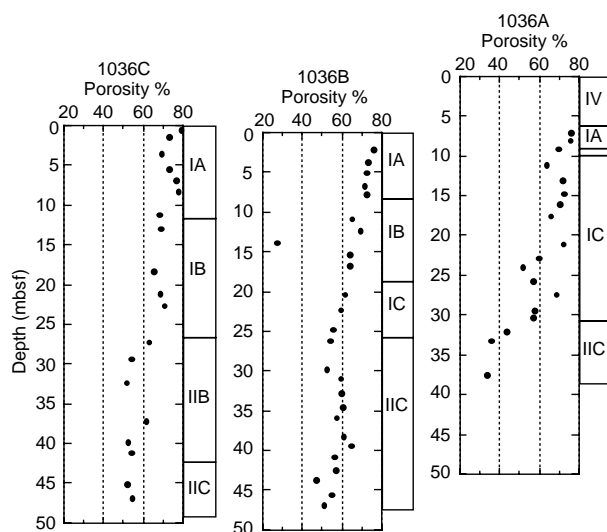


Figure 34. Index properties measurements of porosity in Holes 1036C, 1036B, and 1036A. Relative elevations of the holes shown on the figure correspond to absolute elevations relative to sea level. Lithologic unit numbers are also shown to the right of the profile for reference.

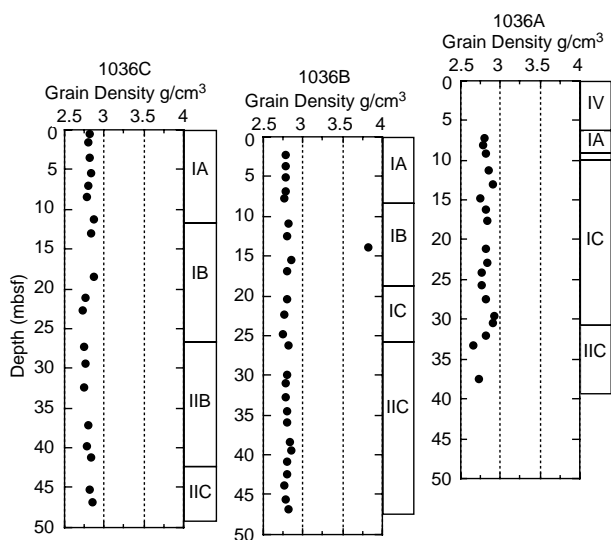


Figure 35. Index properties measurements of grain density in Holes 1036A, 1036B, and 1036C plotted vs. depth below seafloor. Relative elevations of the holes shown on the figure correspond to absolute elevations relative to sea level. Lithologic unit numbers are also shown to the right of the profile for reference.

iron oxides to pyrite and is consistent with a decrease in the pore-water sulfate content (see “Inorganic Geochemistry,” this chapter). Why the boundaries between the low magnetic susceptibility wipeout zones and the “normal” active zones are so sharp is unclear, but they do not appear to correlate with any obvious sedimentological changes.

To illustrate the changes in character between the normal magnetic susceptibility zones and the wipeout zones, a region of magnetic susceptibility and gamma density data in Hole 1036C has been plotted at an expanded scale (Fig. 38). The section between 19 and 24 mbsf has a magnetic susceptibility profile that correlates well with the gamma density profile, with higher magnetic susceptibility values corresponding to higher gamma density values, consistent with the presence of heavy minerals including magnetite and ilmenite in these sections of sediment. However, between 30 and 35 mbsf, there is virtually no magnetic signature at all, despite a gamma density profile similar to that in the shallower zone. From a sedimentological viewpoint, there is no reason to believe that the original mineral provenance of the sediments in the slightly deeper region is any different from the shallow region. Although the magnetic properties were destroyed, we conclude that the differences caused by mineral alteration effects did not change the general proportions of heavy minerals in the sediment.

Table 13. Thermal conductivity measurements, Holes 1036A, 1036B, and 1036C.

Hole	Core	Type	Section	Position (cm)	Depth (mbsf)	Thermal conductivity (W[m·K])
A	1	H	5	120	7.20	0.79
A	1	H	6	60	8.10	1.04
A	1	H	7	15	9.15	1.23
A	1	H	6	130	8.80	0.88
A	2	H	2	20	11.20	1.05
A	2	H	4	80	14.80	0.95
A	2	H	5	62	16.12	1.07
A	2	H	6	60	17.60	0.96
A	2	H	3	85	13.35	1.08
A	3	H	2	60	21.10	0.96

Only part of this table is produced here. The entire table appears on CD-ROM.

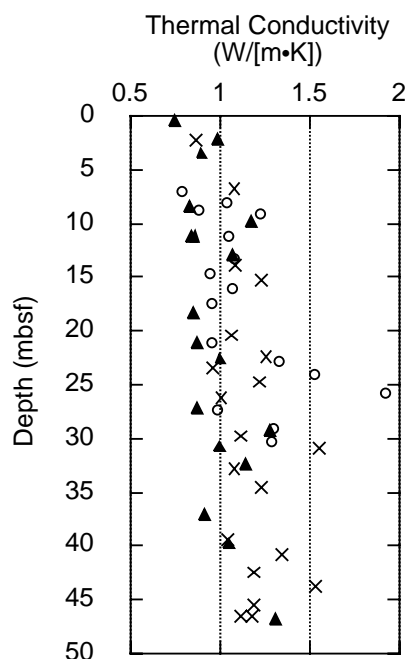


Figure 36. Thermal conductivity measurements for holes at Site 1036 showing plot vs. depth below seafloor. Open circles = Hole 1036A, × = Hole 1036B, and solid triangles = Hole 1036C.

As noted previously, the other interesting phenomenon in the magnetic susceptibility profiles is the relatively high peaks that occur intermittently in a few places within the wipeout zones in the two holes closer to the active vent. In particular, these peaks occur between 18 and 22 mbsf in Hole 1036A and between 25 and 34 mbsf in Hole 1036B. To investigate the detailed nature of these peaks, we looked closely at the two peaks in Section 169-1036B-3H-6 at 26.1 and 26.6 mbsf using the MSSCL. Figure 39 shows gamma density and magnetic susceptibility (both loop and point sensor data) profiles for this section logged at 5-mm increments. It is apparent that although the magnetic susceptibility peaks appear to have little fine-scale structure when logged using the loop sensor, there is a significant amount of structure at the subcentimeter scale as demonstrated clearly by the point sensor. To evaluate the repeatability of this subcentimeter structure, the core section was run through the MSSCL twice using the same set up parameters. The excellent repeatability of these measurements is clearly demonstrated in Figure 39. To further analyze the nature of the magnetic susceptibility structure, a similar log was made on the same interval of the working half. This shows a similar zone of magnetic susceptibility activity, but with a different detailed subcentimeter structure. Examination of the core showed disseminated hexagonal grains of pyrrhotite in significantly higher abundance within the narrow zones of higher susceptibility. The structure of the magnetic susceptibility peaks, therefore, may simply reflect the distribution of pyrrhotite grains within the sediments. Confirmation of this hypothesis would require more detailed rock magnetic analyses of these intervals to rule out significant contributions from other magnetic minerals.

DOWNHOLE MEASUREMENTS CORK Reinstrumentation

Reinstrumentation of the CORKs deployed in Holes 858G and 857D during Leg 139 in 1991 was a primary objective of Leg 169.

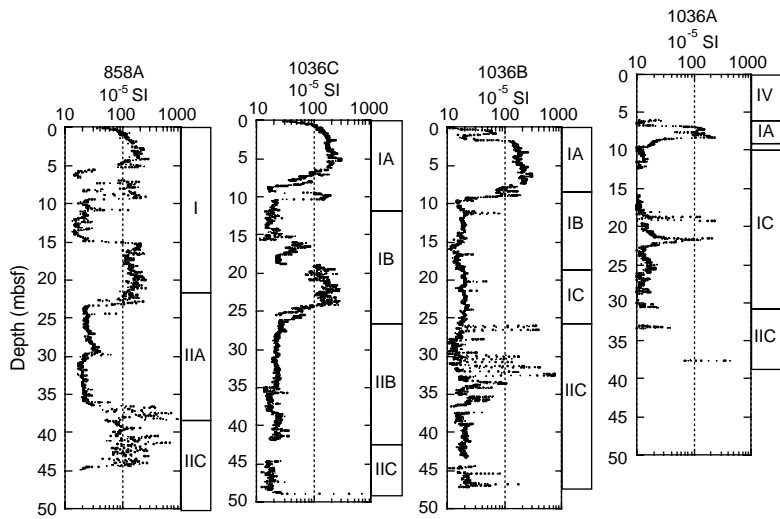


Figure 37. MST profiles of magnetic susceptibility for Holes 858A (Leg 139), 1036A, 1036B, and 1036C. Relative elevations of Holes 1036A, 1036B, and 1036C shown on the figure correspond to absolute elevations relative to sea level. Relative elevation of Hole 858A is adjusted to show the similarity of susceptibility profile to that in Hole 1036C. Lithologic unit and subunit numbers are also shown for reference.

The removal of data loggers and thermistor cables from the old CORKs provided the opportunity to obtain in situ temperature logs and undisturbed fluid samples (see “Inorganic Geochemistry” section, this chapter) from the boreholes before resealing them with new instruments. Hole 858G reCORKing operations at the active Dead Dog hydrothermal site were scheduled first, to be followed by drilling operations at Hole 856H on the inactive BHMS while pressure and thermal conditions at Hole 858G equilibrated. The proposed Leg

169 hole-to-hole hydrologic experiment would continue with the unCORKing of Hole 857D, a reference hole located 1.6 km to the south and outside of the active discharge zone. The temperature and pressure data acquired from reCORKed Hole 858G may detect the transient overpressure induced by the introduction of cold seawater into Hole 857D as it was unsealed and deepened. The intent was to restimulate downhole fluid flow into a fault zone at 610–615 mbsf that was accepting flow measured at 20,000 < 1/min when the hole was drilled

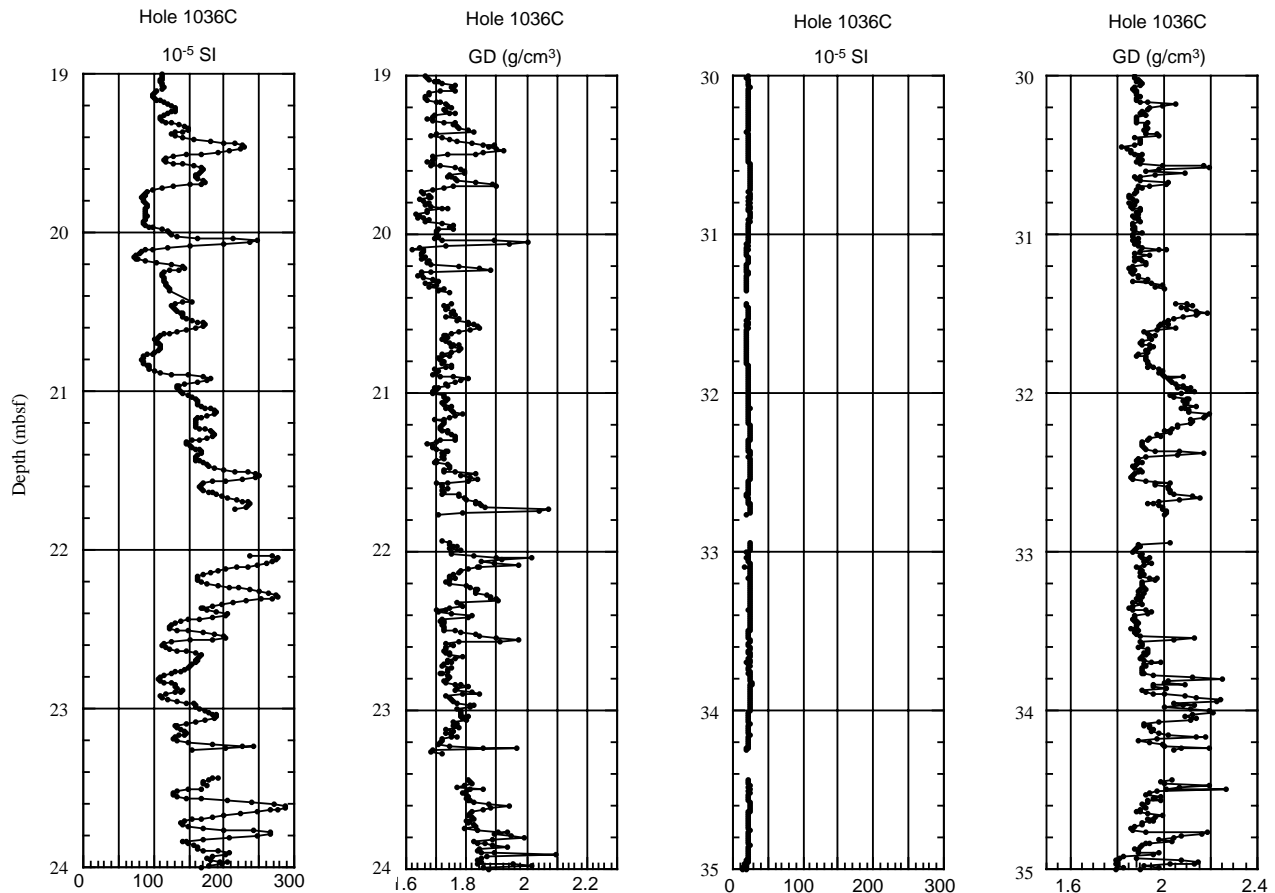


Figure 38. Gamma density (GD) and magnetic susceptibility records from the MST of two selected portions of Hole 1036C, illustrating the change in character between “normal” and MS “wipeout” zones caused by hydrothermal alteration effects.

ature limit of 120°C; the mode of failure at temperatures estimated near 200°C would have been over-aging rather than extrusion (T. Pettigrew, pers. comm., 1996). Fine-grained hydrothermal precipitates were observed on the CORK release rods. Hydraulic hoses of 1-in and 2-in diameter were missing, and hose fittings, nuts, and metal surfaces on the release rods, in the manifold, and along the inside of the CORK housing were corroded.

The shipboard microbiologist sampled the outer and inner surfaces of the CORK body and the submersible/remotely operated vehicle (ROV) landing platform; several species of low-temperature benthic worms and limpets common to vent areas were present. The empty tubes of vestimentiferans, low-temperature, sulfide-dependent vent worms, were observed on the submersible/ROV landing platform and the edges of the CORK chimney (see "Microbiology" section, this chapter). Sediment samples taken by the shipboard paleontologist were barren of foraminifers (see "Biostratigraphy" section, this chapter).

Description of the CORK-Hosted Hydrothermal Chimney Deposit

The inside of the lower CORK housing sitting above the seafloor was encrusted with hydrothermal minerals and formed the first known example of a CORK-hosted sulfide + sulfate chimney (Fig. 42A). The precipitates were predominantly anhydrite with abundant pyrrhotite and pyrite. An open flow channel characterized by the radial growth of hydrothermal minerals had a structure similar to a vent formed at the seafloor.

The width of the host pipe is ~55 cm (21 in), and within this conduit sulfides and anhydrite had precipitated on the inner surfaces to form an irregular chimney structure with walls that varied in thickness from 4 to 10 cm thick. The total length of the chimney was ~170 cm (70 in), and sampling was conducted down the vertical length using a hammer and chisel-type/brute force method. Sample depths were recorded from a 2-m ruler placed down the central conduit (Fig. 42A). Samples from different intervals were bagged and then placed in half-core liners and cut, curated, and sampled for shipboard and post-cruise studies according to ODP curatorial procedures. The samples were curated as Cores 169-858G-17W and 18W. Pieces of corroded, wire-reinforced hydraulic tubing believed to originate in the data logger landing collar were entrained in these deposits. Hose material from the CORK also was observed in polished thin sections.

Three polished thin sections were made from the hydrothermal material sampled from the CORK. The first of these, from 58 to 63 cm downsection from the top of the chimney, is completely composed of anhydrite that forms an interlocking open network of euhedral lath-shaped and fibrous crystals. No opaque minerals were preserved in the thin section. Between 61 and 123 cm depth, pyrrhotite, sphalerite, and pyrite were observed intergrown with anhydrite. The pyrrhotite occurs as two different morphologies: fine-grained aggregates and more common coarse-grained hexagonal crystals. Pyrite partially replaces the pyrrhotite. The mineralogy between 123 and 129 cm is similar; predominantly pyrrhotite and sphalerite with trace pyrite and anhydrite. Hexagonal crystals of pyrrhotite (0.02 to 0.1 mm) occur with finer grained pyrrhotite aggregates that have dark inclusions in the cores. Zinc sulfide also was observed with an hexagonal crystal form suggesting either primary wurtzite or sphalerite after wurtzite.

No chalcopyrite was observed from the chimney deposit in the CORK housing, which may indicate that the temperatures of the fluids were cooler than at depth when these sulfides precipitated. The presence of anhydrite within the chimney deposit indicates temperatures of precipitation in excess of 150°C. Hexagonal pyrrhotite is precipitated at temperatures above 253°C (Barton and Skinner, 1979). The chimney deposit therefore was probably formed at temperatures >250°C, but <300°C. This observation coincides with the temperature measurements made during Leg 169 that indicate fluid temperatures over 220°C at 20 m into the casing, and that the borehole is es-

entially isothermal at 272°C at depths below 85 mbsf. The presence of precipitated sulfide from deep within the casing may indicate that the casing is no longer hydrologically isolated from the sedimentary formation.

Leakage of the First CORK at Hole 858G

Two causes for the failure of the Hole 858G CORK suggested in the Ocean Drilling Program Leg 169 Scientific Prospectus (an informal publication through ODP) are shown schematically with numbered arrows in Figure 41. These schemes are largely based on the initial interpretation of CORK data retrieved during the 1993 *Alvin* dive. A pressure drop prior to an increase in long-term pressure and temperature has been inferred. The first premise holds that fluids moved vertically between the 11¾-in casing and the formation from deep in the borehole. The second premise has fluid migrating upward in the lower CORK body past failed seals. The CORK has two sets of major seals below and above the latch ring that are used to latch the CORK into the casing hanger during deployment and prevent upward displacement of the CORK body caused by pressure buildup in the borehole. The lower seals are located between the CORK and the 11¾-in unperforated casing, and the upper seals between the CORK body and the 20-in-wide reentry cone conductor pipe.

Analyses of the CORK records since the prospectus was written, and the location of hydrothermal deposits in the recovered CORK body, suggest that fluid leakage occurred around the casing before seal failure. Pressure in the borehole was increasing and super-hydrostatic for ~4.5 months prior to failure and reached a maximum of 50 kPa above hydrostatic. Terminal failure resulted as a 20-kPa pressure drop in 1 hr, followed by a more gradual drop to hydrostatic pressure over a 12-hr interval. The amplitude of the tidal signal was ~20% in the 6.5 months before the failure, indicating a sealed system; it increased to 100% at failure. Data logger temperatures increased for 6.5 months preceding failure from a background value of greater than 1°C to a local peak of 10°C and then decreased to 6°C. The terminal pressure drop was accompanied by an increase in logger temperature from 6°C to ~12°C. It is unlikely that fluids flowed into the chimney area from the borehole before, during, or after Hole 858G was uncORKed, as no indication of flow paths, in the form of precipitates, was observed below or immediately above the lower CORK seals.

An alternative explanation is sketched as Premise 3 in Figure 41. The following discussion draws on information provided by E. Davis, K. Becker, A. Fisher, T. Pettigrew, and R. Zierenberg that was used as justification to reCORK the hole. Shallow-level, high-temperature fluids began to flow laterally into the annulus between the 16-in and 11¾-in casing from the known permeable zone drilled between 25 and 50 mbsf (Shipboard Scientific Party, 1992b). One avenue of entry could have been through a breach in the 16-in casing hanger located at 25 mbsf (L. Holloway, pers. comm., 1996); after several months, the formation warmed up and the water exiting through the CORK assembly may have approached the >200°C temperature of the incoming fluid. Mixing of these fluids with seawater entering through the reentry cone and orifices in the bulkhead and lower anchor ring at the sediment/water interface (Fig. 41) kept the data logger at temperatures <12°C. In contrast, the CORK body below the mud skirt was in contact only with the rising fluids and heated sediment, and the upper main seals softened and failed entirely at 6.5 months with 50 kPa pressure across them. The lower seals may have failed previously, allowing uphole flow to follow a "straight" path inside the 11¾-in casing through orifices in the manifold and adjacent latch ring. This flow merged with the annular fluid flow between the two casing strings and traveled past the upper seals. Logger temperatures increased sharply, and continued to rise slowly to ~15°C at the time of data recovery.

The influence of Hole 858F on the hydrogeologic regime at Hole 858G since installation of the first CORK in 1991 remains unclear. This uncased exploratory hole was drilled 10 m north of Hole 858G

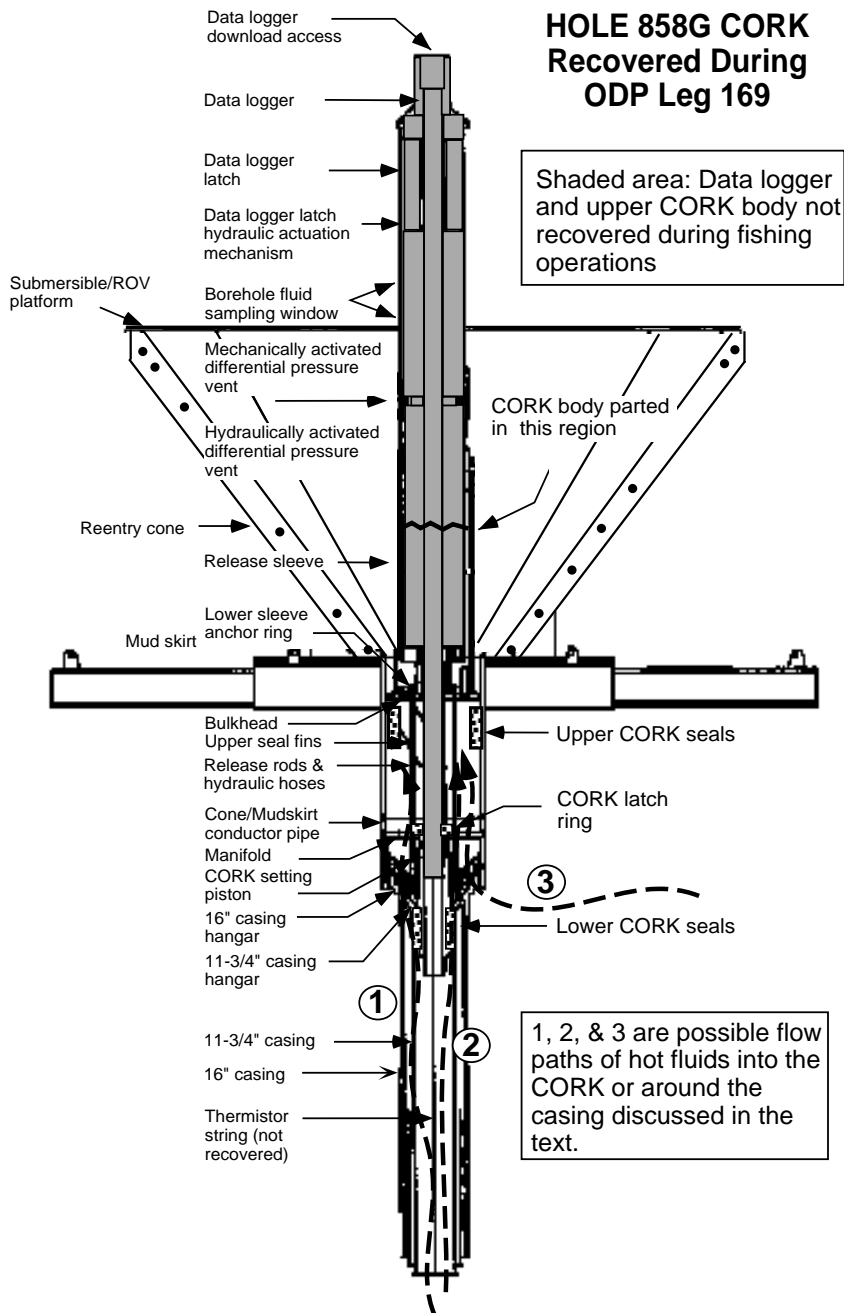


Figure 41. Schematic diagram of the Hole 856G CORK deployed during Leg 139 and reinstrumented during Leg 169. The zigzag black line estimates where the CORK body parted during recovery operations; shaded areas represent the data logger and upper CORK body that were successfully fished, but lost from the fishing tool during retrieval. The thermistor string and sinker bar were left in the borehole. Dashed arrows labeled 1, 2, and 3 show possible flow paths of high-temperature fluids (discussed in the text) that resulted in failure of the CORK and venting of fluids above the reentry cone in the vicinity of the data logger.

and not adequately sealed with cement; the downward flow of cold seawater into the formation through this hole severely affected the short-term pressure and temperature records collected by a submersible three weeks after CORK installation (Davis et al., 1992). The data near the end of the 300-day record retrieved by the *Alvin* in 1993 suggest that Hole 858F may have collapsed in on itself, causing eventual decreases in the tidal signal amplitude and temperature data from Hole 858G and its rise to overpressure, or perhaps allowing Hole 858G to seal itself (E. Davis and A. Fisher, pers. comm., 1996). Examination of data after reCORKing will be the only way to determine

if Hole 858G is sealed; tidal signal attenuation and overpressure will indicate successful reinstrumentation.

Hole 858G Redeployment

ReCORKing operations occurred on 3 September, shortly after in situ temperature measurements and water sampling were conducted. A rotary drill bit and bottom-hole assembly were run into the reentry cone, and circulation and rotation were needed to penetrate past an obstruction encountered at 205 mbsf during the UHT-MSM temper-

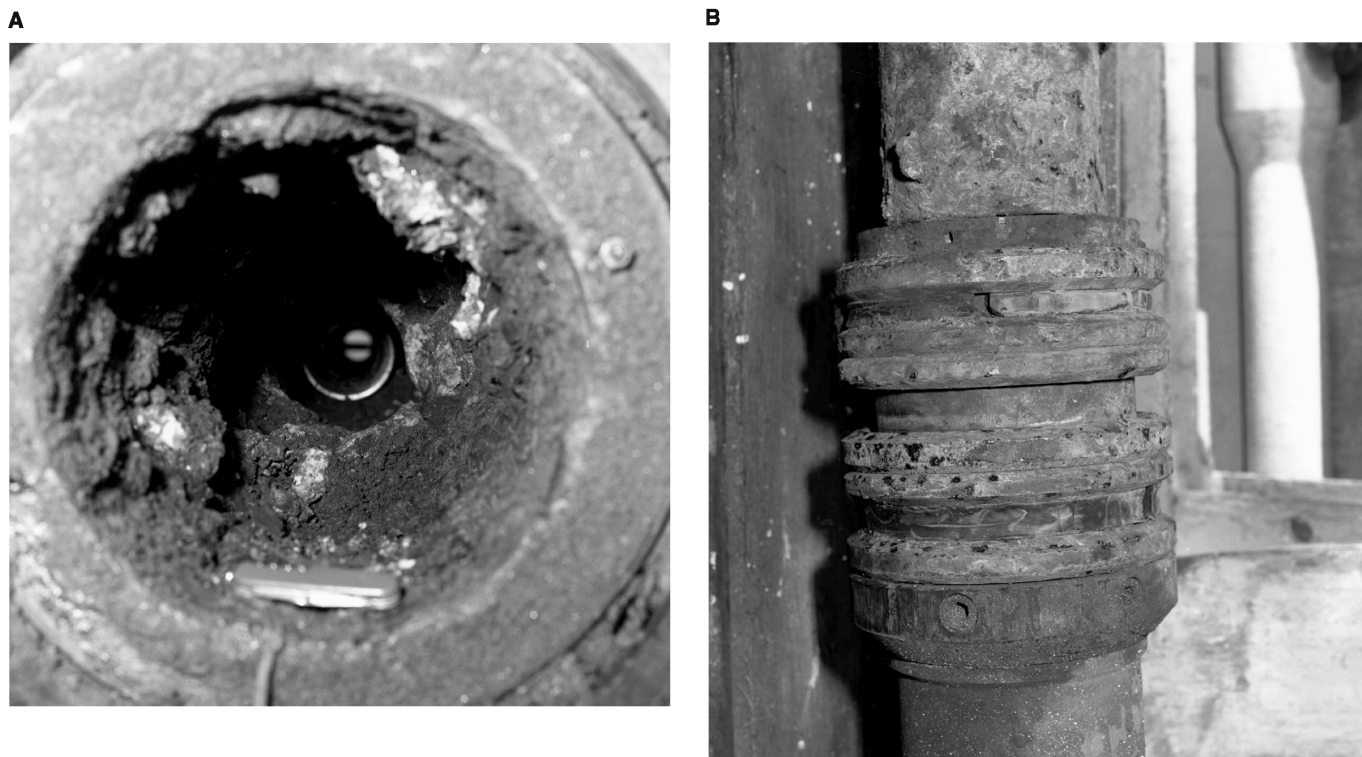


Figure 42. Original Hole 858G CORK after recovery during Leg 169. **A.** Looking down the release sleeve of the body of the CORK showing the sulfide + sulfate precipitates comprising the first observed CORK-hosted hydrothermal vent. An open flow-channel is located at the upper right of the inner wall of the pipe. The annulus in the bulkhead in which the data logger was seated is near the center of the photograph; note that no deposits are visible. A pocket knife is included for scale; the knife is 3.5 in (8.9 cm) long. **B.** Lower main CORK seal assembly located above the stinger and below the 16-in and 11.75-in casing hangars. A baked seal fragment is visible in the seal groove on the left; the seals were extremely brittle, slightly mineralized with fine-grained pyrite, and cracked into shards upon sampling. Corrosion and pitting of the metal surfaces is also visible.

ature log. The hole was drilled to 387 mbsf and cleaned via circulation.

Core 169-858G-19W, a wash core recovered from an unlined core barrel on 4 September from 236 to 296 mbsf, contained loose aggregates of fine-grained pyrrhotite and pyrite with minor anhydrite, along with pieces of thermistor cable jackets and sheaths, wire insulation, and insulating tape. A thin section of a clast from this core revealed that pyrite is the dominant sulfide mineral and that some framboids were observed. Laths and irregular aggregates of pyrrhotite and spheroidal and framboidal pyrite are abundant. Fine-grained chalcocopyrite, sphalerite, and a few grains of galena were also identified. However, the material was not very conducive to being thin sectioned, and minimal opaque mineralogy was preserved. Fluid sampled from the wash core had low magnesium contents consistent with a high temperature origin. Dilution with seawater was relatively small (see "Inorganic Geochemistry" section, this chapter).

Deployment of the new Hole 858G CORK took ~21.5 hr and was performed mostly by Sedco and ODP personnel along with logging scientists responsible for the instrument packages. At the beginning of thermistor string deployment, the stinger below the CORK was lowered into the borehole with the CORK body just above the reentry cone. The box containing the thermistor cable was positioned on the porch outside the Downhole Measurements Lab, the data logger with some slack cable was placed inside the lab, and the iconel sinker bar was out on the rig floor. Lifting tools and grippers, consisting of four bundled 6-ft fine-gauge strands of Kevlar "rope" descending from an eye loop, were used to feed the thermistor string up into the derrick and down into the pipe. The snakes were braided onto the cable while avoiding thermistors and secured with electrical tape and nylon seizing cord so that no slippage would occur along the polyurethane-impregnated cable as tension was applied.

The rig crew attached the sinker bar to the eye loop at the end of the thermistor cable, installed a gripper at ~25 m up the cable, rigged the gripper and cable over a lifting tool, and used the tugger to pick up the sinker bar and seat it in the pipe. The tugger was lowered as the sinker bar and cable were fed down the pipe until the first gripper reached the rig floor. A second gripper was attached ~25 m up the string from the first one and rigged to the second lifting tool. Another tugger was used to pick up the second lifting tool until tension on the first gripper was relieved; it was then untied and removed from the lifting tool. The second lifting tool was lowered until the second gripper was at the rig floor. This process was repeated until the data logger was ready to be deployed. A core barrel clamp was attached below the landing shoulder of the data logger, and it and the slack thermistor cable were picked up with a tugger. The data logger was lowered and positioned in the top of the pipe resting on the clamp. A final check of the logger electronics on the rig floor was performed with a ZEOS laptop computer with a DB9 serial port and a communication cable with custom connector. The communication cable was attached to the logger, and the connector was manually held in place until the short script of interrogatory commands was satisfactorily responded to by the logger. The rig crew rigged the logger to the coring line and ran it down the pipe into the CORK. The successful free-fall deployment of a new submersible/ROV landing platform was confirmed by the VIT camera, and operations at Hole 858G were completed on 5 September.

Hole 857D Recovery

CORK fishing operations at Hole 857D began on 5 September in calm seas and took a little less than 2 days in a complex series of recovery attempts. VIT images clearly showed the canted uppermost

portion of the CORK above the reentry funnel, and a long length of light-colored line that was used and abandoned during the 1993 *Alvin* visit after an attempt to pull the data logger out of the CORK body. The bent upper CORK required that the fishing tool be emplaced over the CORK at an angle, and difficulties latching on were encountered. Similar problems at Hole 858G were linked to interference from the submersible/ROV platform, and a decision was made to remove the platform. To save a pipe trip, the grappling tool was lowered and the platform was dislodged and finally placed 70 m southwest of Hole 857D on 6 September. A fishing attempt was made upon the return to Hole 857D; VIT camera observations showed that the *Alvin* line and the upper portion of the CORK were engaged in the pulling tool, and the pipe was pulled.

The data logger and the upper CORK arrived at the moonpool, but the thermistor cable and sinker bar, as well as the packer union and the stress termination cylinder of the lower CORK body, were left behind in the hole. An attempt was made to dump the data from the logger after the instrument was cleaned up in the Downhole Measurements Lab, but a communication link could not be established. The electrical termination cylinder was removed from the bent data logger, and the potentially reusable 20 thermistor leads inside an oil-filled rubber boot were cut where the leads enter a Teflon dam at the bottom of the boot. The leads were severed ~8 in below the dam during recovery operations. Approximately 24 hr elapsed between the reCORKing of Hole 858G and the removal of the data logger at Hole 857D.

Fishing tools were modified, and after two pipe trips and almost 24 hr, the remainder of the CORK was successfully removed on 7 September. However, the lower CORK fell out of the fishing tool on the pipe trip out of the hole, and may now reside on the seafloor southwest of Hole 857D.

The location of the 300-m-long thermistor string and sinker bar was of paramount concern as preparations were made for temperature logging and water sampling. A wireline spear run in the hole encountered resistance at 16 mbsf; the fish was secured by rotating the tool in the borehole. As the tool was brought to the seafloor, VIT images showed that the fish was part of the thermistor string. Approximately 225 m of the cable was recovered at the rig floor upon the pipe trip out of the hole. Sections of the fluid sampling tubing were clamped and cut as water chemistry samples, and the shipboard microbiologist collected discrete and scraped samples. The thermistor string was subsequently stored in a crate on the helipad.

The thermistor string contained all of its original components in the upper part of the recovered section and was severed at the lower end. The cable, made by Cortland Cable, has an outer diameter of 2 cm, and was especially designed for high-temperature and chemically hostile conditions (Davis et al., 1992). It consists of a central strength member of uniaxial Kevlar rope covered by FEP. Teflon insulation (rated to 200°C) and 10 independent pairs of conductors leading from 10 thermally aged Thermometrics thermistors. The thermistors are encapsulated in epoxy within teflon cylinders and incorporated with the cable inside a protective braid of Kevlar. The fluid sampling tubing, also made of FEP teflon, was attached to the Cortland cable with tie wraps and Teflon tape during Leg 139 (Shipboard Scientific Party, 1992a). Upon recovery, the Kevlar components showed progressive temperature degradation with depth and had a flaky texture. The Kevlar braid was gone in portions of the thermistor string recovered from the deepest parts of the hole, and the uniaxial Kevlar was powdery. The thermistors and conductor leads were in good condition, as were the fluid sampling tubing, tie wraps, Teflon tape, and even the black polypropylene rope incorporated as grips in the original Leg 139 deployment.

The shipboard paleontologist took two samples of the mud inside the large-diameter pipe comprising the upper CORK. The samples from the top and bottom of the pipe both contained typical Holocene subsurface foraminifer assemblages (see "Biostratigraphy" section, this chapter).

The presence of precipitated anhydrite in the water-sampling tube from Hole 857D after recovery of the thermistor string suggests that the hole may have been leaking water before reinstrumentation, perhaps since the failed reCORKing attempt during Leg 146. If this is true, the pressure pulse believed to be generated after the unCORKing and reCORKing of Holes 858G and 857D may not exist.

Hole 857D Redeployment

CORK installation operations at Hole 857D began on 10 September, following temperature measurements, water sampling, and a 2-day coring operation at Hole 1035A, and were completed in 18.5 hr. Clean hole conditions sufficient for deployment of the 898-m replacement thermistor were established after drilling out an obstruction in the cased portion of the hole below 377 mbsf. The hole was cleaned to 929 mbsf; 8 m above the total depth of the hole known from Leg 139 and presumably above the missing part of the thermistor string and sinker bar.

The deployment was routine from an operations standpoint and proceeded very smoothly. Steps were taken in advance of this installation to address several inefficient thermistor string-payout methods used during Hole 858G deployment. Much time had been lost braiding the grippers onto the cable on the rig floor. The grippers were too long and awkward and too few in number. Six new grippers were spliced and formed from manila line with electrical tape and nylon seizing line; the braiding section was 3.5-ft long. The thermistor string was removed from its crate, laid out on top of the alligator boxes aft of the Downhole Measurements Lab, and marked at 30 m intervals with prospective gripper locations. The first six grippers were attached to the bottom part of cable, and the cable then joined with the sinker bar. The "leapfrog" deployment of the 898 m thermistor string took <1.5 hr, with the preparation crew staying two to three grippers ahead of the rig crew. The data logger was given the final software check at 0345 hr, 11 September. The running tool was unjayed from

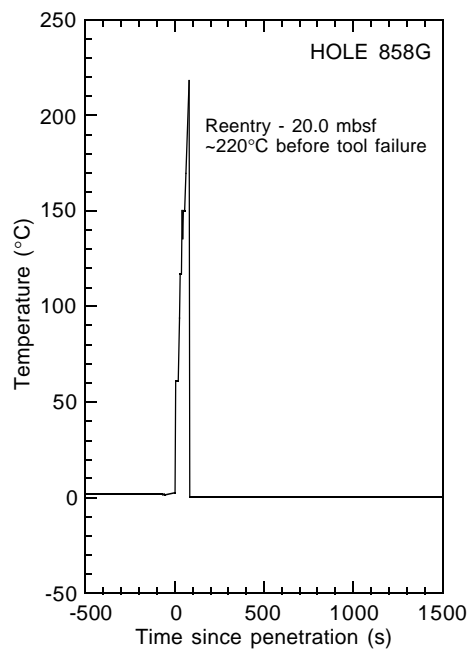


Figure 43. Results of WSTP temperature measurement at 20.0 mbsf in Hole 858G shown in a time-temperature plot. The in situ data were collected on 3 September 1996 after unCORKing operations in the hole were completed. Temperatures, acquired at a 5-s sampling rate, climbed dramatically in a few seconds from bottom-water values to ~220°C before the thermistor failed.

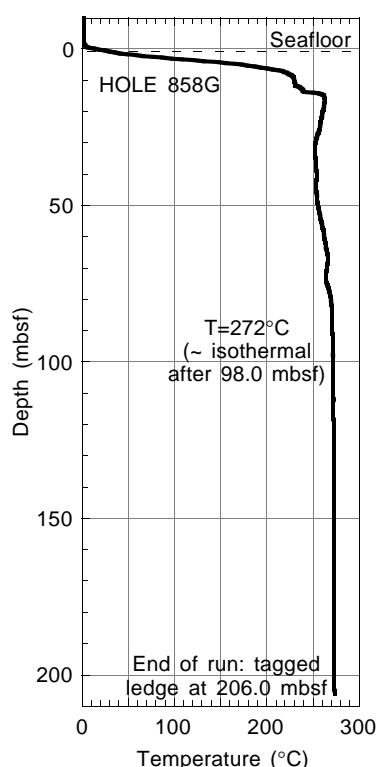


Figure 44. The GRC UHT-MSM tool log acquired on 3 September 1996 in Hole 858G. The run was terminated within the pipe at 206 mbsf after an obstruction was encountered. A very steep thermal gradient exists in the upper 10 m of the hole. The maximum observed temperature is 272°C at 98.0 mbsf, and the log shows that the borehole is effectively isothermal below this depth.

the CORK at 1000 hr, and CORK-related operations were complete at 1500 hr.

Temperature Measurements

Hole 858G

The inaugural temperature run with the GRC UHT-MSM Tool was planned ~24 August after the recovery of the data logger and thermistor string at Hole 858G. Deteriorating weather conditions canceled that plan, and the prepped tool was placed on the bench until the operations shifted back to Hole 858G on 3 September.

There was no evidence that the unCORKed Hole 858G was emitting hot fluid, yet the geothermal gradient downhole was unknown and had the potential for being very high (Shipboard Scientific Party, 1992b). The new UHT-MSM tool was the obvious choice for logging temperatures under these conditions. Concern arose that the slimline tool would encounter the thermistor cable and sinker bar left in the hole, entangle itself, and require a fishing trip that would disturb the in situ borehole conditions and any hydrothermal water samples. The WSTP was thus used first to measure the temperature and collect a fluid sample in the upper part of the hole, and the bit was set at 20 mbsf. Four Temp-Plate temperature sensor tabs with a range of 143° to 204°C were attached to the body of the tool in case the borehole was too hot for the tool's temperature sensing capabilities (~150°C). The tool was run in the hole, and samples were obtained as the probe tip was extended past the end of the bit for 5 min. Upon recovery, the sensor tabs indicated that a minimum temperature of 182°C had been encountered. The internal thermistor registered ~220°C before fail-

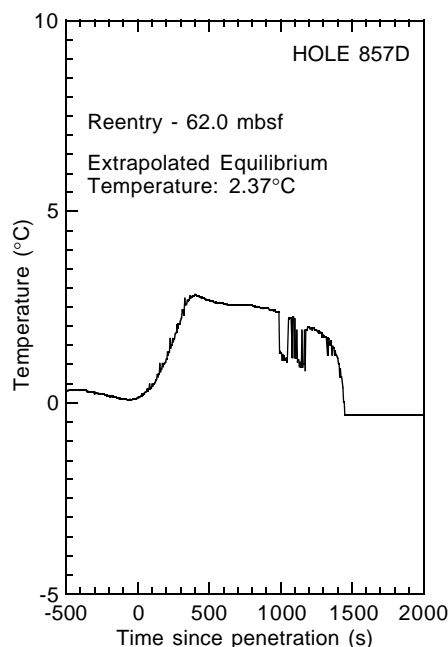


Figure 45. Results of WSTP temperature measurement at 620.0 mbsf in Hole 857D shown in a time-temperature plot. The in situ data were collected on 10 September 1996 after unCORKing operations in the hole were completed. The record shows the effects of inflow into the borehole, and the extrapolated equilibrium temperature of ~2°C is similar to bottom-water temperatures.

ing, as shown in the WSTP temperature record of Figure 43. A hydrothermal fluid sample was collected; analytical results are given in the "Inorganic Geochemistry" Section (this chapter).

The UHT-MSM tool was deployed next with 500 lb of sinker bars on top of it to add weight and increase tension on the wireline. It was run in the hole at 0910 hr to a projected depth of 350 mbsf through the end of pipe set at 20 mbsf. The forward movement of the tool was halted every 20 m, and the tool picked up every 5 m, in a continual check for ledges and the floating thermistor string. The tool was held stationary for a 5-min pressure-depth check at the mudline (2426.0 mbrf) and at 150 mbsf. An obstruction was encountered inside the casing at 206 mbsf, and the run was terminated. A 10-min temperature station was made at 150 mbsf, the tool was held stationary for 5 min in the pipe at 1500.0 mbrf, and then run out of the hole.

The UHT-MSM was highly discolored as it arrived on deck at 1508 hr. High-pressure fluids were discharging from the sinker bar connection. The tool was transported to the Downhole Measurements Lab to cool down before the data were dumped. The dewar flask was unscrewed and removed. Initial concern that the lithium batteries may have been overheated, as the aluminum housing enclosing the battery pack was hot to the touch, encouraged extreme caution in removing the battery pack. After a cooling period of ~1 hr, the data were successfully dumped from memory.

The temperature log is shown in Figure 44. Temperatures increase sharply from bottom-water values at the mudline to ~228°C at 9 mbsf and ~263°C at 16 mbsf, then decrease slightly to ~253°C by 32 mbsf. A temperature of 272°C is observed at 98 mbsf. A gradient of ~1°C/100 m is observed below this depth, and the borehole seems nearly isothermal below 140 mbsf.

Hole 857D

A sinker bar sent down the hole after unCORKing operations were complete on 10 September tagged bottom at 642 mbsf, below the hydraulically conductive fault zone from 610 to 615 mbsf identi-

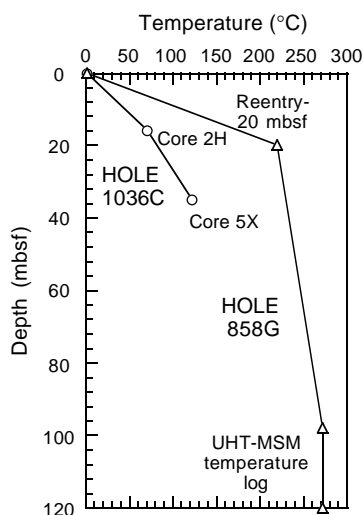


Figure 46. Temperature gradients vs. depth for Holes 1036C and 858G, separated by ~130 m. Curves are forced through a mudline/bottom-water temperature of 2.1°C at 0 mbsf. Gradients in both holes are steep in the upper 18 to 20 m and decrease with depth. The extrapolated WSTP equilibrium temperatures for Core 169-1036C-2H is 71°C at 15.9 mbsf, and for Core 169-1036C-5X is 122.3°C at 34.9 mbsf. The maximum temperature measured with the GRC tool in Hole 858G is 272°C at 98.0 mbsf.

fied during Leg 139. Temperature sensor tabs attached to the bar indicated temperatures less than 108°C. The planned UHT-MSM tool deployment at Hole 857D was canceled owing to erratic behavior in benchtop tests. The WSTP was to be used to measure the borehole temperature and collect a water sample, but an obstruction was encountered at 377 mbsf that had to be drilled before the pipe could be lowered to 621 mbsf to collect the water sample. After the WSTP run, the hole was reamed and cleaned to 929 mbsf.

The results of the WSTP experiment are shown in the temperature-time plot of Figure 45. Strong inflow of bottom water downhole is indicated by an extrapolated equilibrium temperature of 2.37°C and by the seawater composition of the sample (see “Inorganic Geochemistry” section, this chapter).

Hole 1036C

Two WSTP temperature measurements were made in Hole 1036C, located off the edge of Dead Dog Mound and the last hole drilled in the active hydrothermal area of Middle Valley. The extrapolated equilibrium temperatures for APC Core 169-1036C-2H, at 15.9 mbsf, and XCB Core 169-1036C-5X, at 34.9 mbsf, are 71.0°C and 122.3°C, respectively. The temperature gradients with depth for Holes 1036C and 858G given in Figure 46 are not linear with depth. The steeper gradient in the upper 18 to 20 m of the holes suggests the movement of hot fluids in the shallow subsurface that may be bounded at ~30 mbsf by a suspected cap rock layer encountered during Leg 139. Drilling at Holes 1036A and 1036B did not indicate the presence of a layer likely to serve as a hydrologic seal. The presence of such a layer at Hole 1036C is equivocal from the data presently available.

PORE PRESSURE MEASUREMENTS USING PUPPIS

A series of 10 PUPPI deployments were made in and around the AAV, near the Dead Dog Mound, from the *Maurice Ewing* in the summer of 1995. These deployment positions are shown in Figure 47 in relation to the AAV, the Dead Dog Mound, and other seabed features. Deployments were made both adjacent to the vent and at other

locations, both inside and outside the AAV, and at distances up to 450 m from the active vents. These data consistently showed negative residual pore pressures within the AAV and larger negative pressures closest to the vents, supporting conclusively that the drawdown (recharge) of seawater into the mound is currently an active process. The only indication of any slight upward flow was at location PP03, some 200 m to the east of the AAV.

Direct in situ measurement of pore pressure gradients in seafloor sediments is one of the most direct ways to detect and quantify fluid flow through the seafloor and to estimate subsurface pressures at greater depths, because the rates of pore-fluid flow are related to the pore pressure gradient through Darcy’s law (the flux of pore fluid is proportional to the pore pressure gradient multiplied by the permeability). The PUPPI, originally developed at the Institute of Oceanographic Sciences (Schultheiss and McPhail, 1986; Schultheiss, 1990) measures differential pore pressures between ports on a lance buried in the sediments, with a resolution of ~5 Pa (<1-mm head of water). It includes a valve system that enables each pressure transducer to be periodically checked for zero offset drift. A zero reference pressure is achieved by periodically shutting off the pressure port on the lance and opening both sides of the pressure transducer to hydrostatic pressure. The data can thus be drift corrected to compensate for the creep effects that occur in the pressure transducers over a period of time. This type of correction is essential when making long-term measurements.

The PUPPI is a free-fall instrument that can be ballasted with lead or steel weights to penetrate a range of sediment types in water depths of up to 6000 m. Recovery is accomplished using an acoustic command that activates a release mechanism, cutting the connecting pipes and severing the expendable from the recoverable parts. The lance and ballast weight assembly is left on the seafloor, whereas the buoyant instrument package ascends to the surface for recovery.

The primary objectives of the PUPPI deployments during Leg 169 were to (1) confirm the general observation of negative residual pore pressures close to the active vent, (2) examine, with a longer time record, the nature of the dynamic signal previously recorded and to look for any temporal changes (either natural or caused by drilling activities), and (3) observe any changes in the equilibrium pressure (or pressure record in general) caused by the drilling activities with a view to further understanding the hydraulic nature of the surrounding formation.

Operations

The PUPPI launch platform was welded in the gangway gate on the forecastle deck (portside beneath lifeboat No. 4). This provided ~5 to 6 m of freeboard. Launching and recovery of the PUPPIs utilized the main portside crane. A new instrument sling was used to enable the instruments to be partially built on the deck. In this way, the time between launching different instruments from one launch platform was cut from ~2 to 3 hr to <1 hr. To test the acoustic systems and reception, one PUPPI acoustic unit was mounted on the camera frame and tested on a routine run down the drill pipe at Hole 856H during a reentry operation. Before the cruise, anecdotal rumors had suggested that the drillship was acoustically extremely noisy; thus it was thought that the small overside PUPPI transducer might have difficulties in discriminating the PUPPI acoustic returns from the ship noise. This concern was unfounded. Indeed, with the transducer lowered in the moonpool and the computer and command unit located in the subsea shack, excellent signals were received both during the test on the camera frame and during the launch and recovery operations, even over the acoustic noise generated by the thrusters.

Both the launch and recovery operations with the PUPPIs occurred during routine pipe trips, and, therefore, used little if any effective ship time. This is an important factor when considering the implications of this type of measurement in the future.

Despite having the necessary equipment to conduct three deployments, we were limited to two deployments because of logistical con-

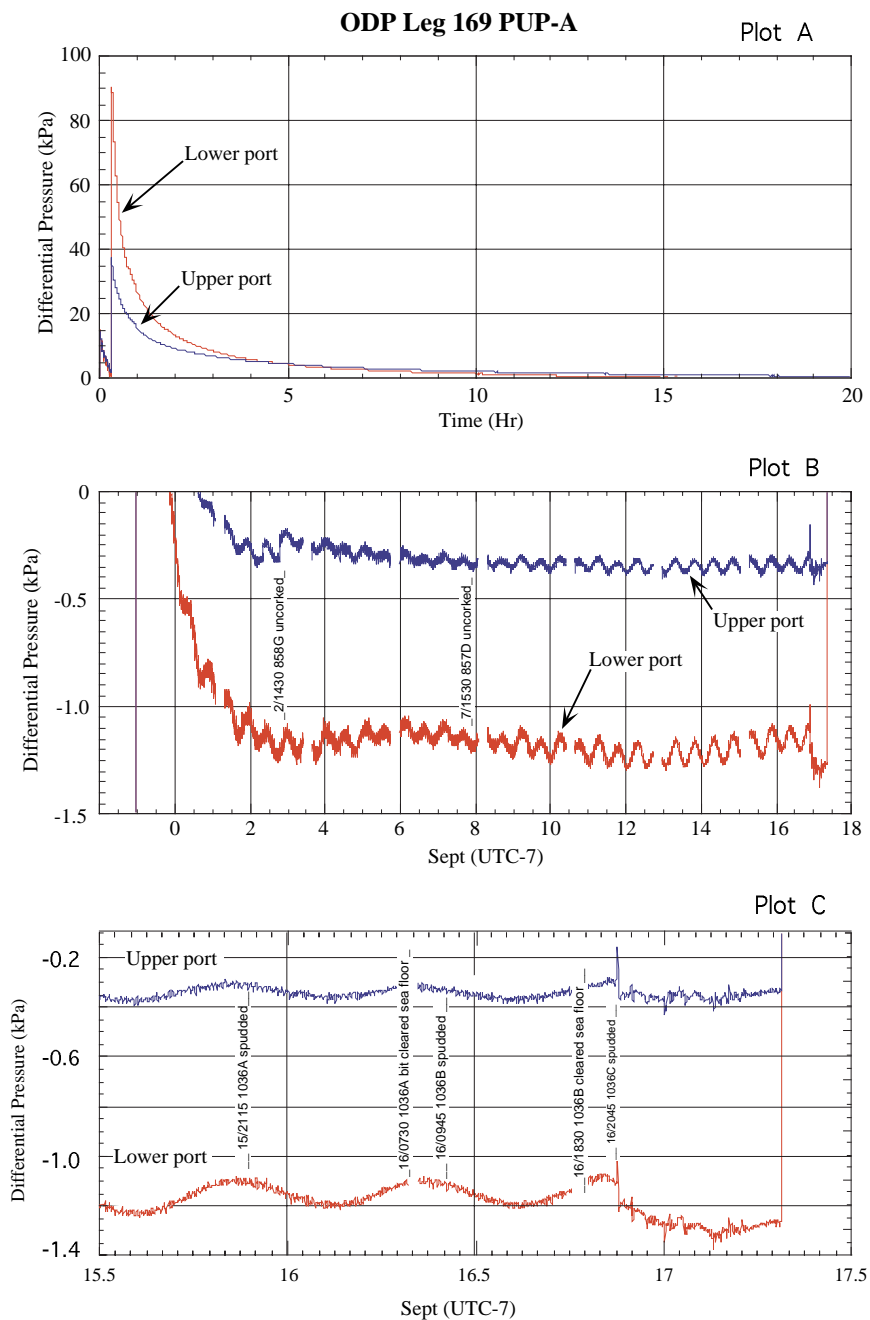


Figure 48. PUP-A data from Site 1036. The lower port is 3 mbsf and the upper port is 1.5 mbsf. **A.** Initial penetration event and decay curve. **B.** Negative residual pore pressure, the tidal cycles, and the dynamic noise. **C.** Possible effects of the drilling process at Site 1036 and the timing of some pertinent operations.

straints. The deployment and recovery positions of the two instruments (PUP-A and PUP-B) are shown in Figure 47 together with the locations of the previous PUPPI deployments. They were deployed near Dead Dog Mound and close to Holes 1036B and 1036C on 29 August and recovered more than 19 days later on 17 September during the pipe trip following the completion of drilling at Hole 1036C.

Results

The purpose of this brief report is not to provide an exhaustive interpretation but to outline the nature of the data recovered. The most serious problem associated with interpreting PUPPI data from this site is the lack of precise knowledge regarding the exact relative positions of instruments and features (e.g., vents and boreholes) on the seafloor. Although the relative positions of the holes and the launch

positions of the PUPPIs are well constrained by the differential Global Positioning System (dGPS) coordinates, the actual positions on the seafloor are subject to horizontal drift of the PUPPIs during their free fall. Previous experiences have indicated that the drift in deep water is limited to perhaps 30 m. However, this is dependent on the water depth and current regime in the area of deployment, as well as any subtle differences in the mechanical construction of the instruments that could conceivably affect the drift during free fall. The recovery positions of the instruments (see Fig. 47) indicate that the instruments may have moved by ~30 m from their launch positions but in different directions, which is difficult to explain. The recovery positions were derived by the visual estimation of the surface position of the PUPPIs at recovery relative to the ship. Consequently, on the scale of this experiment, the positions remain rather uncertain, and we will have to wait until further investigations are made to precisely

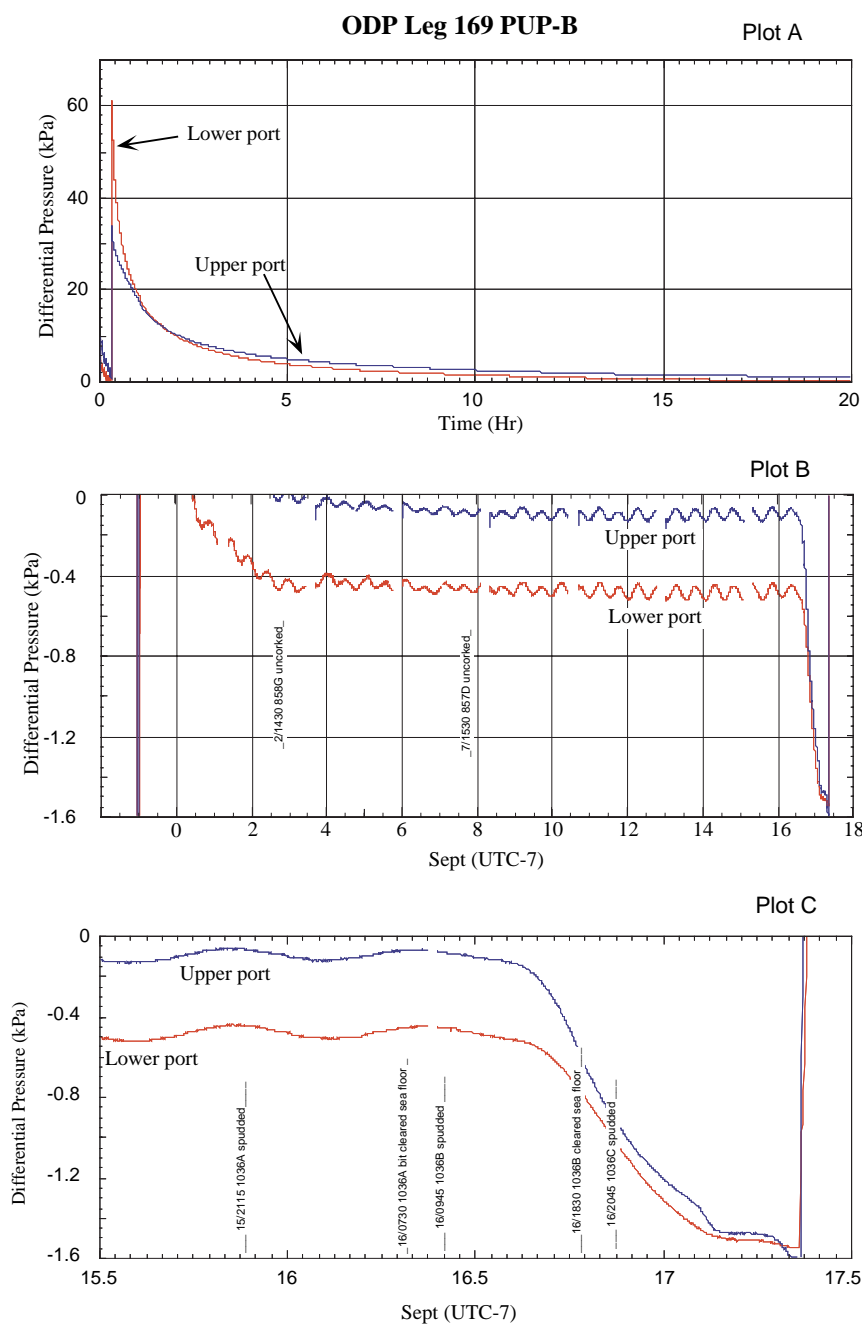


Figure 49. PUP-B data from Site 1036. The lower port is 3 mbsf and the upper port is 1.5 mbsf. **A.** shows the initial penetration event and decay curve. **B.** shows the negative residual pore pressure and the tidal cycles. **C.** shows the effects of the drilling process at Site 1036 during the last 2 days of the deployment and the timing of some pertinent drilling operations.

locate (using submersible, camera, or ROV surveys) the expendable components before a detailed interpretation can be made on some aspects of the data.

The data from the two deployments, PUP-A and PUP-B, are summarized in Figures 48 and 49, respectively. The graphs show summary data sets for each deployment from the two main pressure ports located at 1.5 mbsf (upper port) and 3 mbsf (lower port). The data have undergone preliminary processing, which includes transducer drift correction and the removal of data obtained during the valve operation (which occurred about once every 2 days).

Each figure shows three plots to illustrate the major features of the records. Plot A (initial 20 hr from launch) shows the effects of the instrument free fall through the water column, the penetration event, and the early part of the decay curve. Plot B shows the complete record over 18 days at a greatly expanded pressure scale. This shows the nature of the tidal cycles, the dynamic noise, and the effects of

drilling near the end of the deployments. Plot C is an expanded portion showing the last 2 days of the deployments illustrating more clearly the above features together with annotations showing the timing of various drilling operations at Site 1036.

Both deployments show the following; high maximum insertion pressures (~30–90 kPa), negative residual pore pressure gradients (0.1–0.4 kPa/m), long decay times (4 to 5 days until pressure equilibrium is reached), and well-developed tidal cycles. This indicates that the lances had fully penetrated, that the average upper 3 m of sediment has a low permeability (probably clay/fine silt), and that seawater is being sucked into the mound at these locations. Superimposed on the tidal cycles on PUP-A is a low-level dynamic noise signature observed during previous deployments in this area, that interestingly does not appear on the PUP-B record. The closest previous PUPPI measurements are PP19 and PP36 (see Fig. 47). These records also showed dynamic noise on one record (PP19), but not on the other

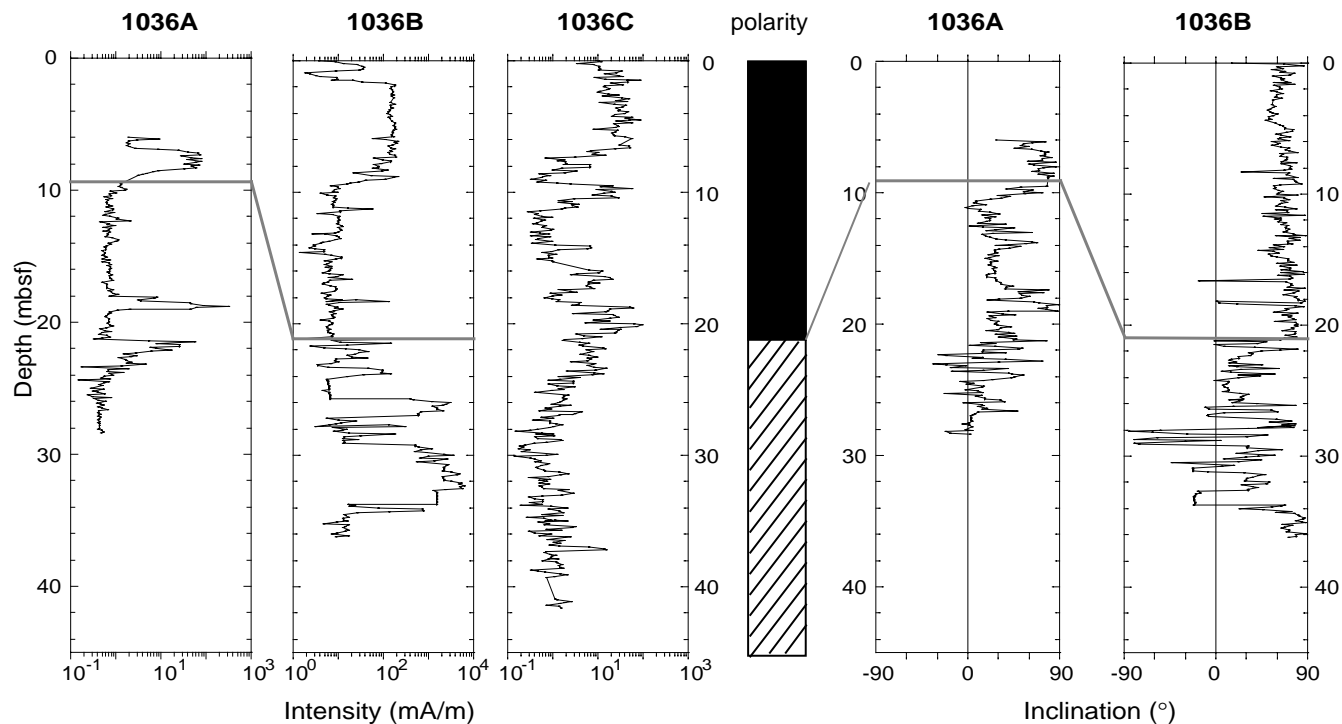


Figure 50. Site 1036 magnetic intensities and inclinations after demagnetization at 20 mT. Column in the middle indicates tentative polarity interpretation (solid = normal polarity and hachured = unreliable results). Stippled line (inclination plots, right side) indicates interpretable base of the Brunhes Chron. Stippled line (intensity plots, left side) indicates respective depths in the intensity columns. See text for explanation.

(PP36). This was considered surprising at the time and tentatively interpreted as a difference in the local hydraulic connectivity to the vent (turbulent/laminar flow). The repeat measurements made during this leg only make this feature of the record even more puzzling.

A subtle reduction in the amplitude of the dynamic noise occurred between 12 and 15 September. This may be a natural variation in the activity of the nearby vent on Dead Dog Mound, but it may also be a result of the nearby drilling operations. Note that this occurred before operations at Site 1036, and if it is to be interpreted as a drilling effect, it should be attributed to the operations at Bent Hill (Site 1035), some 3 km away, or the uncorking of Holes 858G and 857D, which occurred on 2 September at 2130 UTC and 7 September at 2230 UTC, respectively.

The final feature worthy of note on the pore-pressure records is the changes in pore pressure over the last 2 days of the deployments (Figs. 48C, 49C). PUP-A shows a sudden change on 16 September at 2102 hr, just 15 min after Hole 1036C was spudded, according to the drilling records. The mean pore pressure dropped a further 0.2 kPa (at the lower port), and a number of perturbations are visible on the record after this time. In the case of PUP-B, a change in the mean pore-pressure level began ~1400 hr on 16 September and decayed slowly throughout the remainder of the deployment by a further 1.4 kPa (lower port). This event occurred before Hole 1036C was initiated and during operations in Hole 1036B (some 4 hr after Hole 1036B was spudded). Although either of these pressure drops could have been caused by the drilling at Hole 1036A (adjacent to the vent), it is tempting to assign the events at PUP-A to operations at Hole 1036C and the events at PUP-B to operations at Hole 1036B. However, according to the deployment positions, PUP-A was closest to Hole 1036B and PUP-B was closest to Hole 1036C!

Conclusions

The pore pressure records from the two deployments made during this cruise have generally confirmed the data obtained from previous

PUPPI measurements and provided fresh information that should be valuable for constraining models of this hydrothermal system and for investigating hydrothermal systems in the future. In the immediate vicinity of the active vent on Dead Dog Mound, significant negative pore pressures exist at least in the upper few meters of sediment, indicating that seawater is flowing into the mound. The simple hydraulic explanation for this is that the rapid flow from the vent causes suction as a result of the Bernoulli effect.

The dynamic noise in the data has been shown to be variable in the immediate vicinity of the vent, thus suggesting that the hydraulic structure in the sediments/rocks around the vent in the upper few meters is complex. The variation in dynamic noise may be the result of natural changes in the venting process or may have been caused by drilling operations over 3 km away. The effects of local drilling activities are clearly observed by monitoring pore pressure in near-surface sediments. Pore pressures at both sites were further lowered as the result of the drilling process increasing the rate of seawater flow into the mound.

The ability to fully interpret this data is limited by the lack of precise information on the relative positions of PUPPIs, boreholes, and vents. However, this could quite easily be rectified in future experiments by tracking the instruments to on seafloor within an acoustic transponder net. However, it is clear that the technique of using PUPPIs to monitor boreholes is viable, and that it does not require any special shipfitting or indeed ship time, as PUPPI operations can occur during pipe trips. There is significant potential for increasing our understanding of the hydraulic properties in a variety of formations using these techniques in conjunction with downhole and crosshole packer and CORK experiments.

PALEOMAGNETISM

Where recovery permitted, split cores from Site 1036 were measured before and after demagnetization in 5- or 10-cm intervals using

the pass-through magnetometer. The magnetization intensities and directions after AF demagnetization of 20-mT were chosen to represent the paleomagnetic signal of the lithologies drilled (see “Lithostratigraphy” section, this chapter). Magnetization intensities presented for samples from Hole 1036C need to be considered with care, because an unnoticed malfunction of the software (under construction at the time of measurements) significantly affected the raw data, rendering any interpretation of directional data useless. Given the young crustal age at this site, only Holocene through Pleistocene age intervals could be investigated; therefore, any magnetostratigraphy could only be based on identifying short polarity events during the Brunhes Chron (e.g., Nowaczyk and Baumann, 1992). Determination of a magnetic stratigraphy at Site 1036, however, is frustrated by a combination of hydrothermal effects on the magnetomineralogy and by drilling disturbance in sections cored using the XCB.

Holes 1036A, 1036B, and 1036C

Downhole changes of the natural remanent magnetization (Fig. 50) are mostly controlled by variations in the genesis of the minerals that generate the magnetic signal, that is, changes from unaltered to hydrothermally altered sediments and rocks. Only unaltered hemipelagic sediments appear to represent a true record of the Earth’s magnetic field (with inclinations centered around the expected mean value of 67°; Fig. 50). Secondary hydrothermal processes account for magnetostratigraphically spurious magnetizations. The paleomagnetic signal in lithologic Subunits IA and IB for this site very likely represents a true record of the Earth’s magnetic field during part of the Brunhes Chron (C1n; Cande and Kent, 1992). Below these subunits, a magnetostratigraphically interpretable signal is lost. This change coincides with the 100°–150°C isotherm suggested by the onset of anhydrite formation in Subunit IC (see “Lithostratigraphy” section, this chapter) and thus a higher temperature alteration of the sediments. The record of the C1n in Hole 1036B cores extends to ~21 mbsf and corresponds to an interval of medium to weak magnetization intensities (several tens of mA/m to <1 mA/m), whose downhole variation clearly reflects the different lithological Subunits IA and IB. The downhole pattern of magnetization intensities is mirrored in samples from Hole 1036A (6–18 mbsf) and, hence, suggests a correlation of these two intervals. This assumption is confirmed by the magnetic susceptibility (see “Physical Properties” section, this chapter) which mimics the downhole trend of the remanent magnetization intensities. The indication is that the latter are roughly a function of varying concentrations of remanent magnetic minerals, and so is susceptibility. As already noted, however, the record of the Brunhes Chron in cores from Hole 1036A is lost by 9 mbsf. This indicates that an alteration process that postdates the deposition of lithologic Subunits IB through IC (at ~18 mbsf) affected the sediments. The difference may well correspond to the lateral distance of the respective holes from the vent at the top of Dead Dog Mound. Below Subunit B, inclinations trend from shallow positive to negative (Fig. 50). This does not seem to be an accurate record of the Earth’s magnetic field, but rather an effect of the hydrothermal alteration of the sediments. It is unclear which process caused these spurious directions. However, both the inclination and the intensity records of the magnetic signal in cores from Holes 1036A and 1036B are similar and, thus, suggest that these directions may be significant. Furthermore, equivalent features of the paleomagnetic signal have been recorded at corresponding depths at Site 858 (Shipboard Scientific Party, 1992b). Demagnetization of discrete samples to higher field strengths performed during Leg 139 revealed a trend back to normal polarities (i.e., Brunhes Chron; C1n). Again, the extent of the alteration of the primary magnetic signal appears to be a function of the intensity of alteration of the sediments following a hydrothermal isotherm dipping away from the vent. Despite differences in the depth of destruction of the inclination signal, the matching downhole intensity pattern suggests that

at least the upper 20 m of Holes 1036A and 1036B still reflect a primary magnetic signal that has not been extensively altered by secondary processes.

Conclusions

Hydrothermal activity significantly affects the paleomagnetic signal at Site 1036 and overprints the record of the Brunhes Chron as a function of the varying distance of the respective holes from the active vent. A detailed rock magnetic study on the drilled intervals is essential to understanding the effects of the hydrothermal alteration (decreasing from Holes 1036A through 1036C) on the magnetic signal at Site 1036, and awaits further shore-based efforts.

REFERENCES

- Ames, D.E., Franklin, J.M., and Hannington, M.H., 1993. Mineralogy and geochemistry of active and inactive chimneys and massive sulfide, Middle Valley, northern Juan de Fuca Ridge: an evolving hydrothermal system. *Can. Mineral.*, 31:997–1024.
- Baker, P.A., and Cross, S.L., 1994. A note on the carbon, sulfur, and nitrogen contents of hydrothermally altered sediments, Middle Valley, Juan de Fuca Ridge. In Mottl, M.J., Davis, E.E., Fisher, A.T., and Slack, J.F. (Eds.), *Proc. ODP, Sci. Results*, 139: College Station, TX (Ocean Drilling Program), 307–312.
- Baker, P.A., Cross, S.L., and Burns, S.J., 1994. Geochemistry of carbonate nodules and cements and implications for hydrothermal circulation, Middle Valley, Juan de Fuca Ridge. In Mottl, M.J., Davis, E.E., Fisher, A.T., and Slack, J.F. (Eds.), *Proc. ODP, Sci. Results*, 139: College Station, TX (Ocean Drilling Program), 313–328.
- Baross, J.A., and Deming, J.W., 1995. Growth at high temperatures: isolation and taxonomy, physiology, ecology. In Karl, D.M. (Ed.), *The Microbiology of Deep-sea Hydrothermal Vent Environments*: Boca Raton, FL (CRC Press), 169–217.
- Barton, P.B., Jr., and Skinner, B.J., 1979. Sulfide mineral stabilities. In Barnes, H. L. (Ed.), *Geochemistry of Hydrothermal Ore Deposits* (2nd ed.): New York (Wiley), 278–403.
- Becker, K., Morin, R.H., and Davis, E.E., 1994. Permeabilities in the Middle Valley hydrothermal system measured with packer and flowmeter experiments. In Mottl, M.J., Davis, E.E., Fisher, A.T., and Slack, J.F. (Eds.), *Proc. ODP, Sci. Results*, 139: College Station, TX (Ocean Drilling Program), 613–626.
- Bernard, B.B., Brooks, J.M., and Sackett, W.M., 1976. Natural gas seepage in the Gulf of Mexico. *Earth Planet. Sci. Lett.*, 31:48–54.
- Berndt, M.E., Seyfried, W.E., and Beck, J.W., 1988. Hydrothermal alteration processes at mid-ocean ridges: experimental and theoretical constraints from Ca and Sr exchange reactions and Sr isotopic ratios. *J. Geophys. Res.*, 93:4573–4583.
- Bessler, J.U., Smith, L., and Davis, E.E., 1994. Hydrologic and thermal conditions at a sediment/basalt interface: implications for interpretation of field measurements at Middle Valley. In Mottl, M.J., Davis, E.E., Fisher, A.T., and Slack, J.F. (Eds.), *Proc. ODP, Sci. Results*, 139: College Station, TX (Ocean Drilling Program), 667–675.
- Bischoff, J.L., and Dickson, F.W., 1975. Seawater-basalt interaction at 200°C and 500 bars: implications for origin of seafloor heavy metal deposits and regulation of seawater chemistry. *Earth Planet. Sci. Lett.*, 25:385–397.
- Bischoff, J.L., and Seyfried, W.E., 1978. Hydrothermal chemistry of seawater from 25°C to 350°C. *Am. J. Sci.*, 278:838–860.
- Brunner, C.A., 1994. Planktonic foraminiferal biostratigraphy and paleoceanography of late Quaternary turbidite sequences at Holes 856A, 857A, and 857C, Leg 139. In Mottl, M.J., Davis, E.E., Fisher, A.T., and Slack, J.F. (Eds.), *Proc. ODP, Sci. Results*, 139: College Station, TX (Ocean Drilling Program), 39–58.
- Buatier, M.D., Karpoff, A.-M., Boni, M., Früh-Green, G.L., and McKenzie, J.A., 1994. Mineralogic and petrographic records of sediment-fluid interaction in the sedimentary sequence at Middle Valley, Juan de Fuca Ridge, Leg 139. In Mottl, M.J., Davis, E.E., Fisher, A.T., and Slack, J.F. (Eds.), *Proc. ODP, Sci. Results*, 139: College Station, TX (Ocean Drilling Program), 133–154.
- Butterfield, D.A., McDuff, R.E., Franklin, J., and Wheat, C.G., 1994. Geochemistry of hydrothermal vent fluids from Middle Valley, Juan de

- Fuca Ridge. In Mottl, M.J., Davis, E.E., Fisher, A.T., and Slack, J.F. (Eds.), *Proc. ODP, Sci. Results*, 139: College Station, TX (Ocean Drilling Program), 395–410.
- Campbell, A.C., Bowers, T.S., Measures, C.I., Falkner, K.K., Khadem, M., and Edmond, J.M., 1988. A time series of vent fluid compositions from 21°N, East Pacific Rise (1979, 1981, 1985) and the Guaymas Basin, Gulf of California (1982, 1985). *J. Geophys. Res.*, 93:4537–4550.
- Cande, S.C., and Kent, D.V., 1992. A new geomagnetic polarity time scale for the Late Cretaceous and Cenozoic. *J. Geophys. Res.*, 97:13917–13951.
- Cragg, B.A., and Parkes, R.J., 1994. Bacterial profiles in hydrothermally active deep sediment layers from Middle Valley (NE Pacific), Sites 857 and 858. In Mottl, M.J., Davis, E.E., Fisher, A.T., and Slack, J.F. (Eds.), *Proc. ODP, Sci. Results*, 139: College Station, TX (Ocean Drilling Program), 509–516.
- Davis, E.E., and Becker, K., 1994. Thermal and tectonic structure of the Escanaba Trough: new heat-flow measurements and seismic-reflection profiles. In Moreton, J., Zierenberg, R.A., and Reiss, C.A. (Eds.), *Geologic, Hydrothermal, and Biologic Studies at Escanaba Trough, Gorda Ridge, Offshore Northern California*. U.S. Geol. Surv. Bull., 2022:45–64.
- Davis, E.E., Becker, K., Pettigrew, T., Carson, B., and MacDonald, R., 1992. CORK: a hydrologic seal and downhole observatory for deep-ocean boreholes. In Davis, E.E., Mottl, M.J., Fisher, A.T., et al., *Proc. ODP, Init. Repts.*, 139: College Station, TX (Ocean Drilling Program), 43–53.
- Davis, E.E., and Fisher, A.T., 1994. On the nature and consequences of hydrothermal circulation in the Middle Valley sedimented rift: inferences from geophysical and geochemical observations, Leg 139. In Mottl, M.J., Davis, E.E., Fisher, A.T., and Slack, J.F. (Eds.), *Proc. ODP, Sci. Results*, 139: College Station, TX (Ocean Drilling Program), 695–717.
- Davis, E.E., Mottl, M.J., Fisher, A.T., et al., 1992. *Proc. ODP, Init. Repts.*, 139: College Station, TX (Ocean Drilling Program).
- Davis, E.E., and Villinger, H., 1992. Tectonic and thermal structure of the Middle Valley sedimented rift, northern Juan de Fuca Ridge. In Davis, E.E., Mottl, M.J., Fisher, A.T., et al., *Proc. ODP, Init. Repts.*, 139: College Station, TX (Ocean Drilling Program), 9–41.
- Davis, E.E., and Wang, K., 1994. Present and past temperatures of sediments at Site 857, Middle Valley, northern Juan de Fuca Ridge. In Mottl, M.J., Davis, E.E., Fisher, A.T., and Slack, J.F. (Eds.), *Proc. ODP, Sci. Results*, 139: College Station, TX (Ocean Drilling Program), 565–570.
- Duckworth, R.C., Fallick, A.E., and Rickard, D., 1994. Mineralogy and sulfur isotopic composition of the Middle Valley massive sulfide deposit, northern Juan de Fuca Ridge. In Mottl, M.J., Davis, E.E., Fisher, A.T., and Slack, J.F. (Eds.), *Proc. ODP, Sci. Results*, 139: College Station, TX (Ocean Drilling Program), 373–385.
- Edmond, J.M., Campbell, A.C., Palmer, M.R., German, C.R., Klinkhammer, G.P., Edmonds, H.N., Elderfield, H., Thompson, G., and Rona, P., 1995. Time series studies of vent fluids from the TAG and MARK sites (1986, 1990): Mid-Atlantic Ridge: a new solution chemistry model and a mechanism for Cu/Zn zonation in massive sulfide ore bodies. In Parson, L.M., Walker, C.L., and Dixon, D.R. (Eds.), *Hydrothermal Vents and Processes*. Geol. Soc. Spec. Publ. London, 87:77–86.
- Fisher, A.T., Fischer, K., Lavoie, D., Langseth, M., and Xu, J., 1994. Geochemical and hydrogeological properties of sediments from Middle Valley, northern Juan de Fuca Ridge. In Mottl, M.J., Davis, E.E., Fisher, A.T., and Slack, J.F. (Eds.), *Proc. ODP, Sci. Results*, 139: College Station, TX (Ocean Drilling Program), 627–647.
- Gieskes, J.M., Elderfield, H., Lawrence, J.R., Johnson, J., Meyers, B., and Campbell, A., 1982. Geochemistry of interstitial waters and sediment, Leg 64, Gulf of California. In Curray, J.R., Moore, D.G., et al., *Init. Repts. DSDP*, 64 (Pt. 2): Washington (U.S. Govt. Printing Office), 675–694.
- Gieskes, J.M., Gamo, T., and Brumsack, H., 1991. Chemical methods for interstitial water analysis aboard *JOIDES Resolution*. *ODP Tech. Note*, 15.
- Gieskes, J.M., Simoneit, B.R.T., Brown, T., Shaw, T., Wang, Y.-C., and Magenheimer, A., 1988. Hydrothermal fluids and petroleum in surface sediments of Guaymas Basin, Gulf of California: a case study. *Can. Mineral.*, 26:589–602.
- Goodfellow, W.D., and Blaise, B., 1988. Sulfide formation and hydrothermal alteration of hemipelagic sediment in Middle Valley, northern Juan de Fuca Ridge. *Can. Mineral.*, 26:675–696.
- Goodfellow, W.D., and Franklin, J.M., 1993. Geology, mineralogy and chemistry of sediment-hosted clastic massive sulfides in shallow cores, Middle Valley, northern Juan de Fuca Ridge. *Econ. Geol.*, 88:2033–2064.
- Goodfellow, W.D., Grapes, K., Cameron, B., and Franklin, J.M., 1993. Hydrothermal alteration associated with massive sulfide deposits, Middle Valley, Northern Juan de Fuca Ridge. *Can. Mineral.*, 31:1025–1060.
- Goodfellow, W.D., and Peter, J.M., 1994. Geochemistry of hydrothermally altered sediment, Middle Valley, northern Juan de Fuca Ridge. In Mottl, M.J., Davis, E.E., Fisher, A.T., and Slack, J.F. (Eds.), *Proc. ODP, Sci. Results*, 139: College Station, TX (Ocean Drilling Program), 207–289.
- Grimalt, J., and Albaiges, J., 1987. Sources and occurrence of C₁₂-C₂₂ n-alkane distributions with even carbon-number preference in sedimentary environments. *Geochim. Cosmochim. Acta*, 51:1379–1384.
- Gröschel-Becker, H.M., 1996. Formational processes of oceanic crust at sedimented spreading centers: perspectives from the West African continental margin and Middle Valley, northern Juan de Fuca Ridge. [Ph.D. dissert.]. Univ. of Miami, Coral Gables, FL.
- Kawka, O.E., and Simoneit, B.R.T., 1987. Survey of hydrothermally-generated petroleum from the Guaymas Basin spreading center. *Org. Geochem.*, 11:311–328.
- Kvenvolden, K.A., Rapp, J.B., Hostettler, F.D., Morton, J.L., King, J.D., and Claypool, G.E., 1986. Petroleum associated with polymetallic sulfide in sediment from the Gorda Ridge. *Science*, 243:1231–1234.
- Kvenvolden, K.A., Rapp, J.B., Hostettler, F.D., and Rosenbauer, R.J., 1994. Laboratory simulation of hydrothermal petroleum formation from sediment in Escanaba Trough, offshore from northern California. *Org. Geochem.*, 22: 935–945.
- Kvenvolden, K.A., and Simoneit, B.R.T., 1990. Hydrothermally derived petroleum: examples from Guaymas Basin, Gulf of California and Escanaba Trough, Northeast Pacific Ocean. *AAPG Bull.*, 74:223–237.
- Langseth, M.G., and Becker, K., 1994. Structure of igneous basement at Sites 857 and 858 based on Leg 139 downhole logging. In Mottl, M.J., Davis, E.E., Fisher, A.T., and Slack, J.F. (Eds.), *Proc. ODP, Sci. Results*, 139: College Station, TX (Ocean Drilling Program), 573–583.
- Leif, R.N., Simoneit, B.R.T., and Kvenvolden, K.A., 1991. Simulation of hydrothermal petroleum generation by laboratory hydrous pyrolysis. In Manning, D.A.C. (Ed.), *Organic Geochemistry: Advances and Applications in the Natural Environment*: Manchester (Manchester Univ. Press), 300–303.
- Leybourne, M.I., and Goodfellow, W.D., 1994. Mineralogy and mineral chemistry of hydrothermally altered sediment, Middle Valley, Juan de Fuca Ridge. In Mottl, M.J., Davis, E.E., Fisher, A.T., and Slack, J.F. (Eds.), *Proc. ODP, Sci. Results*, 139: College Station, TX (Ocean Drilling Program), 155–206.
- Magenheimer, A.J., and Gieskes, J.M., 1992. Hydrothermal discharge and alteration in near-surface sediments from the Guaymas Basin, Gulf of California. *Geochim. Cosmochim. Acta*, 56:2329–2338.
- Mao, S., Eglinton, L.B., Whelan, J., and Liu, L., 1994. The thermal evolution of sediments from Leg 139, Middle Valley, Juan de Fuca Ridge: an organic petrological study. In Mottl, M.J., Davis, E.E., Fisher, A.T., and Slack, J.F. (Eds.), *Proc. ODP, Sci. Results*, 139: College Station, TX (Ocean Drilling Program), 495–508.
- Nowaczyk, N., and Baumann, M., 1992. Combined high resolution magnetostratigraphy and nannofossil biostratigraphy for late Quaternary Arctic Ocean sediments. *Deep-Sea Res. Part A*, 39:567–601.
- Palmer, M.R., and Edmond, J.M., 1989. The strontium isotope budget of the modern ocean. *Earth Planet. Sci. Lett.*, 92:11–26.
- Parkes, R.J., Cragg, B.A., Bale, S.J., Getliff, J.M., Goodman, K., Rochelle, P.A., Fry, J.C., Weightman, A.J., and Harvey, S.M., 1994. A deep bacterial biosphere in Pacific Ocean sediments. *Nature*, 371:410–413.
- Peter, J.M., Goodfellow, W.D., and Leybourne, M.I., 1994. Fluid inclusion petrography and microthermometry of the Middle Valley hydrothermal system, northern Juan de Fuca Ridge. In Mottl, M.J., Davis, E.E., Fisher, A.T., and Slack, J.F. (Eds.), *Proc. ODP, Sci. Results*, 139: College Station, TX (Ocean Drilling Program), 411–428.
- Quinterno, P.J., 1994. Quaternary foraminifers from Escanaba Trough, northeastern Pacific Ocean. In Morton, J.L., Zierenberg, R.A., and Reiss, C.A. (Eds.), *Geologic, Hydrothermal, and Biologic Studies at Escanaba Trough, Gorda Ridge, Offshore Northern California*. U.S. Geol. Surv. Bull., 2022:337–359.
- Rohr, K.M.M., and Gröschel-Becker, H., 1994. Correlation of well logs, physical properties, and surface seismic reflection data, Middle Valley, Juan de Fuca Ridge. In Mottl, M.J., Davis, E.E., Fisher, A.T., and Slack,

- J.F. (Eds.), *Proc. ODP, Sci. Results*, 139: College Station, TX (Ocean Drilling Program), 585–596.
- Rohr, K.M.M., and Schmidt, U., 1994. Seismic structure of Middle Valley near Sites 855–858, Leg 139, Juan de Fuca Ridge. In Mottl, M.J., Davis, E.E., Fisher, A.T., and Slack, J.F. (Eds.), *Proc. ODP, Sci. Results*, 139: College Station, TX (Ocean Drilling Program), 3–17.
- Rohr, K.M.M., Schmidt, U., and Gröschel-Becker, H., 1993. Regional patterns of hydrothermal alteration of sediments as interpreted from seafloor reflection coefficients, Middle Valley, Juan de Fuca ridge. *Geophys. Res. Lett.*, 20:1867–1870.
- Schultheiss, P.J., 1990. In situ pore pressure measurements for a detailed assessment of marine sediments: state of the art. In Demars, K., and Chaney, R. (Eds.), *Geotechnical Engineering of Ocean Waste Disposal*. ASTM STP 1087:190–205.
- Schultheiss, P.J., and McPhail, S.D., 1986. Direct indication of pore water advection from pore pressure measurements in Madeira Abyssal Plain sediments. *Nature*, 320:348–350.
- Schultz, A., Delaney, J.R., and McDuff, R.E., 1992. On the partitioning of heat flux between diffuse and point-source seafloor venting. *J. Geophys. Res.*, 97:12299–12314.
- Seyfried, W.E., Jr., and Bischoff, J.L., 1979. Low temperature basalt-alteration by sea water: an experimental study at 70°C and 150°C. *Geochim. Cosmochim. Acta*, 43:1937–1948.
- Shipboard Scientific Party, 1992a. Site 857. In Davis, E.E., Mottl, M.J., Fisher, A.T., et al., *Proc. ODP, Init. Repts.*, 139: College Station, TX (Ocean Drilling Program), 283–429.
- , 1992b. Site 858. In Davis, E.E., Mottl, M.J., Fisher, A.T., et al., *Proc. ODP, Init. Repts.*, 139: College Station, TX (Ocean Drilling Program), 431–569.
- Simoneit, B.R.T., 1977. Diterpenoid compounds and other lipids in deep-sea sediments and their geochemical significance. *Geochim. Cosmochim. Acta*, 41:463–476.
- , 1978. The organic chemistry of marine sediments. In Riley, J.P., and Chester, R. (Eds.), *Chemical Oceanography* (2nd ed.) (Vol. 7): New York (Academic Press), 233–311.
- , 1985. Hydrothermal petroleum: genesis, migration and deposition in Guaymas Basin, Gulf of California. *Can. J. Earth Sci.*, 22:1919–1929.
- , (Ed.), 1990. Organic matter in hydrothermal systems -maturation, migration and biogeochemistry. *Appl. Geochem.*, 5:1–248.
- , 1992. Natural hydrous pyrolysis[0151]Petroleum generation in submarine hydrothermal systems. In Whelan, J.K., and Farrington, J.W. (Eds.), *Productivity, Accumulation and Preservation of Organic Matter in Recent and Ancient Sediments*: New York (Columbia Univ. Press), 368–402.
- , 1994. Lipid/bitumen maturation by hydrothermal activity in sediments of Middle Valley, Leg 139. In Mottl, M.J., Davis, E.E., Fisher, A.T., and Slack, J.F. (Eds.), *Proc. ODP, Sci. Results*, 139: College Station, TX (Ocean Drilling Program), 447–465.
- Simoneit, B.R.T., Goodfellow, W.D., and Franklin, J.M., 1992. Hydrothermal petroleum at the seafloor and organic matter alteration in sediments of Middle Valley, northern Juan de Fuca Ridge. *Appl. Geochem.*, 7:257–264.
- Simoneit, B.R.T., Kawka, O.E., and Brault, M., 1988. Origin of gases and condensates in the Guaymas Basin hydrothermal system (Gulf of California). *Chem. Geol.*, 71:169–182.
- Simoneit, B.R.T., and Lonsdale, P.F., 1982. Hydrothermal petroleum in mineralized mounds at the seabed of Guaymas Basin. *Nature*, 295:198–202.
- Stakes, D.S., and Franklin, J.M., 1994. Petrology of igneous rocks at Middle Valley, Juan de Fuca Ridge. In Mottl, M.J., Davis, E.E., Fisher, A.T., and Slack, J.F. (Eds.), *Proc. ODP, Sci. Results*, 139: College Station, TX (Ocean Drilling Program), 79–102.
- Taylor, B.E., 1990. Carbon dioxide and methane in hydrothermal vent fluids from Middle Valley, a sediment-covered ridge segment. *Eos*, 71:1569.
- Teagle, D.A.H., Alt, J.C., Chiba, H., and Halliday, A.N., in press. Dissecting an active hydrothermal deposit: the strontium and oxygen isotopic anatomy of the TAG hydrothermal mound, Part II: Anhydrite. In Herzog, P.M., Humphris, S.E., Miller, D.J., and Zierenberg, R.A. (Eds.), *Proc. ODP, Sci. Results*, 158: College Station, TX (Ocean Drilling Program).
- Thornton, E.C., and Seyfried, W.E., Jr., 1987. Reactivity of organic-rich sediment in seawater at 350°C, 500 bars: experimental and theoretical constraints and implications for the Guaymas Basin hydrothermal system. *Geochim. Cosmochim. Acta*, 51:1997–2010.
- Tivey, M.A., 1994. High-resolution magnetic surveys over the Middle Valley mounds, northern Juan de Fuca Ridge. In Mottl, M.J., Davis, E.E., Fisher, A.T., and Slack, J.F. (Eds.), *Proc. ODP, Sci. Results*, 139: College Station, TX (Ocean Drilling Program), 29–35.
- Turner, R.J.W., Ames, D.E., Goodfellow, W.D., Leitch, C.H.B., Franklin, J.M., and Hoy, T., 1993. Character of hydrothermal mounds and nearby altered hemipelagic sediments in the hydrothermal areas of Middle valley, northern Juan de Fuca Ridge: shallow core data. *Can. Mineral.*, 31:973–995.
- Von-Damm, K.L., 1995. Controls on the chemistry and temporal variability of seafloor hydrothermal fluids. In Humphris, S.E., Zierenberg, R.A., Mullineaux, L.S., and Thomson, R.E. (Eds.), *Seafloor Hydrothermal Systems: Physical, Chemical, Biological, and Geological Interactions*. Am. Geophys. Union, 91:222–247.
- Von Damm, K.L., Edmond, J.M., Grant, B., Measures, C.I., Walden, B., and Weiss, R.F., 1985. Chemistry of submarine hydrothermal solutions at 21°N, East Pacific Rise. *Geochim. Cosmochim. Acta*, 49:2197–2220.
- Wheat, C.G., and Mottl, M.J., 1994. Data report: Trace metal composition of pore water from Sites 855 through 858, Middle Valley, Juan de Fuca Ridge. In Mottl, M.J., Davis, E.E., Fisher, A.T., and Slack, J.F. (Eds.), *Proc. ODP, Sci. Results*, 139: College Station, TX (Ocean Drilling Program), 749–755.
- You, C.-F., Spivack, A.J., Gieskes, J.M., Martin, J.B., and Davisson, M.L., 1996. Boron contents and isotopic compositions in pore waters: a new approach to determine temperature induced artifacts-geochemical implications. *Mar. Geol.*, 129:351–361.
- Zierenberg, R.A., 1994. *Data Report: Sulfur content of sediment and sulfur isotope values of sulfide and sulfate minerals from Middle Valley*. In Mottl, M.J., Davis, E.E., Fisher, A.T., and Slack, J.F. (Eds.), *Proc. ODP, Sci. Results*, 139: College Station, TX (Ocean Drilling Program), 739–748.

Ms 169IR-104

NOTE: For all sites drilled, core-description forms (“barrel sheets”) and core photographs can be found in Section 3, beginning on page 299. Smear-slide data and thin-section data can be found on CD-ROM. See Table of Contents for material contained on CD-ROM.